

Alma Mater Studiorum – Università di Bologna

DOTTORATO DI RICERCA IN

Ingegneria Civile, Chimica, Ambientale e dei Materiali

Ciclo XXXIII

Settore Concorsuale: 09/D2

Settore Scientifico Disciplinare: ING-IND/24

**Synthesis, Modification and Characterization
of Polymeric Membranes for CO₂ Separation**

Presentata da: *Riccardo Casadei*

Coordinatore Dottorato

Prof. Luca Vittuari

Supervisore

Prof. Marco Giacinti Baschetti

Co-Supervisore

Prof. Loris Giorgini

Esame finale anno 2021

Table of Content

| | |
|--|----|
| Abstract | 3 |
| Introduction | 4 |
| 1) Background..... | 6 |
| 1.1 Carbon Capture..... | 6 |
| 1.2 Membranes for Gas Separation | 12 |
| 1.2.1 Gas Separation Membranes – Base Concepts | 12 |
| 1.2.2 Solution Diffusion | 15 |
| 1.2.3 Facilitated Transport Membranes (FTM)..... | 17 |
| 1.2.4 Mixed Matrix Membranes (MMM)..... | 21 |
| 2) Materials | 24 |
| 2.1 Facilitated Transport Materials..... | 24 |
| 2.1.1 PolyVinylAmine (PVAm) | 25 |
| 2.1.2 NanoFibrillated Cellulose (NFC) and Carboxymethylated Nanocellulose (cNFC) | 29 |
| 2.1.3 Arginine..... | 34 |
| 2.2 Solution-Diffusion Materials..... | 35 |
| 2.2.1 Pebax [®] 2533 (P2533)..... | 36 |
| 2.2.2 Graphene Oxide (GO) | 38 |
| 2.2.3 Benzoyl-P2533 (BP2533)..... | 42 |
| 3) Methods | 43 |
| 3.1 Processes and Reactions | 43 |
| 3.1.1 Lupamin [®] 9095 Purification..... | 43 |
| 3.1.2 Blending: PVAm + cNFC nanocomposites..... | 44 |
| 3.1.3 Graphene Oxide Materials Synthesis..... | 45 |
| 3.1.4 Blending: Pebax [®] 2533 + GO Nanocomposites | 46 |
| 3.1.5 Pebax [®] 2533 Modification: Benzoyl-P2533..... | 47 |
| 3.1.6 Controlled Crosslinking of PVAm with Glutaraldehyde..... | 49 |
| 3.2 Chemical and Physical Characterizations..... | 51 |
| 3.2.1 Fourier Transform Infrared Spectroscopy (FTIR)..... | 51 |
| 3.2.2 Thermogravimetric Analysis (TGA) | 51 |
| 3.2.3 Differential scanning calorimetry (DSC)..... | 51 |
| 3.2.4 Scanning Electron Microscopy (SEM)..... | 52 |
| 3.2.5 Nuclear Magnetic Resonance (NMR) | 52 |
| 3.2.6 X-ray Photoelectron Spectroscopy (XPS) | 53 |
| 3.2.7 Water Absorption | 53 |
| 3.2.8 Crosslinked PVAm Weight loss in water: dipping test | 55 |

| | |
|---|-----|
| 3.3 Membrane Preparation | 56 |
| 3.3.1 Solvent Casting..... | 56 |
| 3.3.2 Spin Coating | 57 |
| 3.3.3 Membrane Masking..... | 58 |
| 3.4 Gas Permeation Characterization | 60 |
| 3.4.1 Static Test – Dry..... | 62 |
| 3.4.2 Dynamic Test – Humid..... | 63 |
| 4) Results and Discussion: Polyvinylamine and Nanocellulose | 64 |
| 4.1 Purification of Lupamin®9095 - Polyvinylamine..... | 64 |
| 4.2 Dispersion and Blending | 66 |
| 4.3 Water Absorption | 68 |
| 4.4 Humid Permeability Test..... | 70 |
| 4.5 Controlled Crosslinking..... | 72 |
| 4.5.1 Fast Dipping Test..... | 72 |
| 4.5.2 Long Dipping Test and Weight Loss..... | 74 |
| 5) Results and Discussion: Pebax®2533 and Graphene Oxide | 76 |
| 5.1 GO Dispersion and Blending..... | 76 |
| 5.2 FTIR | 77 |
| 5.3 XPS..... | 79 |
| 5.4 SEM..... | 80 |
| 5.5 DSC | 83 |
| 5.6 Permeation..... | 85 |
| 6) Results and Discussion: Benzoyl-P2533 | 89 |
| 6.1 Product Physical Change | 89 |
| 6.2 FTIR | 89 |
| 6.3 ¹ H-NMR | 91 |
| 6.4 TGA..... | 93 |
| 6.5 DSC | 94 |
| 6.6 Permeability - Gas Transport Characterization | 96 |
| 6.7 Permeance - Thin Coated Membranes..... | 99 |
| Conclusions..... | 100 |
| Acknowledgements..... | 102 |
| References..... | 103 |

Abstract

This doctorate focused on the development of dense polymeric membranes for carbon capture, mostly in post combustion applications, and for natural gas sweetening. The work was supported by the European Project NANOMEMC² funded under H2020 program.

Following the research activity, different materials have been investigated, that rely on two main transport mechanisms: the solution-diffusion, which represent the standard transport through dense membranes, and the facilitated transport, an additional mechanism that can occur along with the previous one if particular materials and conditions are employed. In both cases, proper nano-fillers have been added to the matrix, in order to boost the mechanical and permselective properties of the membranes.

Facilitated transport membranes were based on the use of polyvinylamine (PVAm), as main matrix with fixed-site carriers, and L-Arginine as mobile carrier; the filler, used mostly as reinforcer, was carboxymethylated nanocellulose (cNFC). Thanks to the facilitated transport, humid test showed interesting results, and especially the blend made of PVAm/cNFC/Arg in weight ratio 27,5/27,5/45 crossed the Robeson CO₂/N₂ upper bound, representing current state of the art membranes, with a CO₂ permeability of 271 Barrer and CO₂/N₂ selectivity of 70.

Solution diffusion membranes were based on Pebax[®]2533 matrix which was added with three different graphene oxide (GO)-based materials, namely pristine GO, Porous Graphene Oxide (PGO) and a GO functionalized with polyetheramine (PEAGO). All of them provided a modest but clear increment of permeability of the Pebax matrix, from plus 2% (GO) to plus 8% (PGO), with no change in selectivity. The gas tested with this type of composites were CO₂ and N₂, for Post combustion capture applications.

Pebax[®]2533 was also chemically modified, obtaining the product called “Benzoyl-P2533”, that was fully characterized, and also wide tested in term of permeation using five gas: CO₂, N₂, CH₄, O₂, and He. Such modified material showed an increment of the overall permeability of the material of a fair 10% for all gases tested, apart from helium, that increased of almost 50%.

Introduction

To counter the increment of global temperature due to anthropic emissions of greenhouse gases, first of all carbon dioxide, an energy switch from fossil fuel to renewable sources is by now a necessity. However, such process is extremely slow and difficult, and could take several decades to be accomplished. In the meantime, several technologies have been developed to temporary reduce the emission problem, since nowadays fossil fuels are still the main energy sources: the so called “Carbon Capture” (CC). The approach is to recover CO₂ before it is emitted to the atmosphere, and then store it in safe places (Carbon Capture and Storage, CCS) or use as raw materials to create other substances or products (Carbon Capture and Usage, CCU).

A number of Carbon Capture technologies have been developed, one of which rely on membranes to separate CO₂ from other gases.

Gas separation membranes technologies are widely investigated due to some extremely interesting features, including compactness, ease of installation and maintenance, and extremely low requirement of chemicals resulting to be particularly environmentally friendly.

This doctorate work has been carried out within a European Project called NANOMEMC², whose aim was to develop novel membranes for CO₂ separation, focusing on post combustion carbon capture (PCC) and natural gas sweetening applications.

The University of Bologna role in the network was mainly focused on the membranes material design, and mainly involved materials investigation, modification, blending and characterization, all conducted at laboratory-scale.

The Project was mostly centered on the employment of membranes based on facilitated transport (FTM), added with nano-materials to improve the permeation and mechanical properties.

The facilitated transport material chosen were aminated to selectively carry CO₂, the polymer polyvinylamine and the amino acid arginine. While the filler was cellulose based: carboxymethylated nanocellulose.

More specifically, interesting results were obtained during the first part of the Project by using carboxymethylated nanocellulose plus arginine or polyvinylamine separately; the blend of cNFC and PVAm proved indeed to result in a resistant material also at high humidity and 35°C, while the arginine improved the permselective performances of cNFC. As a consequence, a three-component approach was investigated in the present thesis. All the three components were indeed used at once, to have both fixed and mobile facilitated transport carriers, as well as the mechanical resistance given by the carboxymethylated nanocellulose.

Permeation test were conducted in humid condition, mandatory to trigger the amine-based CO₂ facilitated transport, at 75 and 100 RH%. The gas tested were CO₂, N₂ and CH₄ with feed pressure of 1 bar and temperature mostly 35°C, apart from a set of data at 100 RH% and 50°C.

To improve the mechanical resistance of the blend, a controlled crosslinking of PVAm started to be investigated as well.

A second line of research, within the same NANOMEMC² project, was started following the collaboration with the Korean partner in Hanyang University which suggested to introduced graphene oxide-based nano-filler into Pebax[®]2533 copolymer in order to improve its permselective properties. With this matrix, the filler used were Graphene Oxide (GO) and other two its derivates: Porous

Graphene Oxide (PGO) and GO functionalized with polyetheramine (PEAGO). The considered applications for these composites was post combustion carbon capture, thus CO₂ and N₂ were employed for gas permeation experiments.

Within the doctorate, also the modification of Pebax[®]2533 was investigated trying to further improve its properties and possibly the compatibility with GO based fillers. The Block copolymer was successfully modified during the doctorate work, with the addition of an aromatic ring obtaining a new material named “Benzoyl-P2533”. This new material was fully characterized both chemically and from the permeation point of view using CO₂, N₂, CH₄, O₂, and He.

Pebax based materials will be referred within the thesis as “solution diffusion” membranes, since they do not possess any facilitated transport carrier. For this reason, they were tested for permeation in dry conditions, as humidity should not affect their properties. The temperature and pressure were instead the same as for the other system investigated, 35°C and 1 bar, to facilitate the comparison among the different membranes.

Following the activity described above, the thesis has been structured with a background chapter which present the main information needed to understand the framework in which the doctorate activity was included and to fully understand the different results presented. For this reason, in this chapter the issues related to CO₂ emissions will be recalled together with a brief overview of the different carbon capture technologies, and a more detailed discussion of the main concepts of gas separation membranes.

After the background, the different materials considered for the development of the innovative gas separation membranes will be presented in the Chapter 2, “Materials” that will be divided in two different parts related to facilitated transport and the solution-diffusion membrane materials.

In Chapter 3, all experimental protocols are carefully explained both related to membrane preparation: polymer-filler blending, film deposition and so on, and in terms of materials characterization: chemical and thermal analysis, gas permeation experiments etc.

Then, three chapters about the results and discussion are presented focusing respectively on the facilitated transport materials with nanocellulose, on Pebax-based graphene oxide nanocomposites, and the modified Pebax, Benzoyl-P2533. Lastly, the conclusions of the work are proposed.

1) Background

Initially, in this chapter carbon capture will be considered explaining why it is nowadays one of the most interesting technology to tale the issues related to global warming. A brief overview of the different type of carbon capture will be described to explain the reason that drove us to focus on membrane separation.

The second part of the chapter will be then dedicated to gas separation membranes, describing the technology, the theoretical background and the main advantage and limitation considering the potential application to CCS

1.1 Carbon Capture

In the last decades, the rapid economic growth of developed and developing countries led to a notable increment of the global energy request, and of the use of fossil fuels which still represent the most employed energy source [1,2].

As a consequence, the concentration of combustion products, especially CO₂, kept relentlessly increasing: from 1850 to 2010 the average CO₂ concentration in atmosphere jumped from 280 ppm to 380 ppm and nowadays (2020) it is about 415 ppm [3]. This increase, as visible in Figure 1, has been followed by an increment of the greenhouse effect (closely related to these gases) and consequently to an increase of temperature to level which are not suitable for the maintenance of many existing ecosystems.

One of the most feared consequence is the increment of sea levels, directly related to temperature rising, since it is mostly due to glaciers melting and thermal expansion itself [4,5]. However, this is not the only negative consequence: climate change intensifies desertification [6] as well as promote the formation of cyclones and other extremely powerful and dangerous natural phenomena [7–9] that can cause enormous damage to both human civilization and overall ecosystem.

To avoid irreparable damages to the environment as we know it today, it is today well known that the global warming has to be stopped possibly keeping the average temperature increase below 2°C from the pre-industrial age, and nowadays we already passed from -0,6°C to + 0,2°C, thus + 0,8°C compared to pre-industrial age [10].

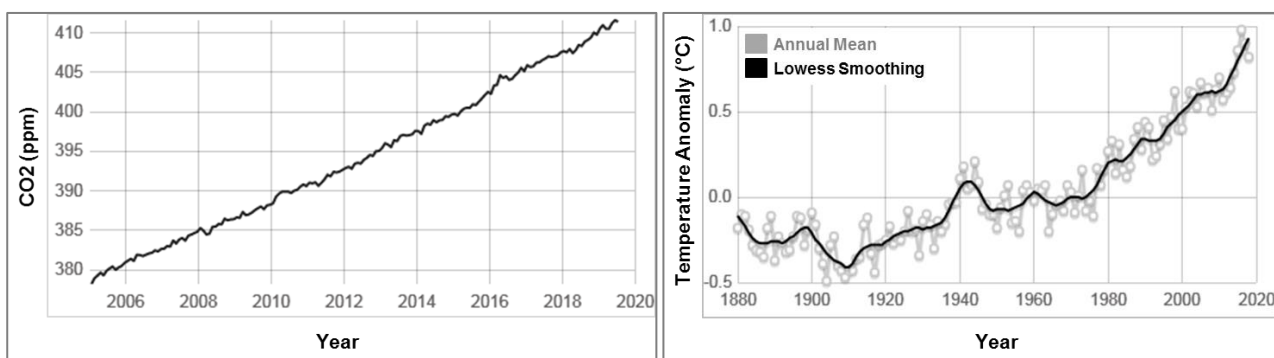


Figure 1: CO₂ and Temperature trend (from climate.nasa.gov [3])

This means that an important reduction of greenhouse gases emissions needs to be obtained in a rather short time, and many studies are analyzing the various hypothetical scenarios and projections, [11–15], with horizons ranging from 2030 to 2100 maximum. Otherwise the average temperature could rise even over $+2^{\circ}\text{C}$, as hypnotized also in the IPCC report, with different possible scenario considered, including one that reach about $+4^{\circ}\text{C}$ (Figure 2).

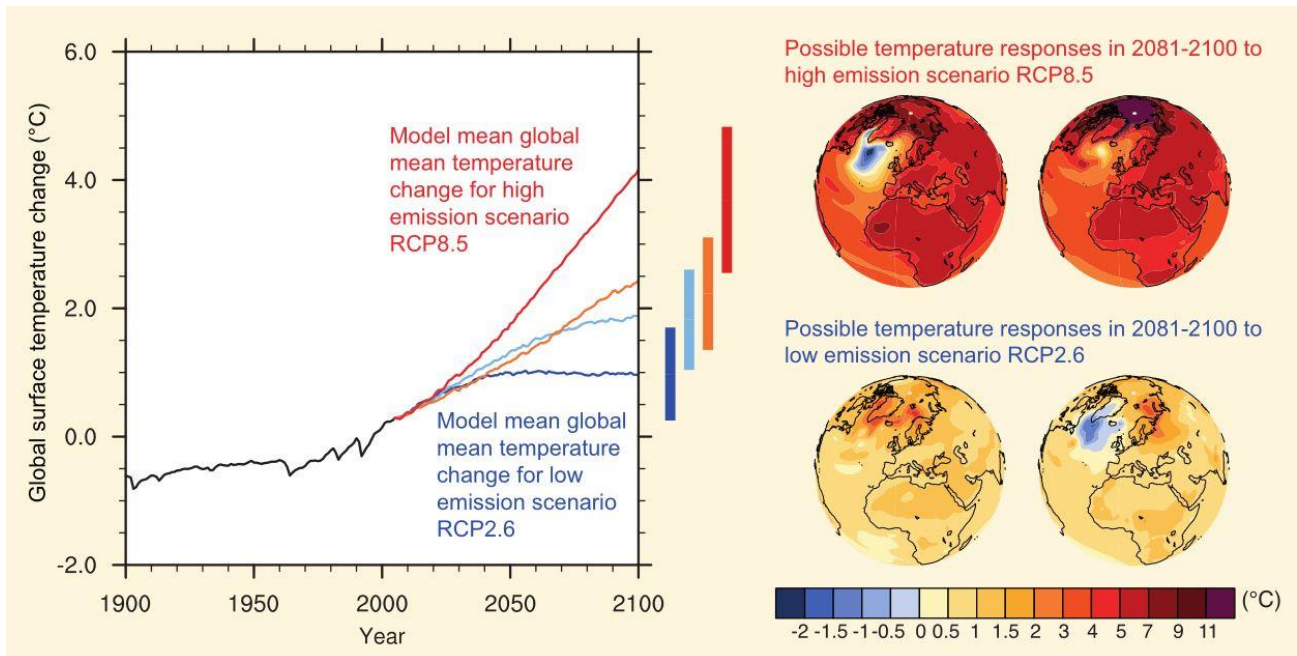


Figure 2: some possible temperature scenarios from IPCC [12]

To counter and contain this, so far, unstoppable increment of greenhouse gases (GHG) concentration, an energy transition from fossil fuels to renewable energies sources is considered the best option. However, such strategy is not instantaneous nor fast at all, and for this reason carbon capture technologies resulted to be interesting and investigated: they basically aim at maintaining the use of fossil fuel-based processes but without emitting GHG into atmosphere, to allow, in the meantime, the development and deployment of new renewable resources-based processes.

In this context, “Carbon Capture” (CC) technologies represent the overall attempt of CO_2 recovery from flue gas, in order to store it in sealed places preventing it to reach atmosphere, usually underground in depleted gas or oil deposits (Carbon Capture and Storage CCS) [16,17]; or to use it for different purposes, such as supercritical fluid extraction, chemical synthesis, food processing/preservation, enhancing oil/gas recovery etc. (Carbon Capture and Utilization CCU). [18]. The branch of these processes that aim to sequester CO_2 produced by massive combustion located in a specific area, such like power plants or other large plants, it is called Post-Combustion Carbon Capture (PCC) and represent the most interesting approach from the industrial perspective as, theoretically it does not requires modification of the existing production plants.

The other two most important approaches to carbon capture are instead the Pre-Combustion and the Oxy-Combustion [19,20], all these three main processes are schematized in Figure 3:

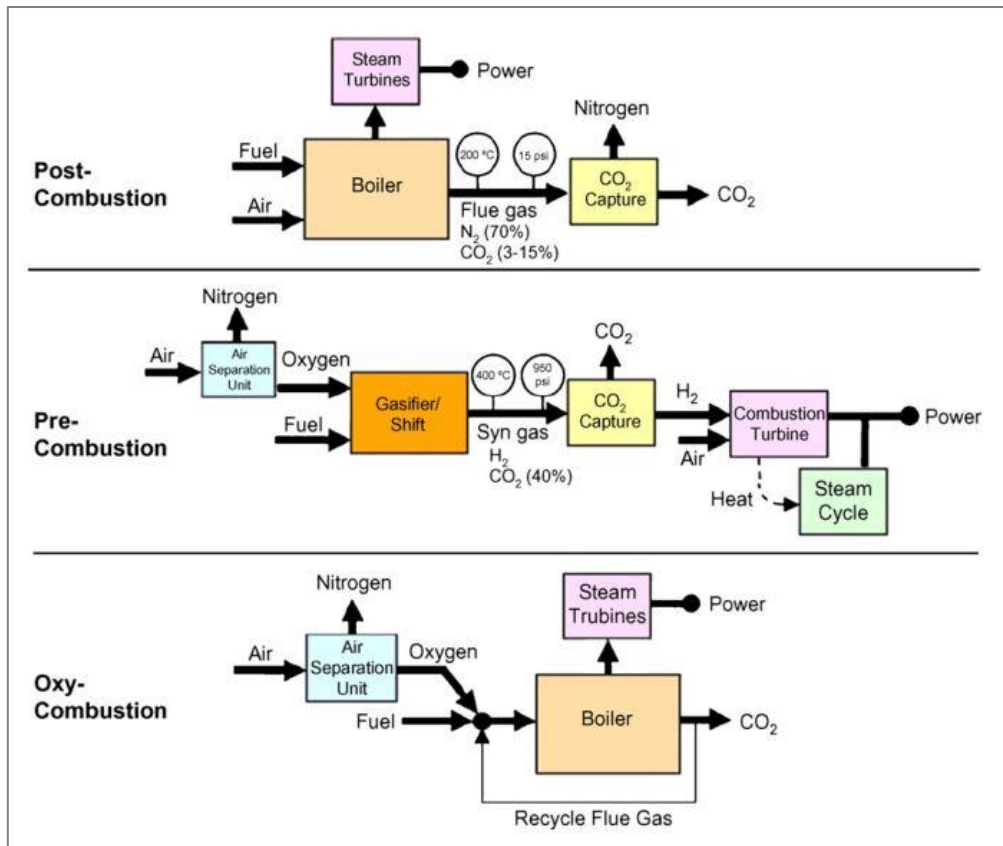
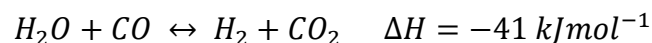


Figure 3: Process scheme of Post-, Pre-, and Oxy-Combustion [21]

As shown into the scheme, in post-combustion carbon dioxide is recovered at the end of the process, since it is one of the main byproducts of the last part, the combustion to gain energy [22]. In this concern the key separation is the one related to the CO_2/N_2 mixture since nitrogen is the most abundant inert flue gas. High selectivity and productivity are usually requested from the separation technology due to the high flowrate to be treated and to the low CO_2 content of the initial streams, as visible in Table 1 and 2 below.

In pre-combustion, the goal is to avoid the production of CO_2 in the main combustion system, so that the CO_2 is usually separated prior to the furnace after a gasifier/water gas shift reactor has been used to obtain pure hydrogen [23]. In this case CO_2 is usually a byproduct of the water gas shift aimed to produce more hydrogen from syngas (CO and H_2) through the typical following reaction:



The separation is therefore based on the CO_2/H_2 mixture and is usually easier than post combustion due to lower flowrate and low H_2 condensability. The process however has, in this case, to be adapted to be run with hydrogen as fuel thus requesting changes in its structure and equipment.

In oxy-combustion the gases key separation factor is O_2/N_2 , since the aim of this process is to burn fuels with nearly pure oxygen, usually separated from air [24]. The main purpose for using oxy-fuel combustion is to generate flue gas with very high concentrations of CO_2 and water vapor, making it possible to separate or capture the CO_2 from the flue gas purely by low-temperature dehydration and desulfurization processes. Also in this case, however, changes in the combustion process have to be

considered as the removal of nitrogen highly increases the combustion temperature if no other inert is introduced.

Table 1: Flue from some typical industrial processes [25]

| Components | Pre- combustion | Post combustion | Iron blast Furnace | Cement Production – |
|------------------|-----------------|------------------------|--------------------|---------------------|
| | CO ₂ | 10 – 35 mol% | 12 – 14 vol% | 20 vol% |
| SO _x | - | 1000 – 5000 ppm | - | 0 – 150 ppm |
| NO _x | - | 100 – 500 ppm | - | 0 – 150 ppm |
| CO | 300 – 4000 ppm | ~ 10 ppm | 22 vol% | 0 – 130 ppm |
| H ₂ S | 500 – 1000 ppm | - | 0 – 5000 ppm | - |
| H ₂ | ~ 20 vol% | - | 4 vol% | - |
| O ₂ | 0.03-0.6 vol% | 4-6 vol% | | |
| Water | Saturated | Saturated | 4 vol% | 12.8 vol% |

Table 2: Flue from some typical industrial units [26]

| Stream sources | CO ₂ concentration %vol (dry) | Pressure range | CO ₂ partial pressure (bar) |
|---|--|----------------|--|
| Gas turbines | 3–4 | Atmospheric | 0.03–0.04 |
| Fired boilers of oil refinery and petrochemical plant | 8 | “ | 0.08 |
| Natural gas fired boiler | 7–10 | “ | 0.07–0.10 |
| Oil fired boilers | 11–13 | “ | 0.11–0.13 |
| Coal fired boilers | 12–14 | “ | 0.12–0.14 |
| IGCC after combustion | 12–14 | “ | 0.12–0.14 |
| Blast furnace (after combustion) | 27 | “ | 0.27 |
| Cement process | 14–33 | “ | 0.14–0.33 |

Going in detail into the CO₂ separation unit, there is a number of promising CC technologies, and the most investigated are the following:

- **Solvent Absorption:** It consist in absorbing CO₂ in an amine-based solvent, typically examples are monoethanolamine (MEA) or diethanolamine (DEA), and successively regenerate it in a stripping column, obtaining in this way a CO₂ flow that can be sent to storage or usage [27,28]
- **Adsorption:** the main principle is similar to the absorption, but in this case CO₂ is adsorbed on the surface of proper solid materials, usually zeolites, carbon-based or properly functionalized compounds [29,30].
- **Membrane Separation:** it is a technology based on selective permeation through a semi-permeable barrier, in order to separate CO₂ from other gases [31,32].
- **Cryogenic Separation:** it consists in frost CO₂ solid at very low temperatures, usually -120 to -140°C, in order to separate it in such solid form and then gasify it [33,34].

- Mineralization: it consists in turning CO₂ to solid in carbonates form (CaCO₃, MgCO₃, FeCO₃ ...) through chemical reactions [35,36].

Among the different approaches, nowadays the most solid and employed technique is the Solvent Absorption, while the others are mostly in R&D or pilot development, at more or less advanced stages [31,32,37].

As already mentioned, most of carbon technology require a further step after the separation: the obtained CO₂ indeed has to be used in other processes or safely stored. While the former option basically “consumes” the CO₂ by using it as a new raw material in view of the creation of a new type of carbon cycle, the latter aim to trap and keep CO₂ confined for a long period to avoid its dispersion in the atmosphere. The most common stoking places, in this case are depleted gas or oil deposits, carbon sites where the extraction is no longer economically viable, or aquifers containing salty water. It has to be noted that also the research of suitable storage sites is currently very active as well as the whole storage process which include often also the transport and the compression of captured CO₂. In general geological storage requires a very efficient gas confinement which has to last for centuries or even millenniums; a leak of just 0,1 % per year would invalidate the CCS efficiency regarding global temperature control [38].

A scheme of CCS and CCU for post combustion applications is displayed in Figure 4.

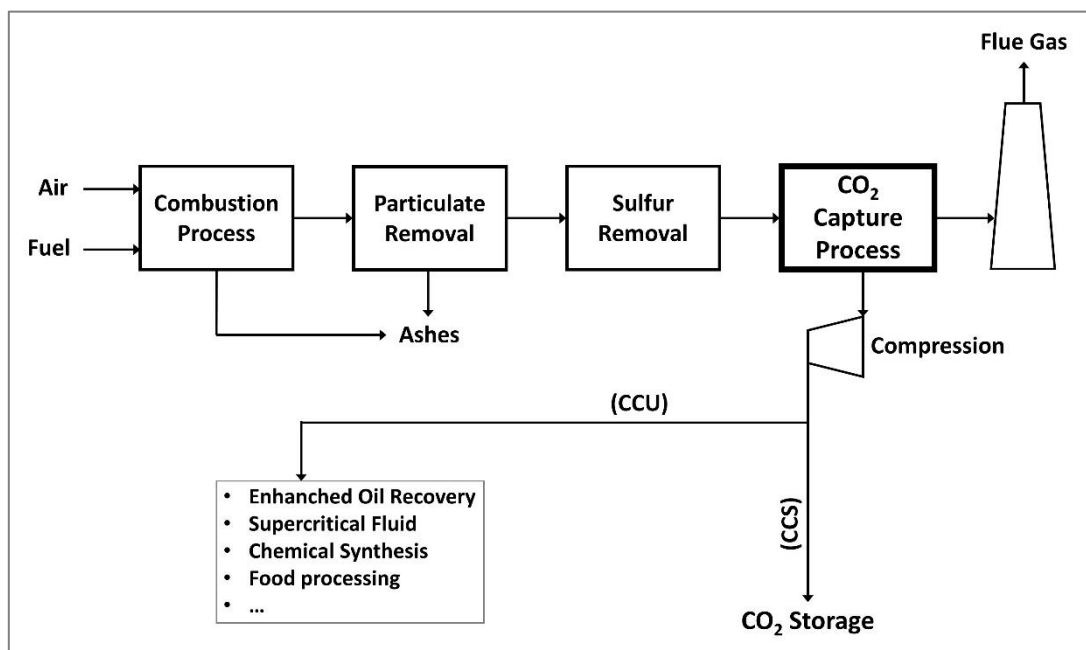


Figure 4: Generic PCC scheme with CCU/CCS options

Since the recovery of CO₂ from flue gas usually does not provide any direct economic benefit [39–41], such technologies are often used also in other more convenient processes, such as the natural gas sweetening [42–44]. Along with natural methane, indeed, different quantities of acid gases like CO₂ and H₂S are always present and they have to be removed in order to make the gas suitable for being distributed and used. In this approach therefore the use of CO₂ separation techniques may generate direct revenues, thus making the application more appealing. The availability of data from

industrial applications and possibly the reduction of the implementation costs indeed can pave the street towards the application also in the less convenient processes such as Carbon Capture.

In both flue gas and natural gas CO₂ removal, the features that make membranes interesting for the gas separation process are the same: low capital and installation costs, low environmental impact due to low chemical usage and disposal, facile installation and maintenance, high modification and tunability potential to improve their performances and/or attenuate their drawbacks. While the main shortcuts are usually related to plasticization and aging processes that tends to limit their performances, to limited thermal and chemicals stability which decrease their operative lifetime, and more in general to the poor balance between permeability and selectivity, the main performance parameters of membrane separation, that usually follow opposite trends (rising selectivity decreases permeability and vice versa). A better analysis of the main features of the membranes for gas separation a more detailed explanation of this technology will be discussed in the next Chapter 1.2.

Gas Separation Membranes: Features and Challenges

By the membrane material design point of view, so far, the greatest efforts have regarded the improvement of the permselective performances, since it is the very base requirement to build an effective process.

The main challenge here is represented by the typical trend of permeability versus selectivity in membranes (dense and not), where usually when one rise, the other decrease, and vice versa, and such intrinsic limitation is explicated with the Robeson's upper bounds, charts of permeability of a gas (es. CO₂ vs selectivity of this gas with another one (es. CO₂/N₂ or CO₂/CH₄),

1.2 Membranes for Gas Separation

Membrane-based separation technologies are those processes where the mixture of two or more compounds is separated by a semi-permeable barrier into a permeate and retentate flow. In such process, the most permeable species concentrate into permeate stream, while the less permeable cannot easily cross the membrane and concentrate into retentate stream (see figure 5).

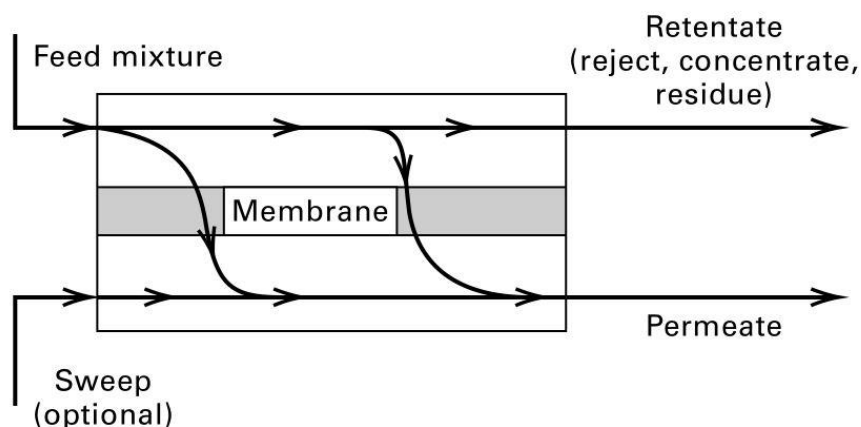


Figure 5: Typical gas separation membrane scheme [45]

In the last decades, membranes for gas separation is getting more and more interesting due to certain key feature of this technology: low environmental impact due to the vestural absence of chemicals to carry one the separation, low capital cost and low energy consumption and maintenance costs (as there is not needs to regenerate the sorbent), great compactness and modularity which facilitate the operation in confined spaces and remote location and allow to have high flexibility in operation as well as easy and fast installation/uninstallation, [25,26,46].

Of course there also several possible drawbacks which have up to now prevented the wide spread use of membranes in many field, this are mainly related membrane materials limitations such as for example the plasticization and the aging processes [47,48] that tends to limit their performances, the limited mechanical, thermal and chemicals stability which decrease their operative lifetime [49,50], and more in general the somewhat limited separation performances (with respect to other technologies) which makes membranes usually not convenient for separation processes where the feed is already extremely diluted or if a very high grade purification is needed, as in these case they are not generally able to operate with high efficiency and low costs [51]. To better understand the characteristic feature of this technology a brief description of the main parameters and transport mechanisms are given below.

1.2.1 Gas Separation Membranes – Base Concepts

To perform the separation of interest, membranes relay on a driving force pushing the process which usually obtained through concentration (ΔC) or pressure (Δp) gradient across the membrane itself. In gas separation processes, then, the driving force is often a pressure gradient, and the flow through the membrane of the compound i can be described by Equation 1:

$$J_i = \frac{P_i \cdot \Delta p_i}{L} = \varphi \cdot \Delta p_i \quad (1)$$

Where J_i is the specific flow of the compound i across the membrane, L is the membrane's thickness, P_i is the permeability of the compound i for that specific membrane, Δp_i is the gradient of partial pressure of i between the two sides of the membrane (upstream and downstream), and φ is the permeance of the compound i .

The *Permeability* indicates the flow through the membrane with a certain known thickness, per unit of surface and driving force, and is the most employed parameter to describe the potential properties of a membrane material. With the proper experimental condition, indeed, the ability of a given membrane to obtain separation is related to the different permeability of the species present in the feed. Permeability, for gas separation membranes is usually measured in “Barrer”, a non SI units proposed in honor of Richard Maling Barrer [52,53], as shown in Equation 2 and 3.

Permeability is basically a material property and for this reason it is mainly used to describe the potentiality of materials to carry on a certain type of separation.

When the membrane efficiency is of interest, however, another quantity is often used: the *Permeance* (φ), which represent the actual flow through the membrane per unit of surface and driving force, without taking into account the thickness parameter at all. Thus, Permeance is mostly used to describe the real flow through the overall final membrane, which is usually composed by many different layers and cannot be described by a single permeability value. Its unit of measure is usually the “Gas Permeance Unit” (GPU), as shown in Equation 4 and 5.

The final parameter which often appears in the study of membrane separation is finally the *Selectivity* (also called as “separation factor”) that indicates which gas passes preferentially, thus describing the membrane's separation capability (Equation 6).

Frequently, gas permeation experiments are carried out testing one gas at time. In these cases, the *Ideal Selectivity* is calculated afterwards, from the ratio of the two permeabilities obtained separately (Equation 7).

$$\text{Permeability (SI)} = \frac{\frac{\text{mol}}{\text{s}} \cdot \text{m}}{\text{m}^2 \cdot \text{Pa}} = \frac{\text{mol}}{\text{s} \cdot \text{m} \cdot \text{Pa}} \quad (2)$$

$$\text{Permeability (Barrer)} = \frac{\frac{\text{cm}^3_{(\text{STP})}}{\text{s}} \cdot \text{cm}}{\text{cm}^2 \cdot \text{cmHg}} \cdot 10^{10} \quad (3)$$

$$\text{Permeance (SI)} = \frac{\frac{\text{mol}}{\text{s}}}{\text{m}^2 \cdot \text{Pa}} = \frac{\text{mol}}{\text{s} \cdot \text{m}^2 \cdot \text{Pa}} \quad (4)$$

$$\text{Permeance (GPU)} = \frac{\frac{\text{cm}^3_{(\text{STP})}}{\text{s}}}{\text{cm}^2 \cdot \text{cmHg}} \cdot 10^6 \quad (5)$$

$$\text{Selectivity } \alpha_{i,j} = \frac{y_i^d / y_j^d}{y_i^u / y_j^u} \quad (6)$$

$$\text{Ideal Selectivity } \alpha'_{i,j} = \frac{P_i}{P_j} \quad (7)$$

The just exposed definitions represent the basic performance parameters of the field and are generally given for all the different types of membrane which in general can be described and classified in many ways considering their structure, geometry, composition and son on; Figure 6 present some of the possible classification parameters.

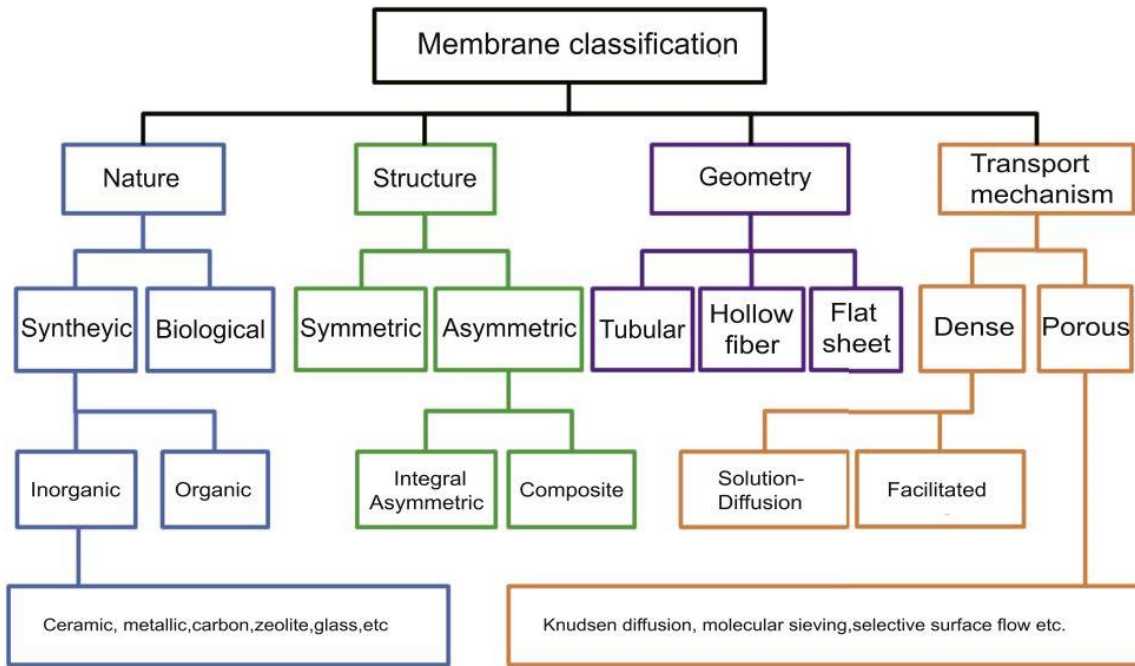


Figure 6: Membrane Classification Parameters [54]

Referring to Figure 6, the membranes can therefore be described by considering their:

- *Nature*: which is the source (synthetic/biological) and chemical type of the material (organic/inorganic). Organic (polymeric) membranes have the great advantage of being cheaper and with a more feasible processability compare to the inorganic ones.
- *Structure*: that is how the membrane is structured, e.g. if it has the same structure organization on both sides (symmetric) or it changes through the perpendicular axe, in term both structure and porosity of the same material (integral asymmetric) or made of different layer (composite). Both industrially and in laboratory scale, membranes are usually asymmetric composite, since a support layer for the selective one is always needed. However, at laboratory scale it is also thick self-standing membranes are tested to have a clear view of the materials properties.
- *Geometry*: it is basically the shape of the membrane, the most common being flat sheet, tubular and hollow fiber membranes. Flat sheet membranes are the most simple to be prepared for permeation tests at lab-scale.
- *Transport mechanism*: is the mechanism through which the gas can cross the membrane, and it depend by its physical structure. For porous (or in the case of gas separation, micro- or nano-porous) membranes the mechanism is dominated by molecular sieving or knudsen diffusion,

where the pores act as sieve. For dense membranes (without pores) the transport is called solution-diffusion, where the gases get solubilized inside the material and then diffuse through it. Facilitated transport is a possible additional mechanism of transport for dense membranes, where a target molecule is carried selectively by a certain reactive site called “carrier”.

Usually, the porous membranes have higher permeability but lower selectivity, while the dense have higher selectivity and lower permeability. For the sake of clarity, all the different transport mechanisms which can happen within a membrane have been cited, but since in this work only dense membranes have been investigated, only solution-diffusion and facilitated transport mechanism will be taken into account in more details.

Lastly, to their outstanding impact in gas separation membranes field, it is rightful to introduce the concept of Mixed Matrix Membranes (MMM). With the MMM approach, a dense polymeric matrix is filled with organic or inorganic fillers, that are capable of to exhibit highly efficient separation performances often through the porous mechanism explained before, obtaining a final membrane that virtually possess both advantages provided from the dense polymers and from the sieving fillers. Such concept will be deeper discussed in Section 1.2.4.

1.2.2 Solution Diffusion

Dense polymeric membranes usually rely on solution diffusion mechanism of transport, which occurs in 5 main steps [55], schematized in Figure 7:

- 1) The compounds in the feed diffuse to the upstream surface of the membrane;
- 2) Then they solubilize into the membrane’s material itself;
- 3) Once absorbed, they diffuse through the membrane, reaching the downstream side;
- 4) They desorb from the downstream surface of the membrane;
- 5) Lastly, they diffuse to the permeate flow.

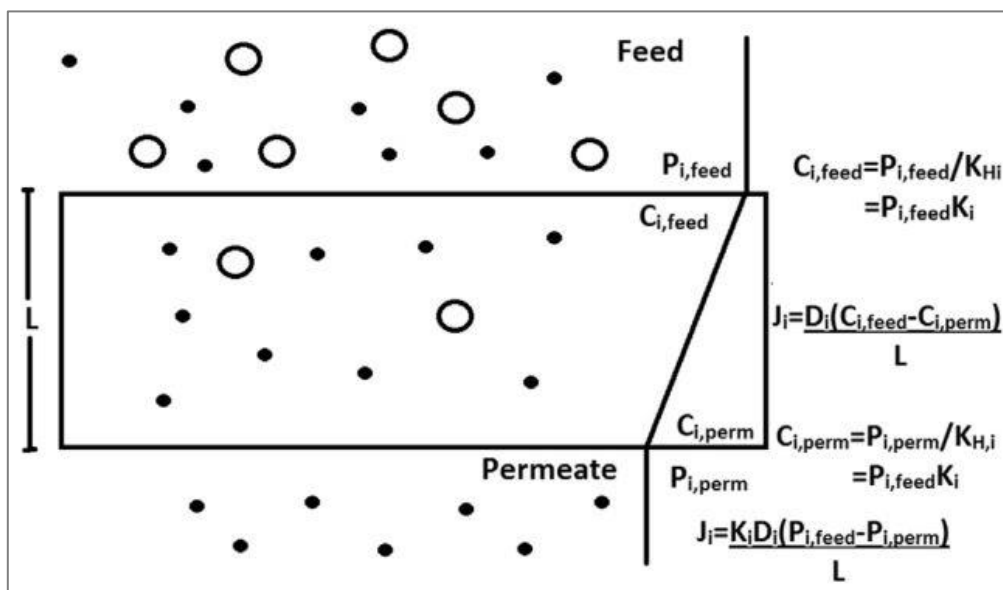


Figure 7: Solution Diffusion Scheme [26]

As a consequence of the mechanism just explained, it results clear that the flow across the membrane (in term of permeability) made of a given material is related to both its Solubility (coefficient S), and its Diffusivity, (coefficient D), and results to be the product of these two quantities as reported in Equation 8 [26,55,56]:

$$P_i = S_i \cdot D_i \quad (8)$$

This result comes directly from the knowledge the basics ruled governing sorption and diffusion. On one side, due to low gas condensability, solubility of gases in polymer usually follows the Henry's law so that, for a given temperature, the amount of solubilized gas per unit of polymer volume is proportional to the partial pressure of gas in equilibrium with it, as shown in Equation 9, which also represent the definition of the Solubility coefficient.

$$C_i = \frac{p_i}{H_i} = p_i \cdot S_i \quad (9)$$

Where C_i is the concentration of the compound i solubilized, p_i is its partial pressure, H_i is the Henry's constant.

The diffusive process, on the other side, is usually described by Fick's law of diffusion, which in the case of flat membranes with diffusion coefficient D , can be written as showed in Equation 10:

$$J_i = \frac{D_i \cdot \Delta C_i}{L} \quad (10)$$

Where ΔC_i is the concentration gradient through the membrane, with thickness L .

Substituting the Equation 9 into Equation 10, Equation 11 is obtained:

$$J_i = \frac{S_i \cdot D_i \cdot \Delta p_i}{L} \quad (11)$$

Which by comparison with equation 1 directly gives the results in Eq. 8.

Similar considerations can be done also regarding the ideal selectivity previously discussed, which can be divided in a sorption and a diffusion part as shown in Equation 12:

$$\alpha_{i,j} = \frac{P_i}{P_j} = \frac{D_i}{D_j} \cdot \frac{S_i}{S_j} = \alpha_D \cdot \alpha_S \quad (12)$$

where α_D , is the diffusion selectivity, mainly related to the kinetic parameters governing the gas molecule mobility inside the membrane, and α_S represent the solubility selectivity a thermodynamic parameter, related to the ability of gas to desolve inside the polymeric membrane.

In general, therefore, permeability can be improved by increasing the diffusion speed (which usually scale with the kinetic diameter of the molecules) and increasing the selectivity (often related to gas condensability). Unfortunately, in general, in solution diffusion membranes every attempt to increase in permeability also bring a decrease in selectivity and vice versa as suggested by the Robeson's plot were an experimentally determined upper bound is clearly visible, that contain the most promising

membranes for the separation of a specific couple of gas [57]. Since in this doctorate, separation of carbon dioxide and methane was mostly investigated, in Figure 8 the Robeson's plots are showed for the CO₂/N₂ and CO₂/CH₄ systems.

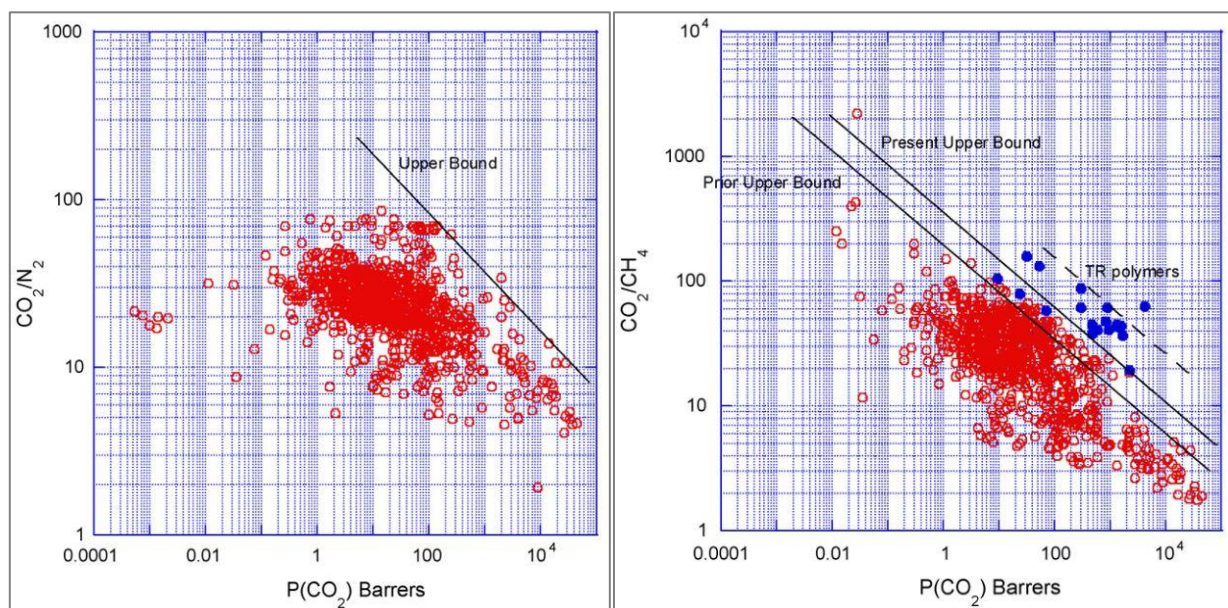


Figure 8: Robeson Plot for CO₂/N₂ (left) and CO₂/CH₄ (right) [57]

The upper bounds displayed in Figure 8 were obtained in 2008, while the previous ones, obtained in 1991, were lower in both selectivity and permeability. The upper bounds are indeed updated regularly with the development of new materials [58], showing that the effort made during the years actually works to improve the overall permselective properties of membranes.

For this reason, despite this limitation solution diffusion membranes are by far the most used in real applications and are of great importance in many different types of processes well beyond the gas separation. For additional information, in this concern the interested readers can refer to the many work available in the open literature such as for example the work from Khalilpour et al. who provided a fine review about transport mechanisms in dense membranes [26], or that of Wijmans and Baker [55] that present a deeper discussion of solution diffusion model for different types of membrane separation processes.

1.2.3 Facilitated Transport Membranes (FTM)

Facilitated transport (dense) membranes, along with the already mentioned solution-diffusion transport, possess also an additional transport mechanism based on the presence of a selective carrier inside the membrane. This type of transport indeed relies on a chemically selective and reversible bond between the target compound (in this case CO₂) and the carrier's molecules that facilitate its transport across the membranes.

Such approach very high potentiality in view of membrane performance improvements, due to the fact that with the proper carriers it is virtually possible to highly improve both permeability of the target compound and its selectivity towards other species, "moving" the upper bound forward in both direction.

Moreover, FTM can possibly grant economic advantages, since facilitated transport is usually active already at low pressure so that it eliminates the need of an important upstream compression to have a sufficient pressure gradient across the membrane.

By the strict chemical point of view, this is a mechanism already widely present in nature: for example ionophores that bound certain ions and make them cross cellular membranes, hemoglobin that bound and carry selectively oxygen, and many other compounds-selective and carry proteins are basically all examples of facilitated transport.

The aim in R&D is to mimic such mechanism in order to create extremely selective separation processes, to separate e.g. metal ions [59], olefin/paraffin [60], or gas separation.

The latter approach has already been investigated with success in literature [25,46,61–67] and especially Prof. Winston Ho group reached interesting high performances and develop level and already starting the scale-up [68–70], proving that such approach has high potential and it is totally worth to be investigated, studied and improved. Even if very appealing, indeed, most FTM are still far from industrial deployment as they still present some limitation often related to resistance and stability.

Technically speaking the FTMs can be divided in two main groups based on the Carrier mobility; we have indeed:

- *Mobile Carrier membranes*: where the carrier is not fixed, represented by a low molecular weight molecule that can move freely into the polymer backbone, bonding the target compound and carrying it through the membrane until the permeate side, where it is released.
- *Fixed Carrier membranes*: where the carrier is fixed, a part of the matrix itself, and the target compound react or interact locally, flowing and jumping through the reactive sites of the carrier until reaching the permeate side.

In general, these two types of FTM represents the two limits of the trade-off existing among the membrane stability and the membrane performances. Mobile carriers indeed have higher ability to transport the target molecules across the membrane, but being mobile they can also leak from the membranes thus causing a deterioration of its separation performances. Fixed carrier on the other hand are more stable, but in general less able to facilitate the target molecule diffusion.

Whichever the carrier type may be, then, FTM transport performances are affected by target compound concentration into the feed stream, especially if the concentration is high enough to saturate all the reactive sites. This “carrier saturation” phenomenon indeed leads to a decrement of selectivity and/or permeability of the membrane. Such behavior is caused by the decrement in concentration gradient inside the membrane, that become basically fully saturated from the target molecule.

Amine-Based CO₂ Facilitated Transport

FTM membranes have been considered for post combustion as the operative conditions result to be very favorable for their application; the feed pressure are low indeed and the CO₂ concentration is limited as well as already shown low as well as already shown in Table 1 and 2 reported in section 1.1. In addition, the peculiar acidic character of CO₂ can be easily exploited to bound it to selected carrier.

Among the many possible choices, amines are in general the most employed compounds for CO₂ removal, due to their basic nature which allows easy interaction with the acidic one of the carbon dioxide.

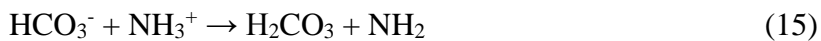
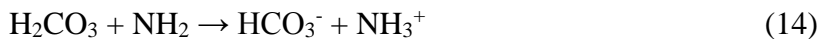
Indeed, also in the field of solvent absorption technology, the solvents employed to absorb CO₂ are often amine-based: some common examples are Monoethanolamine (MEA), the secondary amine Diethanolamine (DEA) and the tertiary amine Methyldiethanolamine (MDEA) [71,72].

For similar reasons, also in membranes technology amines are one of the most employed compounds to generate FTM, where the most common fixed sites material is Polyvinylamine (PVAm) neat or with modifications or additions, but also other aminated polymers like polyallylamine (PAA) or chitosan; while for mobile carriers amino acids are withdrawing great attention [25,31,62,73,74].

Also in NANOMEMC² Project the facilitated transport materials chosen for CO₂ separation were amine-containing materials, used as both fixed and mobile carrier. In particular the fixed carrier was PVAm, which possess on of the highest concentration of primary amines among the polymers, while for the mobile carrier Arginine amino acid was chosen, that possesses both a primary amine and a guanidine group. A better description of these materials will be given in the next chapter.

The main possible reaction mechanisms that can occur within an amine based FTM membrane in presence of CO₂ follow two pathways, the bicarbonate and carbamate ones:

Bicarbonate Mechanism (schematized in Figure 9)



From which, simplifying, the following reversible reaction is obtained:



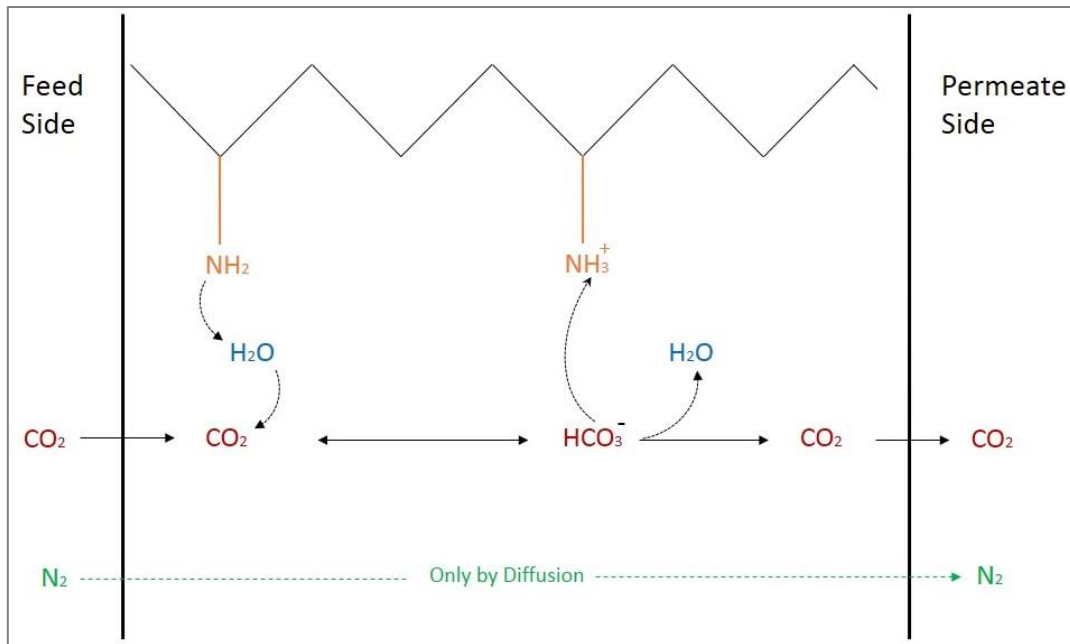
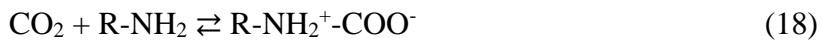


Figure 9: Amine-based CO₂ FTM – Bicarbonate mechanism

Carbamate Mechanism (Schematized in Figure 10)



From which, simplifying, the following reversible reaction is obtained:

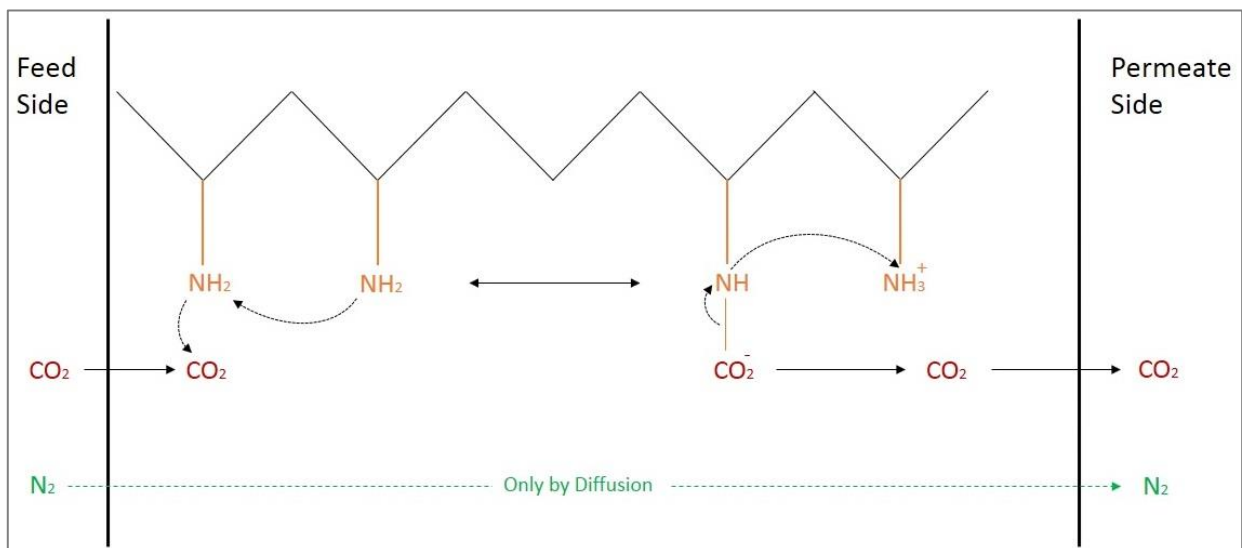
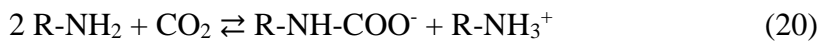
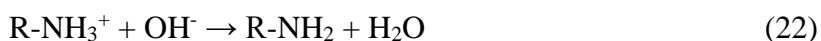


Figure 10: Amine-based CO₂ FTM – Bicarbonate mechanism

The main difference between the two mechanisms, is that the bicarbonate one (Equations 13-17) requires water to occur and allows a stoichiometrically double CO₂ uptake compare to the carbamate: this latter indeed, as shown in Equations 18-20, to transport one CO₂ molecule has to employ two reactive sites, while in the bicarbonate path only one at time. As a consequence, the humid bicarbonate mechanism resulted the most employed for these systems.

Moreover, in this case it has been proved that the water activity plays a key role in permselective performances, since both CO₂ permeability and CO₂/N₂ selectivity increment with the relative humidity of the system during the test, further confirmation of humid mechanism efficiency [62,63,75–77].

By the pH point of view, instead, since that chemical state (protonation) of amine group vary based on acidity or basicity of the solution, considering the following Equations 21 and 22, It is good protocol to maintain an alkaline pH during the PVAm preparation, in order to favor the neutral form R-NH₂, able to carry the reaction with water and CO₂ and thus trigger the facilitated transport previously explained.



As already mentioned, in this case the carrier itself is able to bond the target and drag it through the membrane, and here H₂O is useful not only for triggering the humid reaction with CO₂, but also to promote the mobile carrier diffusion as well.

It has to be noted however that humidity, in general, also present possible drawbacks: in hydrophilic polymers, PVAm included, the increment of water intake may cause also the swelling of polymeric chains reducing its mechanical stability. As a consequence, compromise needs to be reached between humidity (that is performances) and mechanical strength (that is stability). The latter is usually improved and controlled by making the structure more rigid and resistant through crosslinking reactions [78–80] or the addition of selected reinforcing fillers [63,81–86].

1.2.4 Mixed Matrix Membranes (MMM)

Composites and nano-composites are a particular class of materials where two (or more) different components are blended in order to enhance the property of one (or more) of them. Common examples are I) increasing the mechanical properties of a certain polymeric matrix, continuous phase, by adding a proper dispersed phase filler or II) making more processable a material (usually inorganic), which would not be able to form a continuous phase by itself, by coupling it with a proper compound (usually a polymer) that could represent the glue or compatibilizer matrix that hold together the whole structure [87,88].

Nanocomposites among the different type of composite have become very popular also in the field of gas separation membranes which in this case are often referred as “*Mixed Matrix Membranes*” (MMM).

In MMM, the additional filler may have different goals; it can be used to stabilize the membrane’s mechanical structure, e.g. countering swelling, aging and other physical or chemical phenomena that can compromise its performances. Or it can increase the permselective performances of the membrane itself, as highly permselective fillers exists (such as zeolites or MOF [89–94]) which are

very difficult to be processed as films but can be embedded into a polymeric matrix which provides structural stability to the material. Sometimes the filler can both increment mechanical stability of the matrix as well as its permselective properties.

A number of reviews is already present in literature about the interesting results obtained by this approach, in term of permselective improvements, with both organic and inorganic fillers [95–100], and to make a summary it is possible to say that the main trend is to employ a proper polymer as continuous phase, and adding fillers with at least one dimension of nano-scale size, possibly with a good dispersion, in order to have great Surface/Volume ratio and to be able to prepare thin membranes.

Both matrix and fillers are usually chosen based on their potential gas permselective properties, for example adding highly selective filler into a highly permeable matrix, in order to boost both best features of both component and trying to overcome the Robeson upper bound. For example loading a porous sieving selective filler into a solution-diffusion continuous polymeric matrix.

A general scheme of Pros/Cons of polymeric membranes vs MMM is shown in Table 3:

Table 3: Main Differences between Polymeric only and Mixed Matrix Membranes

| Membrane Type | Advantages | Disadvantages |
|---------------------|---|--|
| Polymeric | <ul style="list-style-type: none"> - Easy synthesis and fabrication - Good mechanical stability - Easy for upscaling and making variations in module form - Separation mechanism: Solution diffusion - Eventual additional Facilitated Transport mechanism | <ul style="list-style-type: none"> - Low chemical and thermal stability - Plasticization - Pore size not controllable - Follows the trade-off of Permeability and Selectivity |
| Mixed Matrix | <ul style="list-style-type: none"> - Enhanced mechanical and thermal stability - Reduced plasticization - compacting at high pressure - Potentially surpass the trade-off between permeability and selectivity - Enhanced separation performance over native polymeric membranes - Separation followed by the combined polymeric and filler-based principle | <ul style="list-style-type: none"> - Brittle at high fraction of fillers - Chemical and thermal stability depends on the polymeric matrix - Not all combination Matrix-Filler are feasible due to possible compatibility issues |

When designing an MMM, the main technical concerns, apart from choosing the best combination of matrix and filler in term of permselective properties, are usually two:

- Compatibility matrix-filler
- Filler dispersion

These two issues are often bonded, since if there isn't a proper chemical compatibility (e.g. polarity) between the filler and the hosting matrix, the former tends to aggregate forming agglomerates sometimes big enough to be clearly visible at naked eye, resulting in an extremely bad shaped heterogeneous membrane.

Such phase segregation is also affected by the type of membrane preparation: the faster the evaporation (or phase inversion) is, the lesser these phenomena will create troubles, even if the best way is always to find proper compatible filler-matrix materials, in order to not have any sort of problems during the manufacturing phase.

The compatibilization is by now well known in MMM field, and there are plenty of works that study the interaction of fillers with matrix and their interfaces [95,97,99,100], that can produce different effects: the correct adhesion of the two different materials, the creation of interfacial voids, the obstruction of the micro-/nano-pores of the filler, or just the already cited phase segregation that lead to preferential pathways into the membrane.

Thus, to avoid or eliminate such morphological problems, an accurate choice of the materials and an adequate design of the membrane preparation process are mandatory.

As a title of example, in Figure 11 are displayed two membranes made of the very same materials and concentrations, Pebax and Graphene Oxide, but obtained through different blending processes: in the one on the left it is possible to notice a very clear segregation behavior of the GO, while in the one on the right the distribution of filler is extremely homogenous (the only visible imperfections are just bubbles of air, that may occur sometimes in solvent casting).



Figure 11: example of two solvent casting membranes made of the same materials and concentrations (Pebax®2533 and Graphene Oxide) but obtained through different blending processes [101].

Within NANOMEMC² Project, and in this PhD work, MMM technology have been the core approach to prepare CO₂ separating membranes, employing nano-scale fillers belonging to two different compound classes: Cellulose-based nanomaterials, and Graphene Oxide based nanomaterials. Details about materials used will be discussed in Chapter 2, while the blending technologies will be presented in Chapter 3.

2) *Materials*

This Chapter is divided in two main sections: the first, 2.1, where facilitated transport materials along with the nano-filler used will be described. In 2.2 instead will be discussed the solution-diffusion matrix made of Pebax[®]2533, its modification and the GO-based materials used as fillers.

A number of solvents and reagents have been used during the work, and where not directly specified in the thesis, they were purchased from Sigma Aldrich and used without any further purification or processing. The Deionized (DI) water used had conductivity of 12,7 $\mu\text{S}/\text{cm}$.

While the gas used for permeation tests (CO_2 , CH_4 , O_2 , N_2 , He) were chromatographic grade with 99.995 to 99,9999% purity.

2.1 Facilitated Transport Materials

In this section the main materials employed in the production and testing of facilitated transport membranes will be described. Both the FTM carriers, Polyvinylamine and Arginine, will be presented and considered together with the nano-filler employed in the membrane production, that is carboxy methylated nanocellulose.

The gas permeation of these materials included mostly single gas test carried out with CO_2 , N_2 and CH_4 , at 35°C and 1 bar upstream, at high controlled humidity, 75 and 100 RH%.

Some high humidity tests have been conducted at 50°C as well, to investigate the change in permselective performances and the mechanical stability of the materials at higher temperatures.

Within the NANOMEMC² Project, such filler has been widely employed especially by PhD Davide Venturi, obtaining interesting results in mechanical stability and permeation performances, mixing it with PVAm and Arginine, separately [61,62,77]. In this work, therefore, a three-component approach has been investigated, by using all these three materials at once.

The matrix blend cNFC and PVAm proved be a material very resistant also at high humidity and 35°C, while the arginine improved the permselective performances of cNFC, thus, the aim of this work was to exploit both the blend resistance and fixed carrier performances of PVAm plus cNFC, and also the increase of performances provided by the mobile carrier Arginine.

For the matrix blend, three different weight ratios of PVAm/cNFC have been attempted: 20/80, 35/65 and 50/50, where the 50/50 resulted to be the most homogeneous and stable; it was therefore chosen for subsequent analysis. Two different amounts of arginine have been added and tested: 25 wt% and 45 wt%. The considered membrane therefore has an overall composition of 37.5/37.5/25 and 27.5/27.5/45 respectively.

The properties and features of these materials will be discussed in the following paragraphs, while the blending protocols are discussed in Section 3.1.2.

Lastly, to mechanically reinforce even further the membranes, especially for high temperature applications, a homogeneous and controlled crosslinking of PVAm with glutaraldehyde was investigated, obtaining some interesting preliminary results. Such crosslinking protocol is described in Section 3.1.6.

2.1.1 PolyVinylAmine (PVAm)

PVAm (Figure 12) was the material chosen as FTM matrix in this work due to its extremely high primary amine content, that can trigger the facilitated transport previously explained.

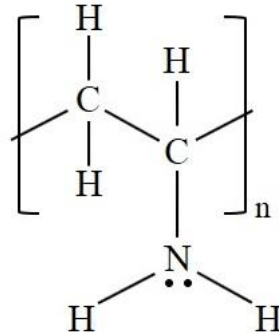


Figure 12: Chemical structure of (neutral) PVAm

It consists in a liner weak cation polyelectrolyte: amines groups' protonation is possible in acid conditions (Equation 21), and the charge density is function of the pH as estimated by Annenkov et. Al. [102] and shown in Figure 13.

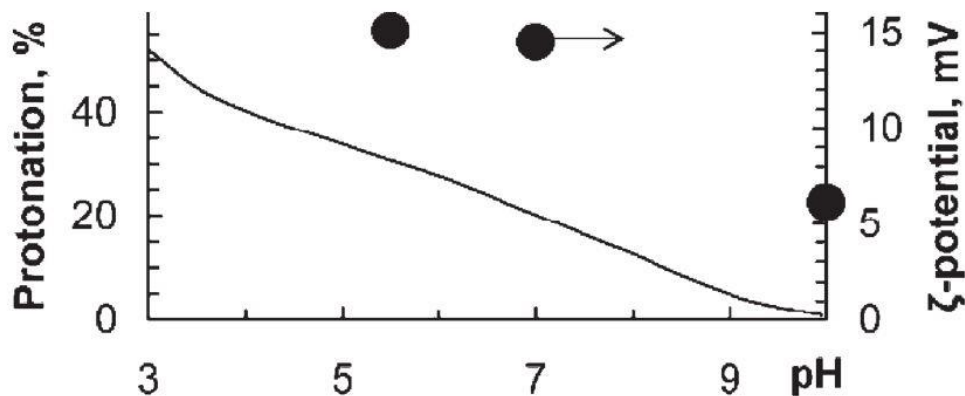


Figure 13: PVAm protonation trend function of pH [102].

Consequently, along with the protonation, also the morphological conformation of the polymer chains themselves change as well (Figure 14):

- At very basic pH levels there are basically no protonated amine groups, resulting in a low ionic force along the chain, with the structure that tend to the random coil shape, helped by the possibility of making hydrogen bonds intra- and inter-chain.
- At very acid pH levels, the structure is saturated by protonated amine groups, thus with a high cationic force along the whole chain, that now repel itself by electrostatic repulsion, favoring a linear conformation.
- At intermediate pH values some amine groups are protonated, while others not, and the charge density (and conformation) is function of the protonation degree: with the rising of -NH₃⁺ groups the cationic force will increase as well as the linear conformation tendency, vice

versa cationic force will decrease with the increment of neutral $-NH_2$ favoring to a random coil conformation [103].

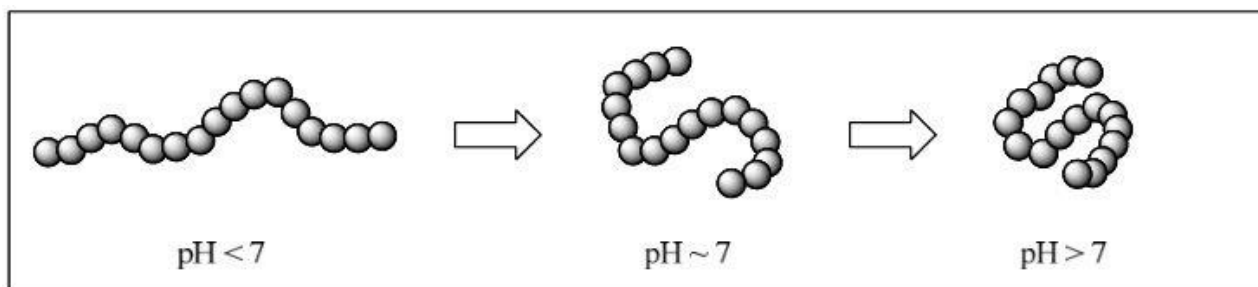


Figure 14: PVAm conformation based on pH [103]

Polyvinylamine is soluble in highly polar solvents, thus, for the storage it is usually kept in water, due to its cheapness and safety.

About reactivity, neutral PVAm is a primary amine with two electrons on nitrogen available to react with many electrophile groups, and to chelate metals behaving as Lewis base.

As a consequence, the possibility of chemical functionalization and modification are a lot, some of them are displayed in Figure 15 from the comprehensive study of Pinschmidt [104]:

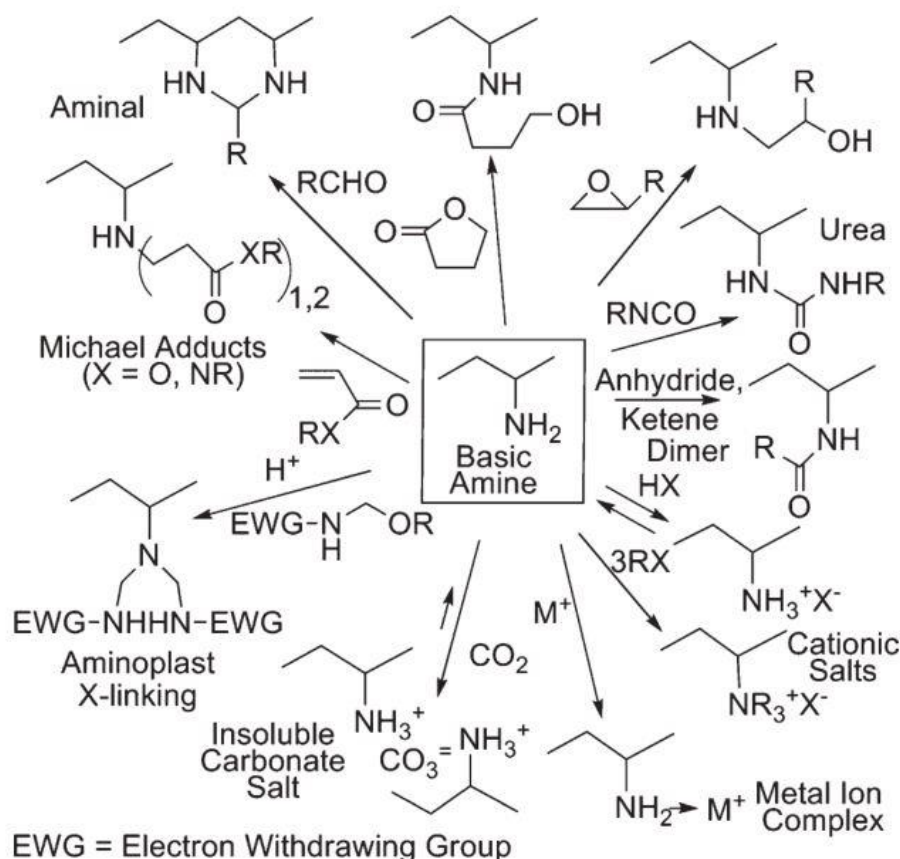


Figure 15: Examples of PVAm reactions

Polyvinylamine cannot be synthesized directly by the monomer vinylamine, since it undergoes to tautomerization, forming the imine end hindering the polymerization process, as shown in Figure 16:

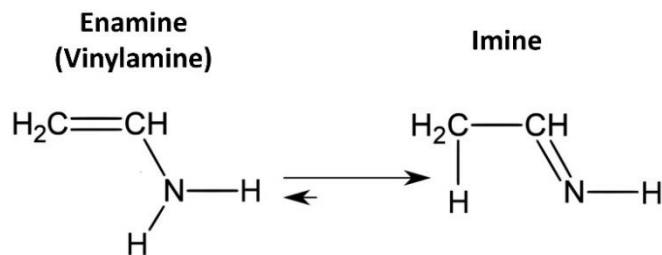


Figure 16: Vinylamine tautomerization

It is therefore necessary to employ different strategies, starting with another polymer that can successively being converted to PVAm. The most common process exploits the synthesis of N-Vinylformamide (NVF), through condensation of acetaldehyde and formamide, followed by catalytic isomerization of the so formed ethylformamide.

Once obtained, NVF is used as monomer to perform a radical polymerization using azo compounds in oils or water as initiators, generating the Poly-N-vinylformamide (PNVF).

Such polymer undergoes to hydrolysis, obtaining as final product: the Polyvinylamine.

The hydrolysis step can be carried out in acid or basic conditions:

- Basic hydrolysis has higher conversion yield, close to 100%; but, as a drawback, it generates the byproduct sodium formate, a salt, that need an additional purification step (e.g. dialysis, ultrafiltration...) to be removed.
- Acid hydrolysis has lower maximum conversion, around 80%, and generate methylformate as byproduct, removable by distillation.

The above described synthesis and polymerization processes are schematized in Figure 17 and 18 below:

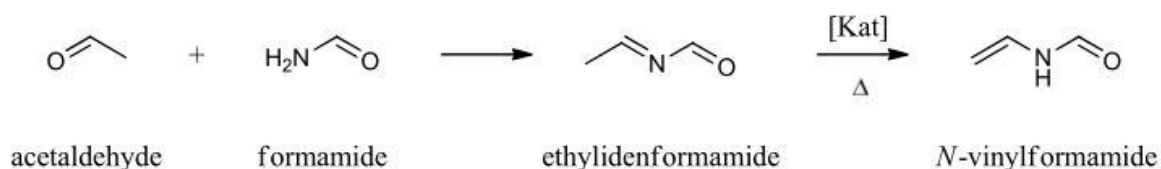


Figure 17: monomer NVF synthesis scheme [103]

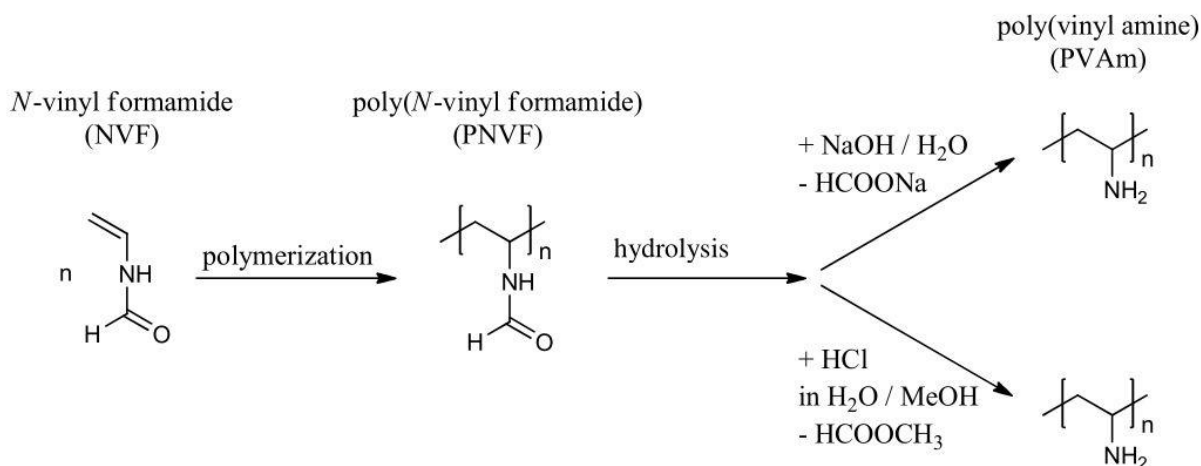


Figure 18: PVAm synthesis scheme [103]

PVAm is today a commercial polymer, employed in different fields. For instance it is used to increase paper's strength [105,106] or in liquid separation field, e.g. heavy metals removal from water, including mercury(II), or nanofiltration [107–112]. In the last years it has attracted even more interest in facilitated transport membranes for gas (CO₂) separation.

The first most notorious work, resulted in a paper, was carried by Hagg et al. in 2005 [113], then such polymer started to be employed from different groups. As an example, the already mentioned Professor Ho and his group obtained extremely interesting results by using PVAm and other amine-based materials [67,75,114,115], but there are many different groups that started to realize the potential of this polymer due to both permselective properties and material versatility for blending, modification etc. [65,67,76,116–121].

Moreover, PVAm is soluble and workable in water, which lead to interesting scale-up possibility thanks to its low cost and safety management, for these reasons PVAm has been picked as the main facilitated transport matrix in NANOMEMC² Project.

For our group, the source of PVAm was the commercial product Lupamin[®]9095, produced and commercialized by BASF s.r.l., that kindly provided us enough material to carry out all our experiments.

Lupamin[®]9095 consists in an aqueous solution of a copolymer made of polyvinylamine and polyvinylformamide at high molecular weight (≈ 340000 Da), with a hydrolysis degree higher than 90%, which represent the relatively amount of amine groups in respect of formamide ones.

Solid content is about 20-22 wt%, which includes both copolymer and salt, and the remaining 78-80 wt% is all water [122,123].

Its very high hydrolysis degree indicates that the reaction protocol involved the basic hydrolysis as final step, as previously explained, leading to the formation of the byproduct sodium formate, a salt which is still present into raw Lupamin[®]9095 product.

In this way, a purification protocol has been carried out to remove such component, which will be discussed in Section 3.1.1 [63], because the relatively high amount of salt would influence too much the final membranes, making them more brittle and prone to excessive water swelling.

Lastly, for brevity sake, even if the copolymer contains a small amount of formamide groups, about 5 wt%, in this work it will be always called just Polyvinylamine or PVAm.

A photo and physical characteristic of the product Lupamin[®]9095 are displayed in Figure 19.

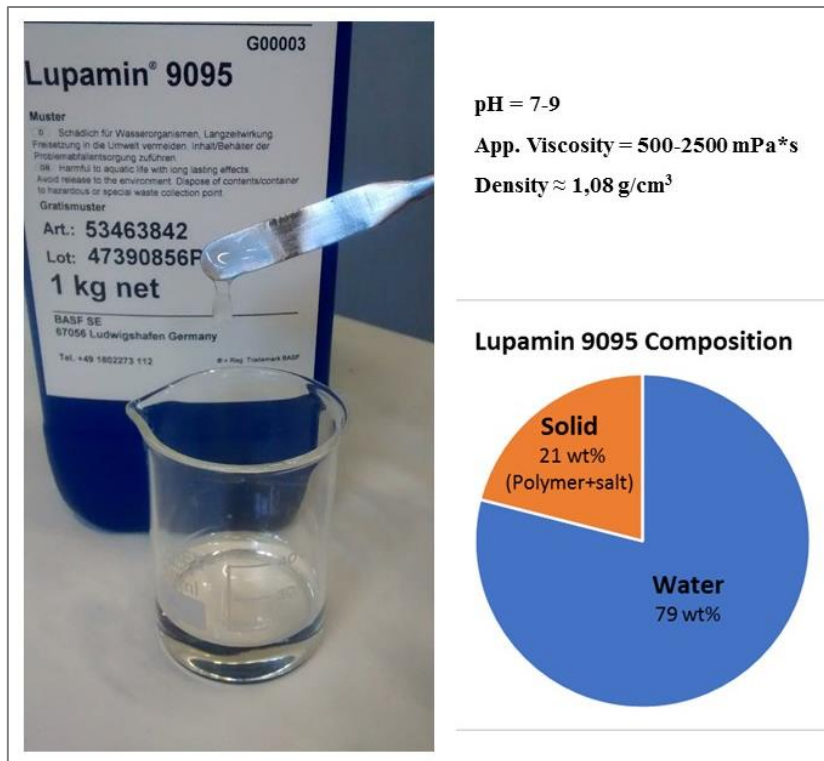


Figure 19: Lupamin®9095

2.1.2 NanoFibrillated Cellulose (NFC) and Carboxymethylated Nanocellulose (cNFC)

Cellulose is a natural linear polymer, the most abundant and surely one of the most important polysaccharides present in nature. It is formed by 300-3000 molecules of glucose bonded together by $\beta(1-4)$ glycosidic bonds and represents one of the basic structural units of plants, including algae and tunicates as well as certain bacteria. It is renewable, biodegradable, and nontoxic, and is the most prominent nanostructured component occurring in wood, cotton, hemp, flax, and other plant-based materials. Cellulose's structure is displayed in Figure 20.

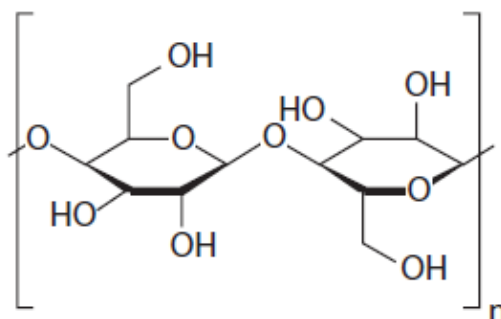


Figure 20: Cellulose chemical structure

Cellulose is organized in microfibrils kept together by hydrogen bonds, and such microfibrils are in turn organized in fibrils and fibers, which represent the macro-structure for the plant's cell.

When cellulose-containing materials are treated in proper ways, fibrils and nanofibrils can be extracted in nano-scale dimension structures, which represent the Nanocellulose.

A scheme of the structures from the plant to the cellulose molecules is displayed in Figure 21.

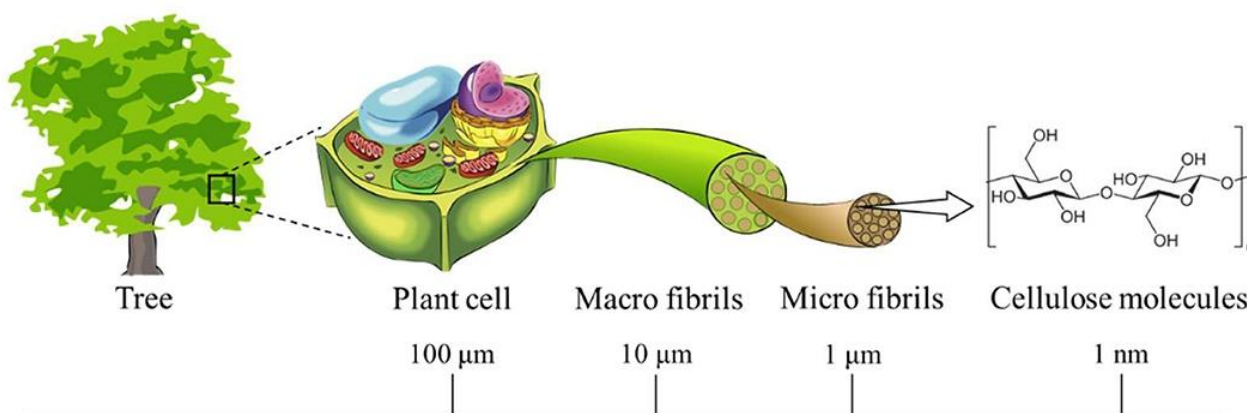


Figure 21: From plants to cellulose scheme [124]

Such material possesses very high physical properties, along with interesting chemical modification and grafting potential, and thus it is highly studied as renewable nano-material, with different reviews available in literature, e.g. the one from Thomas Bejoy et.al [125] or Thomas Paul et.al [126]. Usually, the most common studied application is nano-reinforcement in polymers to make nanocellulose-based nanocomposite materials [84–86]; even if nanocellulose is becoming more and more interesting for a number of application in the field of packaging [127–130], cosmetics [131,132], medicine [133–138] and of course separation as adsorbent or as part of selective membranes [62,139–141].

There are three main classes of nanocellulose, classified according to their morphology and source:

- Cellulose Nanocrystals (CNCs), organized in micro- and nanocrystals, obtained from lignocellulosic matter through acid hydrolysis, the shortest nanocellulose material with 100-250 nm length and 5-60 nm diameter.
- Nanofibrillated Cellulose (NFC), extracted through mechanical and chemical treatments, it has also many amorphous regions and the fibers are longer than CNC's, with several micrometers length and 5-60 nm diameter;
- Bacterial Nanocellulose (BNC), obtained by bacterial synthesis, mainly *Komagataeibacter xylinus*, fed with low mass weight alcohols and sugars, the largest among these three, with several micrometers length and 20-100 nm diameter.

In this work the focus is on the NFC (more specifically on Carboxymethylated NFC) since it has been the nanocellulose-based material employed in NANOMEMC² Project.

Nanofibrillated Cellulose (also called as cellulose nanofibers, nanofibrillar cellulose, cellulose nanofibrils...) is basically a bundle of linear packed cellulose nanofibers and consist of significant amorphous regions, with soft, long chains having (usually) diameters ranging from ten to a few hundred nanometers and lengths in the micrometer scale [125,126].

NFC is usually from lignocellulosic sources is usually extracted by wood pulps, and the most common separation method are of mechanical nature, since multiple mechanical shearing actions can

effectively delaminate individual microfibrils from lignocellulosic fibers. The most common processes include several types of chemical or enzymatic pretreatments of the cellulose pulp which are able to disrupt some of the interfibrillar bonds thus facilitating the fibrillation process. The last step is then usually a high-pressure homogenization, that has been the first approach made and still one of the most common, even if others have been investigated as well, such as high-pressure grinding, ultrasonication, steam explosion. Lastly, to overcome the main hurdle of clogging issues associated with homogenizers, the use of extruders and high consistency milling is recommended for the delamination of fibers.

As previously cited, cellulose represent a very suitable substrate to perform different types of reaction, mostly thanks to the high density of hydroxyl groups on the fibers surface. Few examples are displayed in Figure 22 e 23: from Thomas Bejoy et. Al [125]:

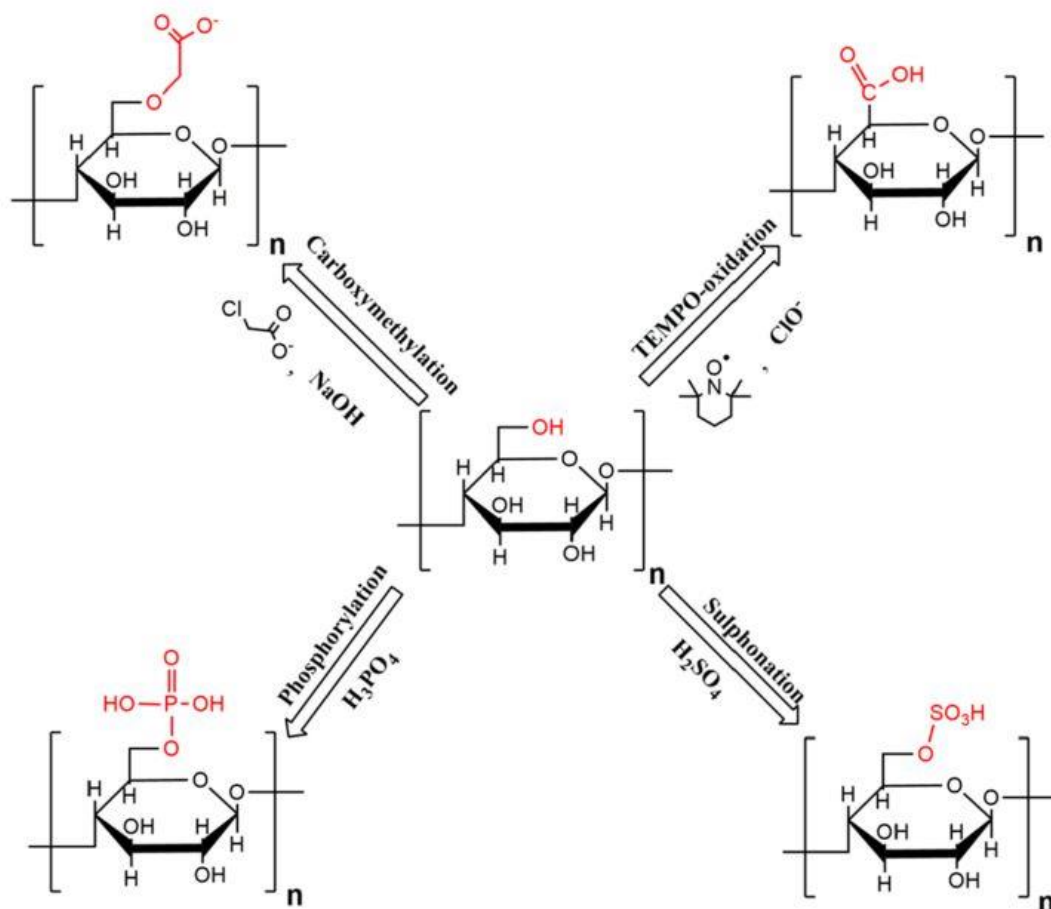


Figure 22: Cellulose's surface modification aimed to enhance hydrophilic character [125]

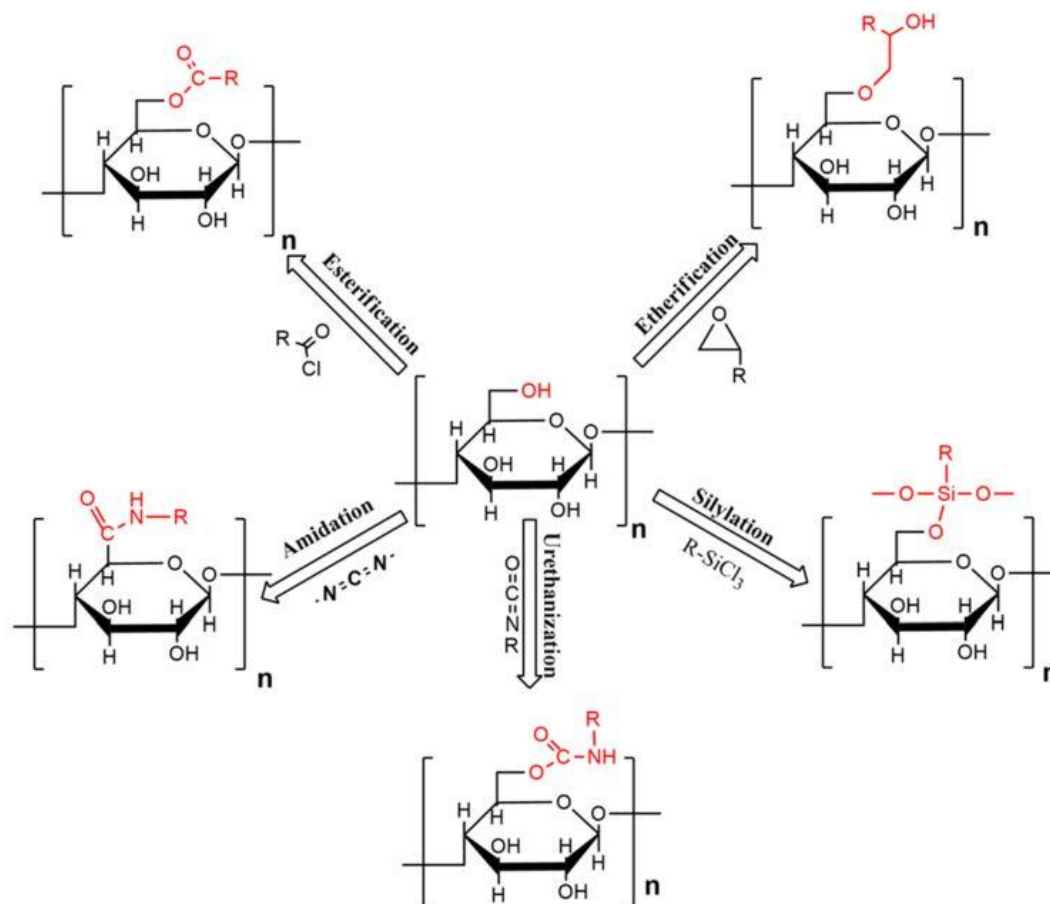


Figure 23: Cellulose's surface modification aimed to provide hydrophobic character [125]

As shown, with the proper electrophile group it is possible to substitute the hydrogen of the hydroxyl group with a wide number of functional groups, providing different chemical behavior to the final product.

One of the most common modifications is called "Carboxymethylation", which is able to increase the polarity of the cellulose structure by substituting the hydroxyl's hydrogens with an acetic acid group, providing also highly charged surface (which can lead to ionic interactions with other molecules), and a lot of acid groups at the surface (for post-modification purpose) in comparison to neat NFC [142]. A generic structure of carboxymethylated cellulose is displayed in Figure 24.

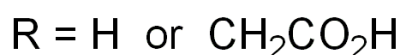
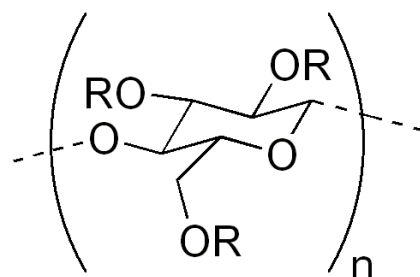


Figure 24: General structure of Carboxymethylated Cellulose

These chemical properties of carboxymethyl nanofibrillar cellulose (here will be always called “cNFC”) were the reason of why it has been chosen as nano-filler for this project: its polar acid groups are most likely compatible with both amine and amino acid groups of PVAm (the FTM matrix) and Arginine (FTM mobile carrier), leading to an overall stable and homogeneous structure, providing a mechanical stabilization of the whole composite and thus aiming to prevent swelling and mechanical instability that may occur in hydrophilic FTM materials previously discussed.

Carboxymethylated nanocellulose (cNFC) was kindly provided by INOFIB (Saint-Martin-d’H è res Cedex, France) as a water suspension with a solid content of 2.9 wt.% and a surface charge of 3600 $\mu\text{equiv/mol}$.

cNFC is usually synthesized by the alkali-catalyzed reaction of cellulose with chloroacetic acid and the protocol used for the modification was based on the one developed by Wågberg et al. [143]. A total of 180 g of eucalyptus fiber was pretreated. The eucalyptus fibers were first dispersed in water and then solvent-changed to 4 L of ethanol. The fibers were then impregnated with a solution of 175.1 g of monochloroacetic acid in 820 mL of isopropanol corresponding to 10 M OH equivalent with respect to cellulose. A solution of 26.5 g of NaOH in 3.3 L of isopropanol was then added to fibers that were heated to just below boiling temperature in a 10-L reactor fitted with a condenser. This carboxymethylation reaction was allowed to continue for 6 h. Following this carboxymethylation step, the fibers were filtered and washed: first with 20 L of deionized water, then with 3 L of acetic acid (0.1 M), and finally with 15 L of deionized water. The fibers were then impregnated with a 3-L NaHCO₃ solution (4 wt.% solution) for 60 min in order to convert the carboxyl groups to their sodium form. Finally, the fibers were washed with 15 L of deionized water and drained on a Buchner funnel.

In order to obtain Nanofibrils of Carboxymethylated cellulose (cNFC), carboxymethylated fibers were mechanically treated using a Masuko Grinder ® device with a speed of 1500 rpm and a gap of 10 μm between the two grinding stones. A gel at 2.9 wt.% cNFC was obtained after 10 passes. An example of such material is displayed in Figure 25.



Figure 25: Water suspension of Carboxymethyl Nanocellulose

2.1.3 Arginine

Arginine was chosen as mobile carrier in the project, to work along with PVAm in CO₂ facilitated transport. It is a polar chiral amino acid, and its L-enantiomer represent one of the essential amino acids in humans. Its structure is reported in Figure 26.

It exploits a basic behavior due to the high amount of amine content, especially the guanidine group HNC(NH₂)₂.

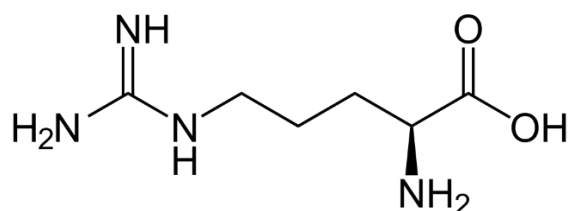


Figure 26: L-Arginine structure

Due to their amine content, arginine (and other amino acids) are attracting attentions as mobile carrier in gas separation [73,74,144] due to their selective interaction with CO₂.

Moreover, arginine is particularly cheap, which could lead to easier scale up, and it has a fairly high mass weight and boiling point: 174 Da, and it start to decompose before evaporating, at about 230°C. Such physical characteristic help to prevent its leakage (and evaporation) into the downstream side, which is one of the main concerns when using mobile carriers.

Furthermore, until reaching its decomposition temperature, Arginine remains substantially stable, as shown in Figure 27 by Weiss et. al [145]:

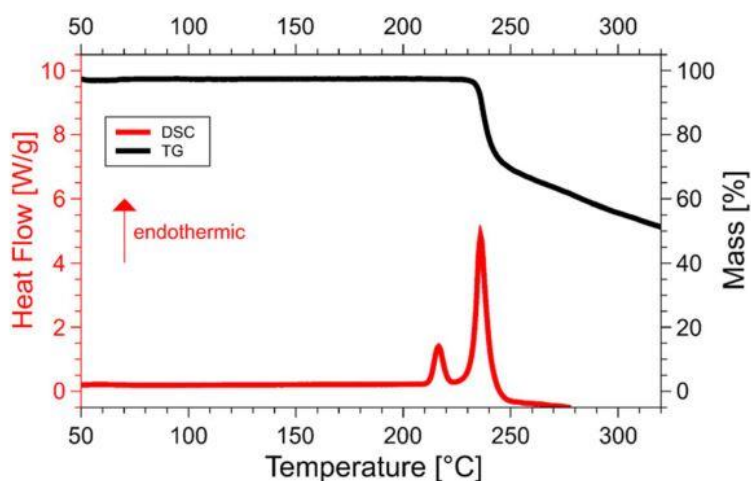


Figure 27: TGA and DSC of Arginine [145]

L-Arginine was purchased from Sharlab Italia s.r.l.

A sample of the material is displayed in Figure 28.



Figure 28: L-Arginine powder

2.2 Solution-Diffusion Materials

In this section the main materials employed in the preparation of membranes based on solution-diffusion transport mechanism will be introduced and described. Most of these membranes are mixed matrix membrane based on Pebax[®]2533, a commercial polymer produced by Arkema, and different types of Graphene Oxide nanofillers. A modification of such polymer developed during the work will also be briefly introduced.

Mixed matrix membranes were developed for post combustion carbon capture applications; thus, permeation tests have been carried out on CO₂ and N₂, at 35°C and 1 bar upstream to make a possible comparison with literature data. The materials used were some of the core-components studied for post combustion membranes, by Professor Ho Bum Park and his group in Energy Engineering Department, Hanyang University where I spent part of the time of my PhD. Professor Park was also involved in NANOMEMC2 project as external South Korean partner.

The present idea was to start a work of matrix-filler compatibilization with the aim of increasing the selectivity of the overall material, whose matrix already has a decently high permeability, making a set of data with different loadings to understand which could have been the best compromise of GO loading.

Following this idea, in the present work, a set of Pebax[®]2533 - GO mixed matrix membranes have been prepared and tested to study their potential application for CO₂ separation in post combustion carbon capture. Different loadings, from 0,02 to 1 wt%, of unmodified GO, used as benchmark filler, were initially considered to optimize the MMM composition. Afterward also Porous Graphene Oxide (PGO), which has similar structure of GO but less polar and with higher surface/volume ratio [146,147] and Graphene Oxide functionalized with Polyetheramine (PEAGO), which should improve both polymer affinity, for a more efficient compatibilization, and CO₂ affinity for better separation performances [148], were used at the best loading obtained with GO, 0,02 wt%.

Finally, the chemical modification of Pebax[®]2533 was also considered through the addition of a benzoyl group in order to improve their compatibility with GO and possibly increase its transport properties. Meshkat et al. [149] indeed has recently described the use of the aromatic benzoic acid into a similar dense polymer, Pebax[®]1657, with interesting permselective improvements, rising CO₂

permeability and both CO₂/N₂ and CO₂/CH₄ selectivity. Thus, even if not in mobile carboxylic acid form but grafted into polymer's backbone, the addition of the aromatic benzoyl group seemed promising in term of permselective improvements.

Since the product material is basically new, to have an initial reasonably wide characterization in term of gas separation, five gas have been tested: CO₂, N₂, CH₄, O₂, and He, all of them at 35°C and 1 bar upstream, which are commonly used as references for many of the previously cited applications and literature comparisons.

The properties and features of the materials will be discussed in the following paragraphs, while the blending protocols are discussed in Section 3.1.4.

Lastly, the chemical modification (grafting) of Pebax[®]2533 will be discussed in Section 3.1.5.

2.2.1 Pebax[®]2533 (P2533)

Among the different polymers, Pebax[®] materials have been often chosen as matrix for gas separation membranes, for their good balance between mechanical resistance, processability and separation performances [150–154].

Pebax is the trade name of a series of Thermo Plastic Elastomers, block co-polymers composed by polyamide and polyether blocks, produced by Arkema company with various types of each moiety and in different ratio [155]. The structure and the most common features of Pebax block copolymer are reported in Figure 29.

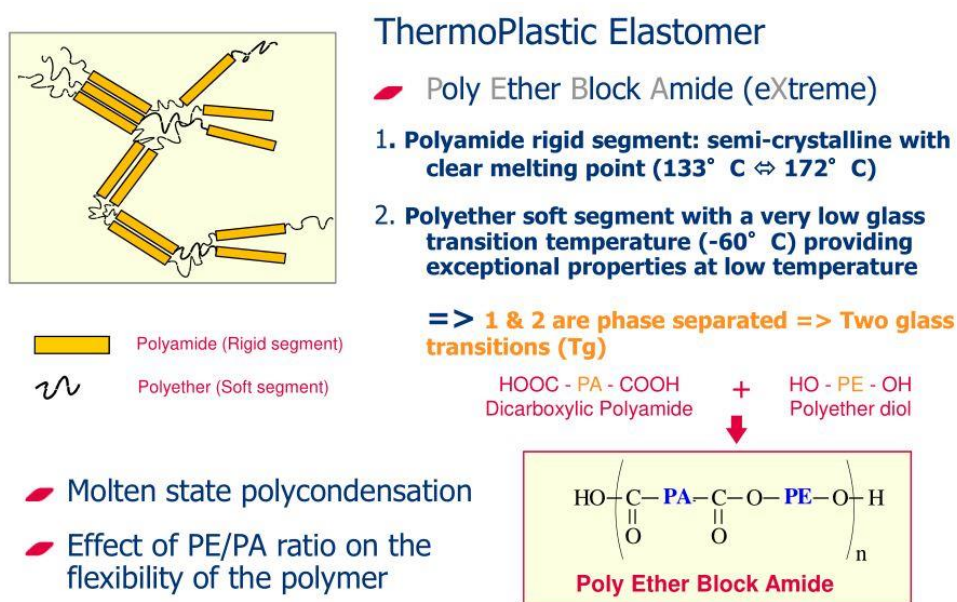


Figure 29: Pebax materials generic structure [155]

They are widely used as membrane matrix in carbon capture, because some of them possess both good CO₂ permeability and CO₂/N₂ selectivity, properties that can be tuned with chemical modification or by the use of fillers, as also reported in the very complete summary from Ho et al. [31].

The type chosen for this work was Pebax[®]2533, a block co-polymer made of polyamide 12 (Nylon 12 or PA12) and a block of polytetramethyleneoxide (PTMO), with a reported mass proportion of

around 20 wt% the former and around 80 wt% the latter [152,156,157], giving a theoretical molar ratio of about PTMO:Nylon12 = 91,6:8,4.

Konyukhova et al. also reported the molecular weights of the two blocks: 530 g/mol for Nylon12 and 2000 g/mol for PTMO [158]. Pebax[®]2533 structure is displayed in Figure 30.

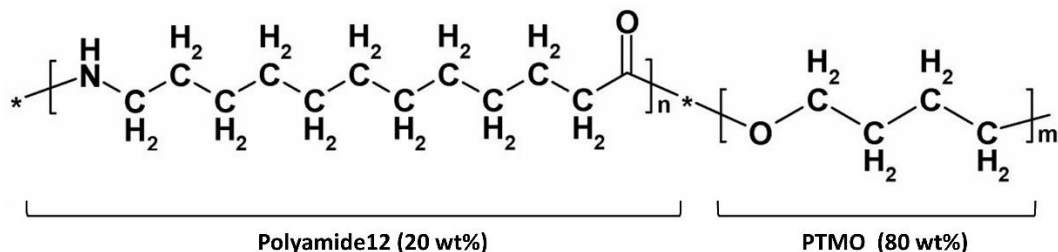


Figure 30: Pebax[®]2533 chemical structure

Pebax[®]2533 is usually employed as absorbent for organic vapors, like perfumes for internal environments or cars, insecticides, and any other application that require a slow desorption of certain gases or vapors.

These uses are due to its high absorption capability, uniform release overtime and easy material processing.

While the type of Pebax more commonly investigated in carbon capture membrane applications is Pebax[®]1657, made of Nylon-6 and PEO with a respective ratio of 40/60 in mass, other materials of the family also possess interesting performances such as the chosen Pebax[®]2533. This type, indeed, exhibits higher CO₂ permeability compared to Pebax[®]1657 (about 130-351 Barrer against 45-80 Barrer) although with lower CO₂/N₂ selectivity (about 25-34 against 43-80) in experiments conducted in mild conditions (pressure upstream of 1-2 bar and temperature from 20 to 35°C) [150,153,159–165].

Pebax[®]2533 was purchased in pellets by Arkema s.r.l. Some pellets are displayed in Figure 31.



Figure 31: Pellets of Pebax[®]2533

2.2.2 Graphene Oxide (GO)

In 2004, physics K.S. Novoselov and A.K. Gejm managed to exfoliate and characterize a single layer of graphite [166], which took the name of “Graphene”, winning the Nobel prize for physics 2010. Graphene is one of the carbon allotropes, a material made of only carbon atoms hybridized sp^2 , where every atom bond three others with an angle of 120° , it is fully planar and only one atom thick, reason why it is considered a two-dimension material.

Exfoliated graphene and its structure are displayed in Figure 32.

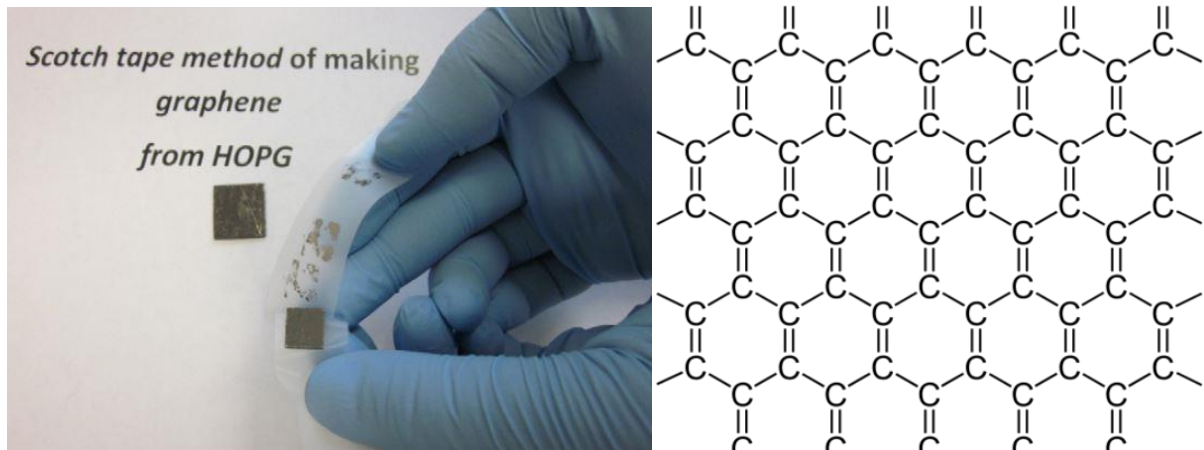


Figure 32: image of mechanically exfoliated graphene [167] (left) and its chemical structure (right)

After its first discovery, many studies have been conducted on graphene, revealing outstanding properties in terms of mechanical resistance and both electric and thermal conductivity [167–170]. The better properties are of course obtained for the pure single layer defect less graphene, but they remains of high interest even if in reality some morphological defects may occur on the sheet, al also pointed out by Park et al., reducing its chemical perfection [171].

Due to this peculiar features graphene has been deeply investigated in different field of science with many papers already published, as schematized in Figure 33 from Zhong et al. [172]:

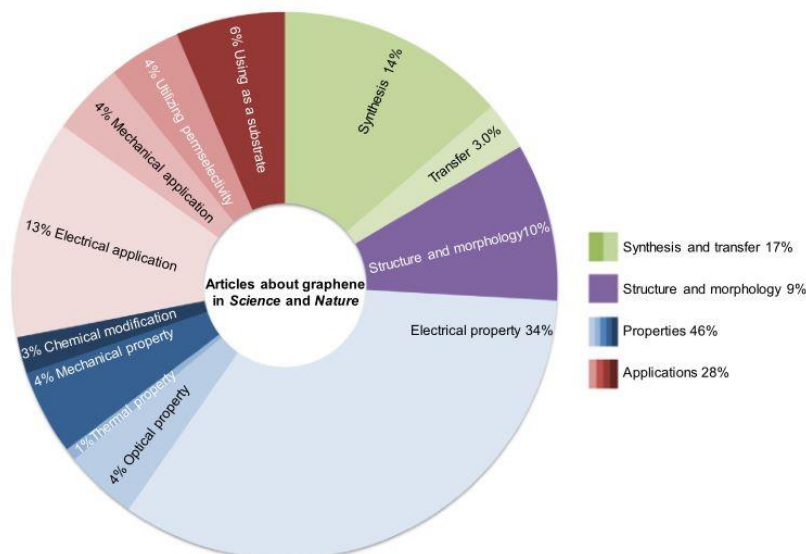


Figure 33: Articles about graphene in Science and Nature

There are different ways to produce graphene, everyone with pros, cons, and quality of product obtained. Figure 34 display the typical chart of quality against cost of the most common production techniques:

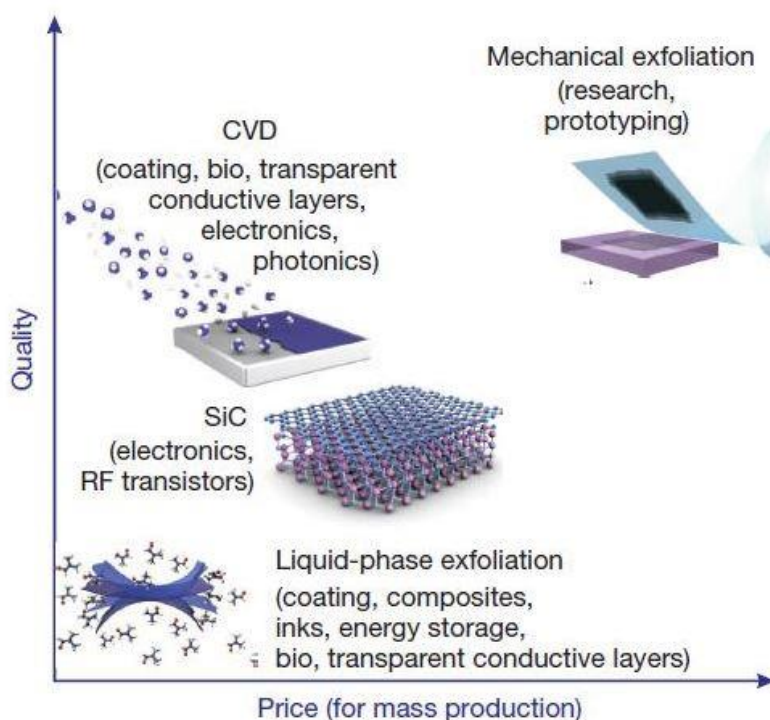


Figure 34: most common graphene synthesis techniques

As shown, the best quality is provided by mechanical exfoliation from graphite, but it is also the slowest and less industrially applicable technique. Another very used technique to form high quality single layer graphene is Chemical Vapor Deposition (CVD), although it is relatively expensive, and the graphene obtained is usually fixed to the surface where CVD was carried out.

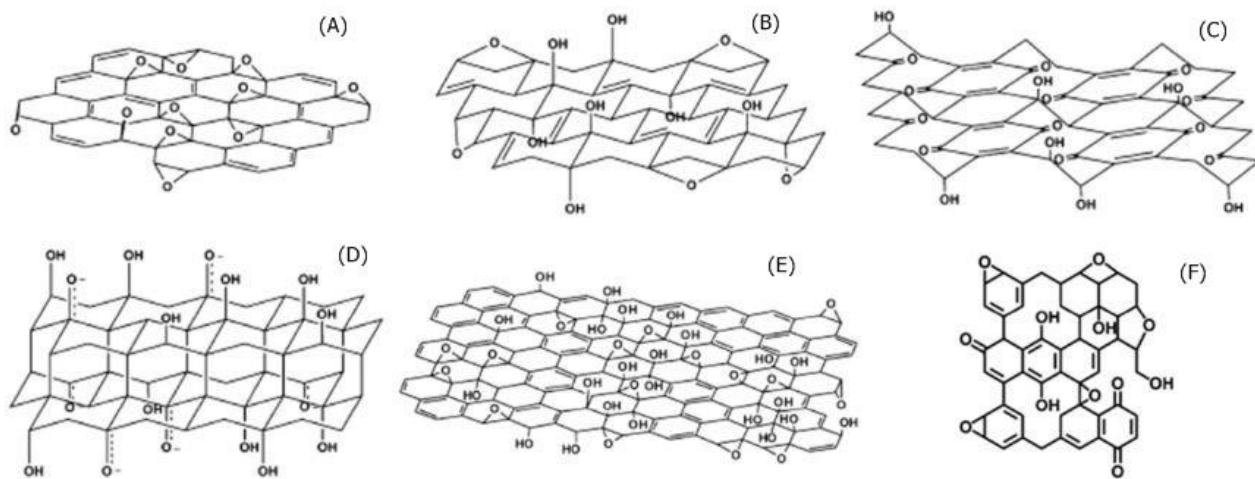
The most common employed technique, due to its ease scale-up and large production potential as well as the lower cost, is the liquid-phase exfoliation, that as drawback has the lowest product quality: by this technique only few or multilayer can be produced. However, it results rather flexible, as it can be tuned to obtain larger or smaller flakes, and it is also compatible with chemical treatments or modification on the graphene itself, which increment its versatility.

By the chemical point of view, graphene is a flat sheet of sp^2 carbon only structure, which is not particularly reactive as it is, but the presence of functional groups could make it an ever more versatile material.

Different modification approaches have been attempted indeed, to functionalize graphene's surfaces, the most common one being its oxidation to obtain the so called "Graphene Oxide" (GO).

The oxidation of graphene results to be the extremely handy due to the insertion of oxygen-based groups, like hydroxyls, ketones, epoxy and carboxylic acid, which give to the material a more polar behavior, and most important, some reactivity: once such groups are grafted, indeed, they can be exploited to carry on different reaction exploiting their high reactivity. For this reason GO is used not only by itself, but is usually the starting point material to carry out other different chemical modifications.

The perhaps most difficult challenge in graphene oxide, is the reproducibility, indeed its very structure is not well defined nor constant, and some models have been proposed as showed in the following Figure 35 from Dreyer et al. [173], among which the Lerf&Klinowski and Szabo&Dekany are the most accredited in literature:



Proposed GO models. (A) Hoffman, (B) Ruess, (C) Scholz-Boehm, (D) Nakajima-Matsuo, (E) Lerf-Klinowski, and (F) Dekany model.

Figure 35: Graphene Oxide structure models [173]

Defects and imperfections along the graphene plane compromise its outstanding physical properties previously mentioned, and this also applies to oxidation grafting: GO indeed has indeed lower properties with respect to pristine graphene with reduction which become more and more pronounced with the increase of the oxygen content and structural defects [174,175].

Despite this reduction GO remains a very interesting materials due to the already mentioned possibility of modification and also because, due to its polarity, it can be effectively stored in water dispersion, making it extremely safe compared to the powder-form, that is very common for graphene storage; in addition it has higher interaction with radiations from the UV-visible to the near infrared opening new field of application. While Graphene is more suitable for electronic and other physical-based purposed like nano-reinforcer etc., Graphene Oxide represents a more interesting tool for the material and chemical point of view.

The most famous protocol to obtain GO from graphene is the Hummer method, and in this work GO was obtained with an improved version of it, developed by prof. Han in Hanyang University [176], as will be discussed in Section 3.1.3. A sample of this material is displayed in Figure 36.



Figure 36: Graphene Oxide synthesized in Hanyang University

Among many possible fillers usually considered, GO-based nano materials have recently attracted much interest and have been widely employed in carbon capture for their capability of enhancing membranes' gas permselective properties and chemical tunability, with many examples already available in literature [146,177–182], and also described in reviews such like the one about 0D and 2D fillers MMM from Janakiram et al. [183], or the one specific for graphene and graphene oxide materials from Yoo et al. [184] or even the wider and more general one provided by Sun et al. [185]. In this work, three Graphene Oxide-based materials have been tested as filler into Pebax[®]2533: Graphene Oxide neat (GO), Porous Graphene Oxide (PGO) and Graphene functionalized with polyetheramine (PEAGO), are displayed in Figure 37:

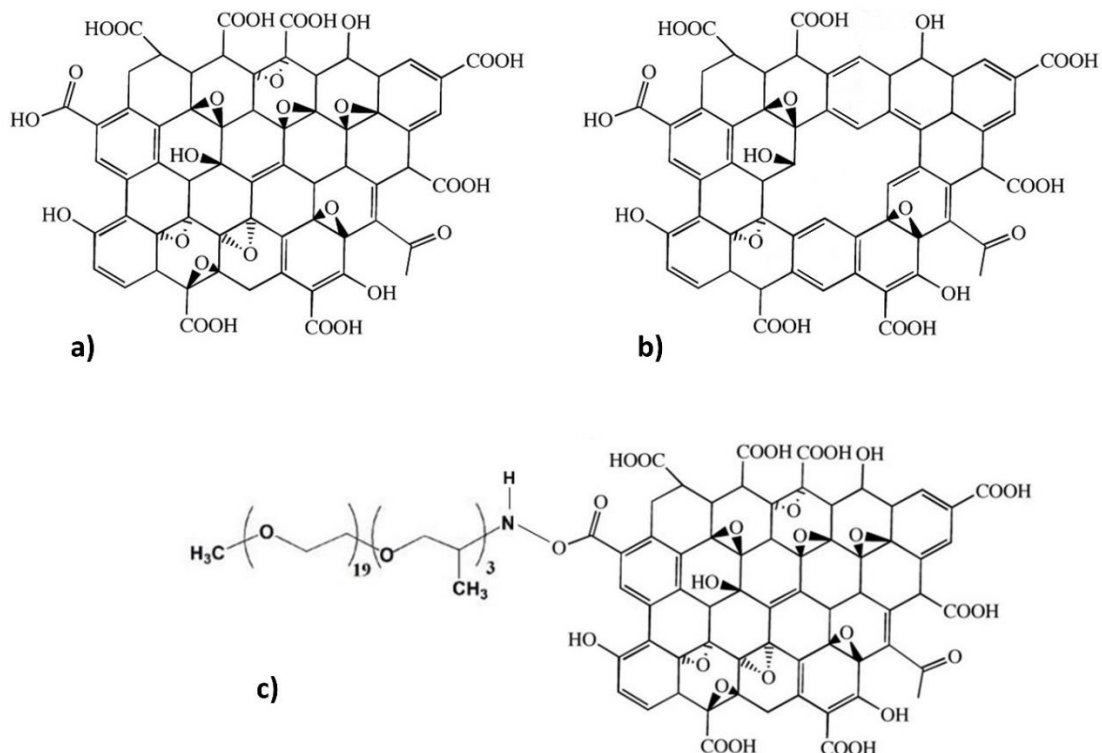


Figure 37: Chemical structure of GO (a), PGO (b), and PEAGO (c).

PEAGO is a modified version of graphene oxide, grafted with a polyetheramine (Jeffamine M-1000), designed by Myung Jin Yoo, in order to make it more soluble in different solvent, and thus in different matrix.

PGO is a type of GO treated to fracture it even further and form holes/defects along the surface itself. The synthesis of both modified GO-based fillers will be discussed in methods Section 3.1.3.

Graphite (used to prepare GO and the other GO-based materials) by Bay Carbon Inc. (Bay City, MI, USA).

2.2.3 Benzoyl-P2533 (BP2533)

During the PhD, Pebax[®]2533 was also chemically modified obtaining a new product, developed for the first time in this work, named Benzoyl-P2533 (BP2533). The modification consisted in the grafting of a benzoyl group upon the nitrogen of the Nylon moiety, with the structure displayed in Figure 38. As said above the main aim was to improve the membrane performance adding a group that proved to be able to increase CO₂ permeability even if in an acidic form [136]. The addition of the benzoyl group directly on the Nylon chain, indeed, even if less polar than the aromatic carboxylic acid reported by Meshkat et al. [136], should be able to cancel the crystallinity of the Nylon12 phase thus improving its transport properties. By substituting the hydrogen of the secondary amine with a high hindering group, indeed the ordering of Nylon chain should be hindered reducing the tendency to form crystals and increasing the polymer chains mobility.

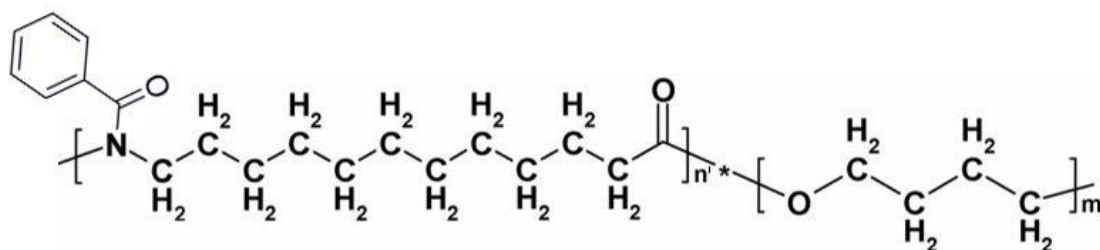


Figure 38: Benzoyl-P2533 chemical structure

Six different protocols were developed to carry out the reaction of Pebax[®]2533 with benzoyl chloride, conducted in pyridine at different conditions, that will be deeply discussed in Section 3.1.5.

Such new product has been fully characterized, by both material and permselectivity points of view, and the results will occupy the entire Chapter 6 of this thesis.

Benzoyl chloride and pyridine were purchased from VWR International.

3) Methods

3.1 Processes and Reactions

3.1.1 Lupamin[®]9095 Purification

As already mentioned in Section 2.1.1, the source of PVAm for this work was the commercial product named Lupamin[®]9095, a polymeric solution that contain also some salts, mostly reaction's byproduct sodium formate and NaCl, which could create problem during membrane production. For this reason, a purification strategy was implemented in order to obtain a PVAm with reduced salt content.

Two different level of purification were developed, [63] obtaining two grades of PVAm, as schematize in Figure 39:

- *PVAm-LG*

Polyvinyl Amine “Low Purification Grade”, obtained by precipitation of Lupamin[®]9095 in ethanol 96 %, with a volume ratio Ethanol/L9095 of 4:1, followed by 60°C drying over-night. This material already presents a low amount of salt, thus resulted to be suitable enough for making homogeneous membranes and resulted to be the most often employed.

- *PVAm-HG*

Polyvinyl Amine “High Purification Grade”, obtained by further purifying PVAm-LG through a solid-liquid Soxhlet extraction (for 48h with 96 % ethanol as solvent) followed by an ion exchange resin treatment with Amberlite IRA958Cl (for 2 h with Solid Content / Resin ratio of 1:15).

This material resulted to be the purest obtained, but the procedure was much more time consuming with respect to PVAm-LG, so that it was used mainly as a reference to understand the role of PVAm purity on the membrane performances.

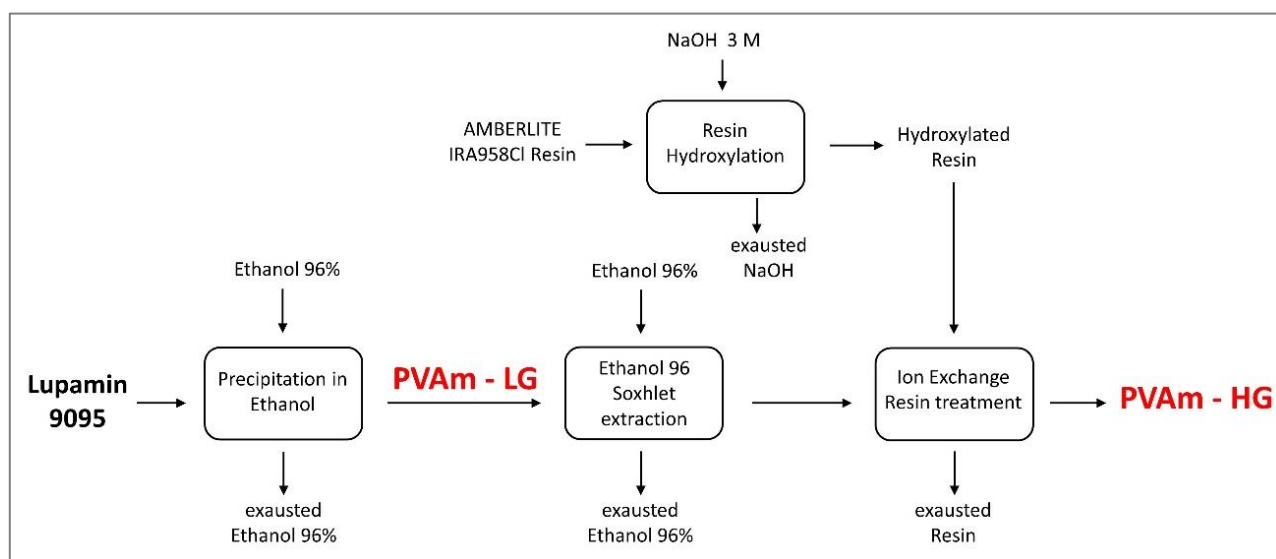


Figure 39: Lupamin[®]9095 purification protocol scheme

3.1.2 Blending: PVAm + cNFC nanocomposites

The efficient and homogeneous dispersion into the polymer matrix is the main concern when making composite membranes.

Often, nanofillers tend to aggregate with each other, forming agglomerates, leading to an overall heterogeneous material which does not have the same properties of the correspondent homogeneous one, and is not reproducible. Thus, the development of an efficient dispersion/compounding method is a crucial procedure in mixed matrix membranes field.

For the dispersion of cNFC into Polyvinylamine, the following protocol (shortly schematized in Figure 40) has been developed, which led to homogeneous well dispersed nano-composited membranes.

The first step was the dilution of 2.90 wt% cNFC water dispersion in order to have, at the end of the blending process, an overall final concentration of solids of 2.00 wt%: the correct amount of water, were added to the cNFC dispersion, then it was magnetic stirred at 500 rpm upon 40°C plate for 1 hour (covered with parafilm).

In samples that required Arginine as well, the correct amount of this amino acid was previously dissolved into the dilution water.

Then, the system was brought at 40°C and a 5000 rpm homogenization was carried out, using the homogenizer Ika Ultra Turrax T18 Digital; after about two minutes, keeping 5000 rpm, the correct amount of PVAm-LG 2,50 wt% was slowly added drop by drop. When all the PVAm solution was added, homogenizer speed was increased to 12000 rpm for 2 minutes. High speed homogenization, was needed as previous analysis showed that PVAm strongly interacts with cNFC causing upon addition the instantaneous formation of aggregates in the form of white flocs.

After the homogenization, 3 minutes of bath sonication (Sonication Bath model FC 10, 220 V, 50/60 Hz, 0,4 Kw, from ENCO s.r.l.) were conducted, in order to remove bubbles and absorbed gas and to stabilize the blend, which was then ready to be used for membranes preparation.

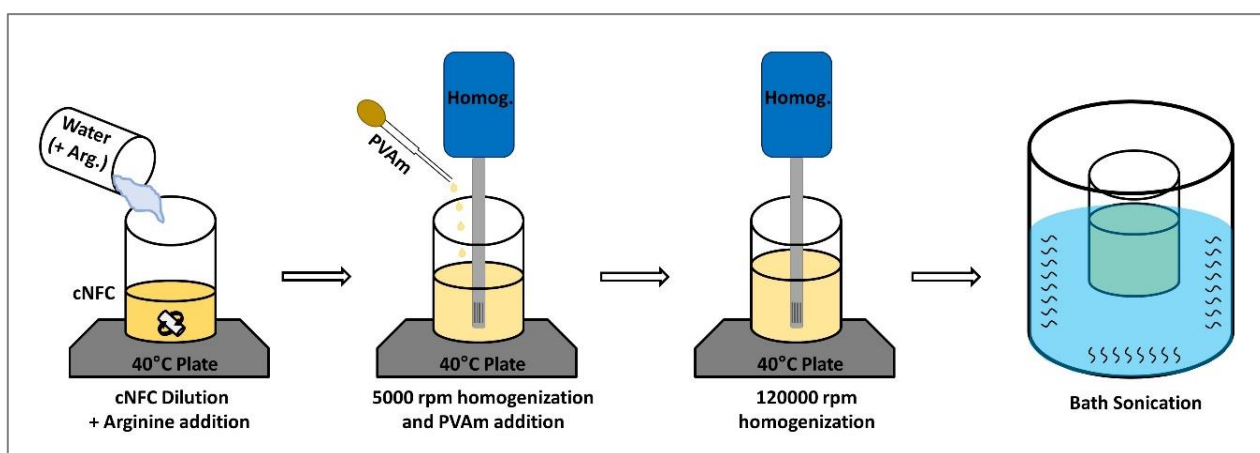


Figure 40: PVAm/NFC/Arg blending protocol scheme

In total, 5 different blends have been performed and investigated: three made of two components, PVAm/cNFC at different mass ratio (50/50, 35/65, 20/80), and two made of three components, obtained by adding 25 wt% and 45 wt% arginine to the 50/50 PVAm/cNFC blend.

The overall blend compositions are summarized in Table 4.

Previous compounding test proved that, to have a mechanically optimized PVAm/cNFC blend, the mass fraction of PVAm had to be maximum half of the total, while it was possible to achieve mechanically resistant and stable blends when exceeding with the cNFC.

Table 4: PVAm/cNFC/Arginine blend ratios

| Blend Type | PVAm (wt%) | cNFC (wt%) | Arg (wt%) |
|--------------|------------|------------|-----------|
| 2 components | 50 | 50 | 0 |
| 2 components | 35 | 65 | 0 |
| 2 components | 20 | 80 | 0 |
| 3 components | 37,5 | 37,5 | 25 |
| 3 components | 27,5 | 27,5 | 45 |

3.1.3 Graphene Oxide Materials Synthesis

Graphene Oxide (GO)

Graphene Oxide has been the main nano-filler for Pebax[®]2533 addition and served as base for preparing the other two nanofillers whose preparation will be described in this section.

GO was prepared through Hammer Method optimized by Prof. Han in Hanyang University [176]: first, 10 g of 99.99 % pure graphite powder was stirred in 380 ml of H₂SO₄ 95 % at 5°C for 10 minutes, then 50 g of 99.3 % pure KMnO₄ were added and the mixture kept in 150 rpm stirring for 12 h at 35°C.

The temperature was then decreased to 5°C and 2500 ml of DI water were added, and lastly 30 ml of H₂O₂ were added as well, still maintaining the mixture in stirring and below 10°C until the solution color changed from dark brown to yellow.

At this point the oxidation reaction was completed, and the product was separated by vacuum filtering the solution, and then washed with a total of 5 L of aqueous HCl (10 wt%) . Finally, the GO was dried at room temperature and without UV exposition for two days before the final wash with 5 L of acetone.

Porous Graphene Oxide (PGO)

Porous Graphene Oxide was prepared starting from a 2 mg/ml GO dispersion in water which was sonicated for 30 minutes to ensure high homogeneity. The dispersion was heated up to 50°C and then NH₄OH and H₂O₂ were then added with a ratio of GO:NH₄OH:H₂O₂ = 20:1:1. The solution was stirred at constant temperature (50°C) for 5 hours, and then cooled to room temperature and centrifuged for 1 hour at 10000 rpm to recover the precipitated PGO. This one was then re-dispersed in DI water and dialyzed for 3-4 days to eliminate any residual reagents or impurities. During the dialysis the pH was continuously monitored, and the process was considered completed when the solution reached neutrality (pH = 7).

Graphene Oxide functionalized with Polyetheramine (PEAGO)

PEAGO was prepared using the method designed Myung Jin Yoo et.al [148]: GO water dispersion has been mixed with Jeffamine M-1000 (PEA) with a mass ratio m_{GO}:m_{PEA}=1:0.75 and stirred for 24 h at room temperature, the pH was then adjusted to 4,5 using HCl 1M and EDC and NHS were added

to the mixture, both with a weight ratio of 1:1 vs GO. The solution was sonicated for 30 minutes and then stirred for 24 hours to complete the modification. PEAGO so obtained was finally washed with 5 L of HCl and then with 5 L of acetone in order to remove any impurities.

3.1.4 Blending: Pebax[®]2533 + GO Nanocomposites

Pebax[®]2533 and graphene oxide are not well compatible materials, and just mixing the latter into the former lead to an extremely heterogeneous structure.

To fix this problem and obtaining homogeneous membranes, a cross-solubility approach has been designed. The two materials were soluble/dispersible in different solvents, as showed in Table 5, but two of the possible solvents, water and ethanol, are actually miscible in each other, thus, the following process has been developed.

Table 5: Pebax[®]2533 and GO compatible solvents

| Material VS Solvent | Water | Ethanol | Buthanol |
|-------------------------|-------------|-----------------|------------------|
| Pebax [®] 2533 | Insoluble | Soluble | Soluble |
| Graphene Oxide | Dispersible | Non-dispersible | Non- dispersible |

Pebax[®]2533 pellets were solubilized in ethanol with a concentration of 2 wt% by stirring at about 700 rpm upon a 150°C hot plate for 5 hours, and then letting it reach room temperature on 500 rpm stirring.

Water was instead used to prepare the stable dispersion of graphene oxide, with a concentration of 0.5 mg/ml, prepared by mixing the dry GO with the desired amount of water and then bath sonicating the solution for 2 hours maintaining the temperature below 35°C. The same procedure was used also for the other two types of graphene considered, PGO and PEAGO.

Once the aqueous dispersion of GO was ready, it was added to the Pebax[®]2533/ethanol polymeric solution on 50°C plate during 1000 rpm stirring for 10 minutes, then poured in a teflon petri dish to make the membrane.

The process is schematized in Figure 41.

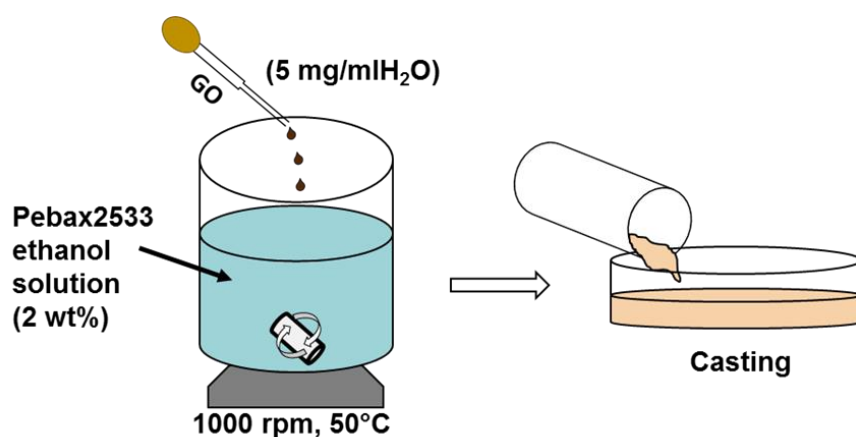


Figure 41: Pebax[®]2533-GO blending protocol scheme

The solution was then left to evaporate at room temperature in order to obtain self-standing membranes. Four different loadings were considered for GO addition: 0.02, 0.1, 0.5 and 1 wt%, in order to study the influence of this parameter on the overall polymer permeability.

Due to the results of permeation test obtained on Pebax[®]2533-GO membranes and the difficulty of dispersion of the other two materials, for PGO and PEAGO only the 0.02 wt% loading was carried out.

3.1.5 Pebax[®]2533 Modification: Benzoyl-P2533

To modify Pebax[®]2533, a grafting upon secondary amine of then Nylon12 moiety was designed, making an acylation with Benzoyl Chloride.

The aim of the modification was to increase the compatibility of the matrix with π -bonded materials like Graphene and Graphene Oxide, and at the same time removing the crystallinity of the Nylon12 moiety, theoretically increasing the overall material's permeability.

To carry on such reaction, pyridine has been used as solvent, that exploited three roles: effectively solubilize the polymer resulting in a stable polymeric solution also at room temperature, providing a catalytic effect for the electrophilic substitution reaction, and neutralizing the byproduct hydrochloric acid.

The overall reaction and catalyst effect schemes are displayed in Figure 42:

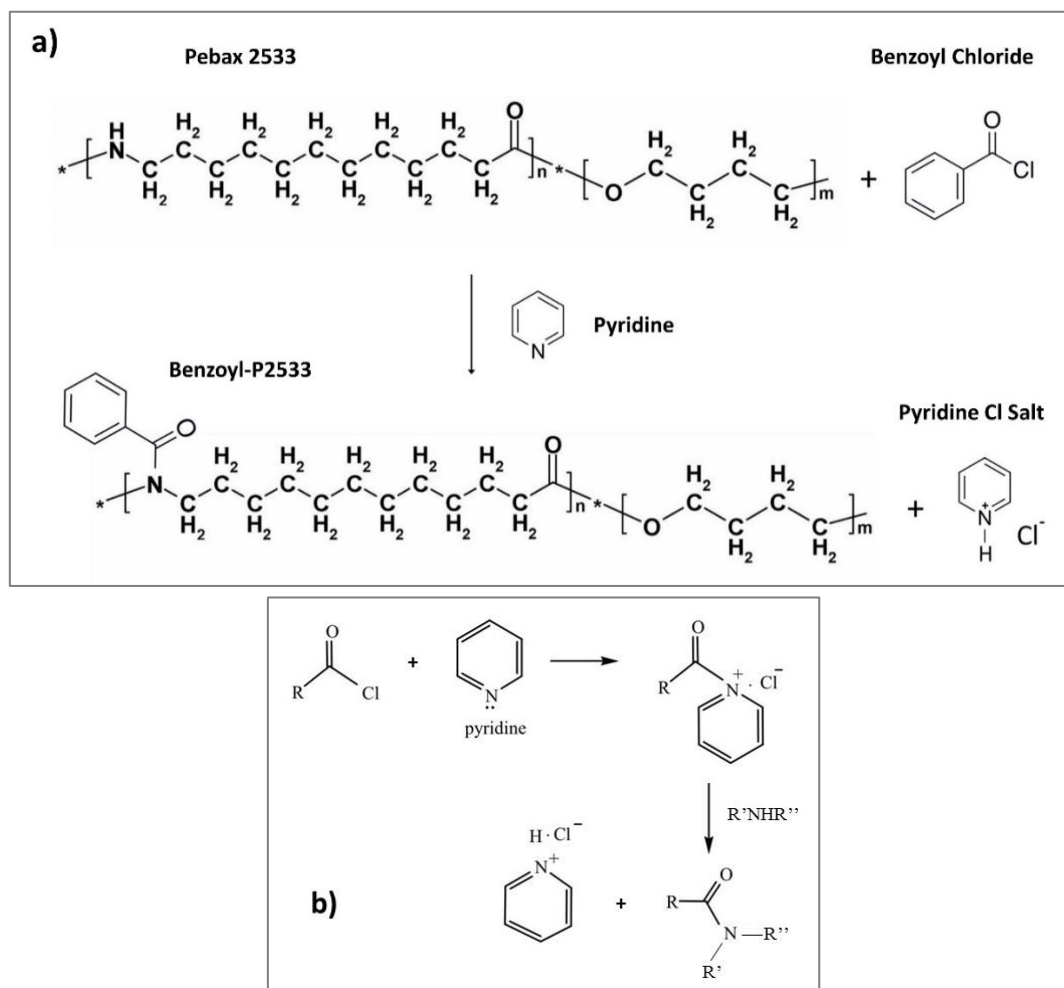


Figure 42: a) Benzoyl-P2533 reaction, b) pyridine catalyst effect

Six different protocols with different intensities have been conducted in order to study the reaction yield, by varying three parameters:

- Molar ratio between the secondary amine moiety of Pebax[®]2533 and Benzoyl Chloride
- Time of reaction
- Temperature

Initially, Pebax[®]2533 was dissolved in pyridine at 2 wt% by stirring overnight on a plate heated at 80°C: once solubilized, the polymeric solution so obtained was stable and limpid also at room temperature for undefined time.

Then, the correct amount of Benzoyl Chloride was added to the Pebax[®]2533 solution, under stirring at 600-800 rpm and at fixed temperature. The mixture has been kept under stirring for a determined time to complete the reaction.

The product obtained was then separated by dropping the polymeric solution to cold deionized water (kept in ice bath, $\approx 0^{\circ}\text{C}$), the amount of water was equal to 50 vol% of pyridine used for the reaction. Such addition caused the precipitation of the product, that was then recovered and washed by stirring in excess of deionized water (mProduct:mH₂O = 1:400) at 40°C 2 hours, four times.

After that, the following purification steps were carried out in order to remove any residual solvent or unreacted reagent:

- the product was recovered and totally dried in vacuum oven at 50 °C overnight, then temperature was increased to 100°C dynamic high vacuum was pulled for 3 hours.
- the dry solid obtained was solubilized in chloroform at 30 mg/ml and slowly dropped in cold methanol (kept in ice bath, $\approx 0^{\circ}\text{C}$), with volume ratio of CHCl₃:CH₃OH = 1:3, obtaining a turbid polymeric solution, which was dropped into cold water (kept in ice bath, $\approx 0^{\circ}\text{C}$), with a volume ratio of CHCl₃:CH₃OH:H₂O = 1:3:8, to obtain a precipitate.
- The solution was removed, and the precipitate was then dried out overnight at 50°C under high vacuum, obtaining the final product.

To clearly summarize the protocols, crossed parameters chosen are shown in Table 6:

Table 6: Benzoyl-P2533 reaction protocols

| Reaction Protocol | Molar Ratio -NH- : BenzCl | Temperature (°C) | Time (hours) |
|-------------------|---------------------------|------------------|--------------|
| #1 | 1 : 2 | 20 | 2 |
| #2 | 1 : 5 | 20 | 2 |
| #3 | 1 : 10 | 20 | 2 |
| #4 | 1 : 5 | 20 | 24 |
| #5 | 1 : 5 | 60 | 2 |
| #6 | 1 : 10 | 60 | 4 |

Among the different protocols, it is possible to notice that #1 #2 and #3 were focusing on understanding the role of reactants molar ratio, which was the only parameter modified while keeping mild condition in terms of temperature and reaction time (2 hours at 20°C).

The #4 and #5 were more aggressive protocols since a fairly high excess of reagent was chosen (1:5) and a much longer reaction time for #4 (24 hours) or higher temperature reaction for #5 (60°C).

Lastly, the most aggressive protocol #6 has been employed: conducting the reaction with a ratio of 1:10, at 60°C, for 4 hours to aim at the total substitution of the polymer.

The product obtained by this reaction was named “Benzoyl-P2533” (BP2533).

3.1.6 Controlled Crosslinking of PVAm with Glutaraldehyde

One of the problems of Polyvinylamine and other highly hydrophilic polyelectrolytes is the swelling and partial solubilization when exposed to high humidity.

In gas separation membranes, this can ruin the physical integrity of the membrane itself or even make the polymer slowly percolate through the support beneath it, compromising the middle- and especially long-term performance of the membrane.

Since PVAm was the main hydrophilic polymeric matrix in NANOMEMC2 project, a method to make such material mechanically stronger and more stable, especially at high temperature, has been investigated, using a controlled chemical crosslinking approach, with the crosslinker Glutaraldehyde (GA). GA is, indeed, well known to be a suitable crosslinker for poly-alcohols and poly-amines [123,186,187] providing an extremely fast crosslinking reaction, which occurs even at room temperature. Since they're part of the polymer chain, the primary amines groups are sterically extremely close and fixed together in PVAm, whose reticulation led most likely to the product shown in Figure 43.

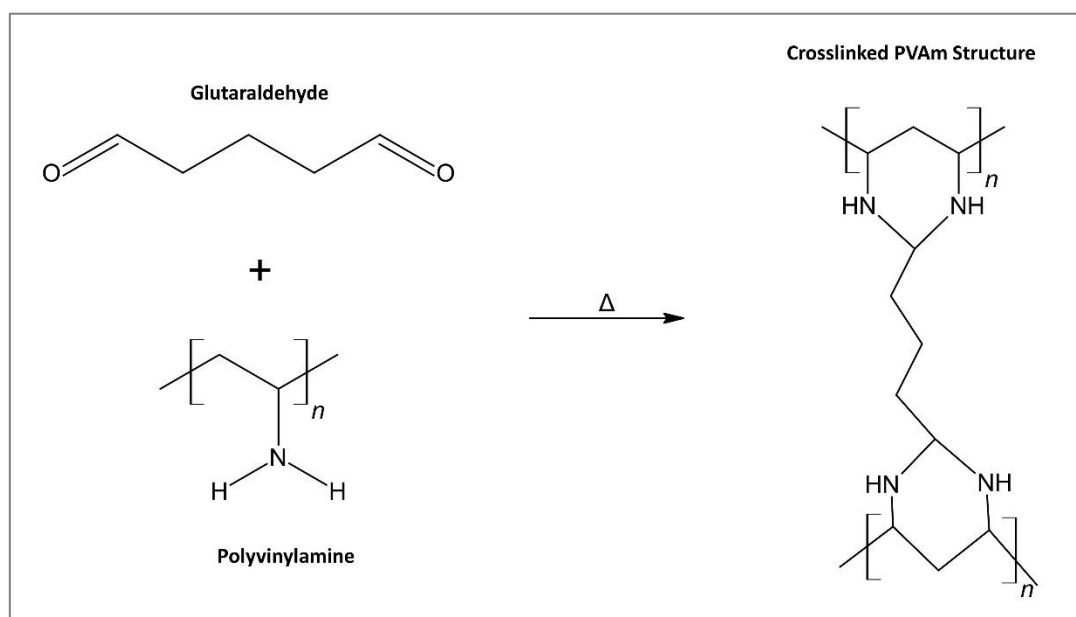


Figure 43: PVAm-GA crosslinking reaction scheme

The concept of this controlled structural reinforce was to make the crosslinking not on the membrane already prepared, but prior in polymeric solution, in order to obtain an overall semi-crosslinked polymer with higher mechanical stability, as well as being accurately tunable in function of the relative amount of crosslinker added.

Otherwise, if treating the membrane already made in a crosslinking bath, all the crosslinking would have occurred only on the surface and in higher concentration, causing the formation of a thin but impermeable layer on top of the membrane.

The protocol, showed in Figure 44, consisted in preparing the PVAm aqueous solution at 2 wt%, then stirring it in ice bath ($\approx 0^{\circ}\text{C}$) for 10 minutes, and then adding the right amount cold GA ($\approx 0^{\circ}\text{C}$ as well) and keep stirring at about 0°C for 10 minutes.

This step was crucial to effectively disperse the crosslinker all over the polymeric solution, so that when the reaction was triggered, it would have occurred homogenously, with no gradient of concentration nor agglomeration.

To start the crosslinking reaction, the bath temperature was raised to 35°C and keep stirred for 1 hour, at the end of which an increment of viscosity was already noticed, based on GA amount.

Lastly, to totally complete the crosslinking, the bath temperature was raised to 60°C , keep stirring for another 1 hour.

To be recovered, the final product was casted into a PTFE petri dish and dried out at 35°C for 48 h, then the solid crosslinked PVAm-GA was ready for different test or vacuum drying followed by solution preparation.

To investigate the effect of such crosslinking, GA was added with different molar ratios, compared to PVAm repeating unit: 1, 5, 10 and 20 mol%, and products obtained were named based on the molar percentage of GA added: PVAmGA1%, PVAmGA5%, PVAmGA10% and PVAmGA20%.

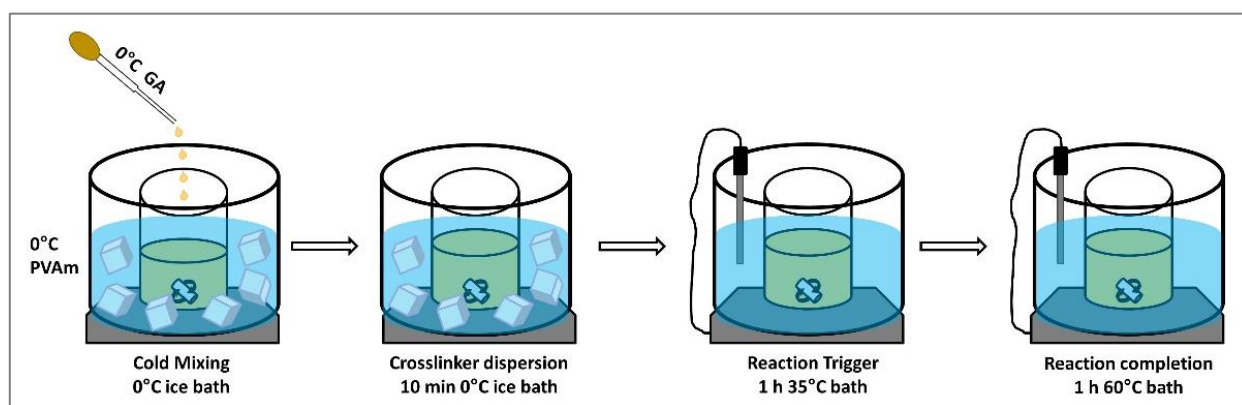


Figure 44: PVAm-GA crosslinking protocol scheme

3.2 Chemical and Physical Characterizations

3.2.1 Fourier Transform Infrared Spectroscopy (FTIR)

FTIR is a type of spectroscopy which uses infrared radiation, that can be absorbed by the compounds through their chemical bonds that are IR-active, and since many bonds satisfy this requirement, FTIR provides information about nearly every functional groups present into materials.

Coupling it with an Attenuated Total Reflection (ATR) setup grants the possibility to analyze directly solid material (e.g. membranes, in this case) which absorb IR radiation not directly (in transmission), but from the evanescence wave that spread to the sample through the crystal beneath it [188].

Overall, FTIR ATR is a fast, not destructive and versatile analysis, and thus is one of the most common for gather qualitative information about chemical structure of materials.

In this Doctorate, the setup employed for such analysis was made of a FTIR model Nicolet 380 (Thermo Scientific), provided with a single bounce ZnSe crystal ATR base (MIRacle™ Single Reflection, Pike Technologies).

All the analysis have been conducted on solid samples, using 32 scans and a resolution of 4 cm^{-1} , managed with Omnic software package.

Such technique has been used for several purposes: checking the chemical structure of the materials used, monitoring the Lupamin®9095 purification progress, qualitatively evaluate the Pebax®2533 modification yield, etc.

3.2.2 Thermogravimetric Analysis (TGA)

TGA is a technique used to determine a sample's weight loss in function of temperature: It basically consists in a micro-balance kept inside an oven with controlled atmosphere.

For post combustion membranes, operating temperature are relatively low, far below 100°C , usually around 60°C which is the typical flue gas temperature leaving the flue gas desulfurization (FGD) unit [189], but an information about the degradation temperature and weight loss of the material is always handy, moreover it permitted to estimate the thermal response in function of the modifications performed.

The apparatus used was a TGA Q600, from TA Instruments.

By the operation point of view, temperature rate was always kept to $10^{\circ}\text{C}/\text{min}$ from room temperature (about $20\text{-}25^{\circ}\text{C}$) to 600°C , with nitrogen atmosphere kept during all the experiment, in order to obtain thermal degradation results only, and not thermo-oxidative. The samples size was maintained between 5 and 25 mg.

3.2.3 Differential scanning calorimetry (DSC)

DSC is a technique which permit to investigate the exothermic and endothermic transitions of materials, such like fusion, crystallization, chain relaxation in polymers and so on.

The technique works by heating at the same time the sample and a standard that has no exothermic or endothermic transitions, keeping them at the same temperature: thus, whenever the sample undergoes to one of the cited thermal transitions, the system has to provide more or less heat to the

sample chamber, and such heat difference is proportional to the transition itself, and represent the actual signal.

In this work DSC served to evaluate the change of crystallinity resulted from the Pebax[®]2533 modification, as well as investigation of graphene oxide based materials inside Pebax[®]2533.

The program used was always made of four cycles, always with a heating rate of 10°C/min:

- 1) Cooling from room temperature to -80°C
- 2) Heating from -80°C to 250°C
- 3) Cooling from 250°C to -80°C
- 4) Heating from -80°C to 250°C

In this way, with the cycles 1 and 2 the thermal history of the material was cancelled, then it was possible to obtain information on the tested material by analyzing cycle 3 and 4.

The apparatus used was a DSC Q2000 from TA Instruments, and the samples size has always been between 5 and 25 mg.

3.2.4 Scanning Electron Microscopy (SEM)

SEM is a type of microscope that produces images using a focused electron beam as radiation source instead of light, allowing to obtain magnification values up to x20000-x30000 and images with resolution of 1 nm or less.

In this work it has been employed to see the dispersion of Graphene Oxide into Pebax[®]2533 membranes, and a magnification of x1000-x5000 proved to be the best range for this purpose.

The apparatus used was a Phenom ProX, with a voltage of 10 kV, and all the samples analyzed have been previously metal-coated in a Quorum sputter SC7620 using Au-Pd disc target, in order to set them totally conductible, a crucial requirement to perform SEM analysis, and resistant to the high vacuum of the instrument.

3.2.5 Nuclear Magnetic Resonance (NMR)

NMR is a type of spectroscopy that allows to observe magnetic field around atomic nuclei, by exciting them with radio waves while kept into a strong magnetic field, usually 100-900 MHz. Such excitation perturbs the alignment of the magnetic nuclear spin and the recovery of this state provide the magnetic resonance, which can be elaborated giving the NMR spectra.

The most common nuclei analyzed in NMR are ¹H and ¹³C, and are extremely useful to identify compounds in organic chemistry, because such resonance is function not only of the nuclei themselves, but also of the electrons around them, in this way it is possible to disguise basically every type of carbon and hydrogen structures in a molecule, allowing outstanding identification power of organic compounds. Moreover, it is an extremely accurate and precise technique, thus it is also one of the best analytical methods for quantitative determinations as well.

In this doctorate, indeed, H-NMR has been used to estimate the molar conversion (in term of substitution degree) of Pebax[®]2533 modification.

The instrument used was a Varian Mercury Plus VX 400 (¹H, 399.9 MHz; ¹³C, 100.6 MHz) spectrometer, chemical shifts are given in ppm from tetramethylsilane (TMS) as the internal reference, and all the analysis have been conducted at room temperature with a CDCl₃ concentration of 5-10 wt/v%.

3.2.6 X-ray Photoelectron Spectroscopy (XPS)

XPS is a spectroscopy technique that generate photoemission of material by irradiating it with X-rays, such electron kinetic energy is measurable and unique for every electron binding, which is unique for every bond.

In this way, XPS represent one of the most powerful qualitative elemental analysis for homogeneous materials or solid surfaces, and in this work, it has been employed to verify the presence of nitrogen into the filler PEAGO after the reaction of Graphene Oxide with Polyetheramine.

XPS spectra were measured using an Omicron ESCALAB (Omicron, Taunusstein, Germany) with a monochromatic Al Ka (1486.8 eV) 300 W X-ray source, and a flood gun to counter charging effects under ultra-high vacuum (UHV, $\approx 1 \times 10^{-9}$ Torr) conditions.

3.2.7 Water Absorption

Water absorption measurements have been carried out on the hydrophilic membranes used in this work, made of PVAm, since such parameter often results useful to understand the behavior of gas permeation in humid conditions [62,63]. To carry out the water absorption test, a customized setup has been employed, previously described and used by Giacinti et.al [190].

The setup is made of a quartz spring kept into an insulated and water jacked column at a controlled and fixed temperature, at the extremity of which is attached a small rectangular sample of known size (in the order of 10x5x0,05 mm), along with an aluminum reference, of known size as well, as shown in the CCD screenshot displayed in Figure 45.

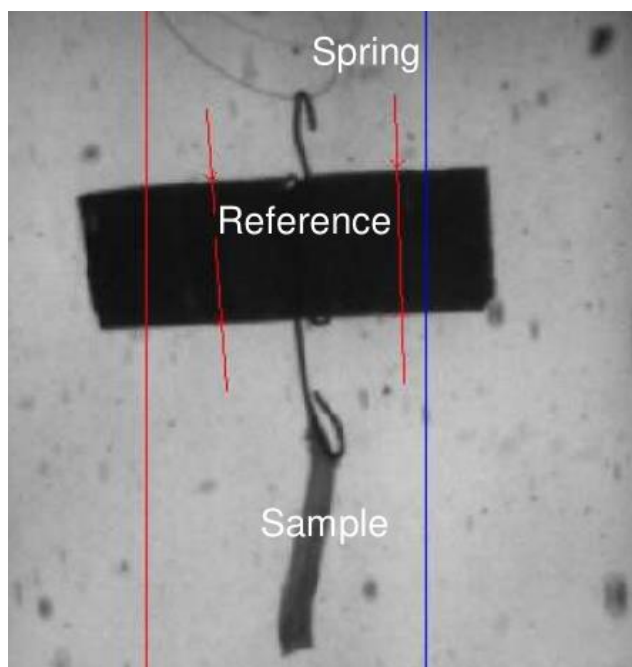


Figure 45: Screenshot of Water Absorption sample

In front of the column is placed a CCD camera that continuously record the sample and especially the aluminum calibrated reference attached to it, which provides higher contrast for the camera and allows, thanks to its known dimension, to evaluate the pixel/ μm conversion factor.

The column is linked to a water tank (S02) that provides water vapor to the system and to a vacuum pump as well, so, exploiting the Antoine Equation 23 and Equation 24, at the known temperature, it is possible to humidify the overall system with the desired solvent pressure, water vapor in this case, allowing to carry out test at different fixed humidity.

$$\ln P^0 = A - \frac{B}{T+C} \quad (23)$$

$$RH\% = \frac{P_{read} - P_{offset}}{P^0} \cdot 100 \quad (24)$$

Where P^0 is the saturated water vapor pressure (100 RH%) at a certain temperature T , while A , B and C are constant parameters specific for any substance.

The actual absorption (and desorption) results, represented by the mass absorbed (or desorbed), can be obtained by the elongation (or reduction) of the spring's length: when the sample absorb (or desorb) vapor, its weight change and the hook gets longer or shorter, such change of length is recorded by the camera and it is proportional to the mass variation though the following Equation 25:

$$[m_{water}]_i = (h_i - h_0) \cdot \frac{k}{g} \quad (25)$$

Where k is the spring elastic constant, h_i the spring length after the absorption (or desorption), h_0 is the initial spring length, g is the gravity acceleration.

The overall experimental setup is displayed in Figure 46.

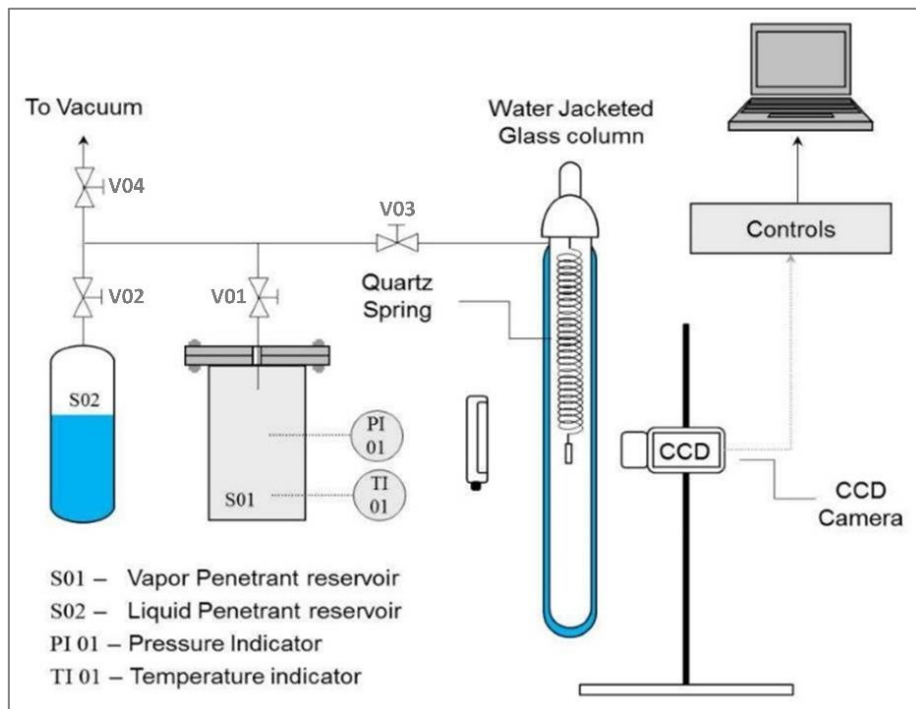


Figure 46: Quartz spring microbalance setup

By the operative point of view, the first step was the measurement of the weight of the sample, which was then hooked to the quartz spring.

Once inside the column at constant temperature, always 35°C, high dynamic vacuum was pulled until no weight loss was recorded, the sample was therefore totally dry and any gas or vapor previously present was eliminated, making the specimen ready for the absorption test.

The column was temporarily isolated by closing V03, and the 4 L reservoir S01, containing both temperature and pressure indicators were opened; at this point water tank S01 was carefully opened to let water vapor fill the system with the desired pressure, and then being closed back.

At this point it was possible to start the absorption test by starting the CCD data acquisition and connecting the column to the humid conditioned system (re-opening V03).

After the equilibrium state was reached, the sample stopped moving downward because unable to absorb more water at the defined RH% and temperature, and that absorption step was concluded.

Then, the column was isolated again, and the system charged with a higher humidity amount, in order to carry out another absorption step with higher RH%, following the same method just explained.

By summing all the mass contributions from each step, it was possible to find the total mass of water absorbed as well as the diffusivity of water in the material.

Usually, low humidity tests required long time and were less accurate due to the slower and smaller absorption, so it has never been conducted an absorption test with a RH% lower than 10 %.

For all the tests conducted, buoyancy effects were neglected in calculation due to the low pressure considered in experiments.

3.2.8 Crosslinked PVAm Weight loss in water: dipping test

To have an idea of the resistance to the swelling and solubility of the different crosslinked PVAm-GAs, a fast and a prolonged dipping tests in water have been conducted.

Both tests were carried in liquid water, since all these membranes were supposed to work at high humidity, even saturated vapor, and in such conditions some micro-drops depositing on the membrane may occur. Thus, the experiment was carried out in much more harsh conditions, so that if a membrane can resist to an extended dip into liquid water, most likely it can withstand against high RH% or few micro-drops.

A first fast and rough test of dipping, to check the eventual swelling of the membranes, consisted in picking with a tweeze a small piece of sample, with dimensions of about 10x5x0,05 mm, immerse it in DI water at room temperature for about 5-10 seconds, and then picked up to see how physically the sample's shape changed.

To investigate the weight loss, a more accurate protocol was developed: it consisted in cutting small layers of dry materials, with dimensions 10x5x0,05 mm (membrane-like shape), then, to weight the mass zero of all the samples, they were treated in 35°C dynamic vacuum oven for 3 hours in order to reach the minimum dry mass without compromising the materials structures, after that the samples were ready to be weighted.

Every sample was then putted into a PE pan containing 45 ml of DI water and let it deep inside the water for 60 h at 35°C.

After the dipping period, all the water was removed and the samples were dried first in ventilated oven at 35 °C for 24 h, then treated with dynamic vacuum at 35°C to reach again the minimum dry mass, and then they were weighted again to check the weight loss.

3.3 Membrane Preparation

In this chapter are described the methods employed to physically realize the membranes used during this doctorate.

Three were the technique chosen: *solvent casting*, *spin coating* and *Mayer rod coating*.

All these techniques have one thing in common: they require the solubilization of the polymer (and eventually the dispersion of the nano-filler). The dissolution requires proper solvent the right temperature as well as an adequate stirring (usually between 400 and 700 rpm). The temperature of the hot stirring plate and the solvent used for the different membranes are listed into Table 7 below.

Table 7: Solubilization parameters for the main materials employed

| Material | PVAm | cNFC | Arginine | Pebax [®] 2533 | GO | BP2533 |
|------------------------|-------|-------|----------|-------------------------------------|--------|------------|
| Suitable Solvents | Water | Water | Water | Ethanol, Butnanol, Chloroform | Water | Chloroform |
| Plate Temperature (°C) | 70 | 40 | Room T | 120 alcohols 40 Chloroform | Room T | 40 |

3.3.1 Solvent Casting

Solvent casting, schematized in Figure 47, has been by far the most employed technique in this doctorate since it allows to obtain homogeneous, even if relatively thick membranes, which is crucial to have good and clear permeation results. It has been used for every type of material, and during the discussions, whenever it is not specified, the results will refer to membranes prepared in this way.

It is the easiest technique to prepare membrane with known thickness, realistically applicable for relatively thick ones (usually 10 to 200 μm), therefore somewhat suitable to laboratory scale because for gas characterizations thick membranes provide more accurate and measurable results.

The procedure consists in solubilizing the polymer into a proper solvent, bath sonicate the solution few seconds to remove the excess of air trapped inside, then dropping the solution into a PTFE petri dish, and let it slowly dry out at low or controlled temperature (for the solvent used within the thesis room temperature under fume hood were appropriate).

After the solvent evaporation, the dry layer of polymer that remain on the bottom of the petri dish is the membrane obtained. The last step is to pull high vacuum at higher temperature overnight to remove any residue of solvent: in this work, high vacuum at 50°C resulted to be always suitable to that aim. Then the membrane is ready to be peeled and tested. Depending on the material, the detachment from the petri dish can be difficult and for this reason teflon is often used for solvent casting in petri dishes because it reduces the membrane adhesion and simplify the peeling operation.

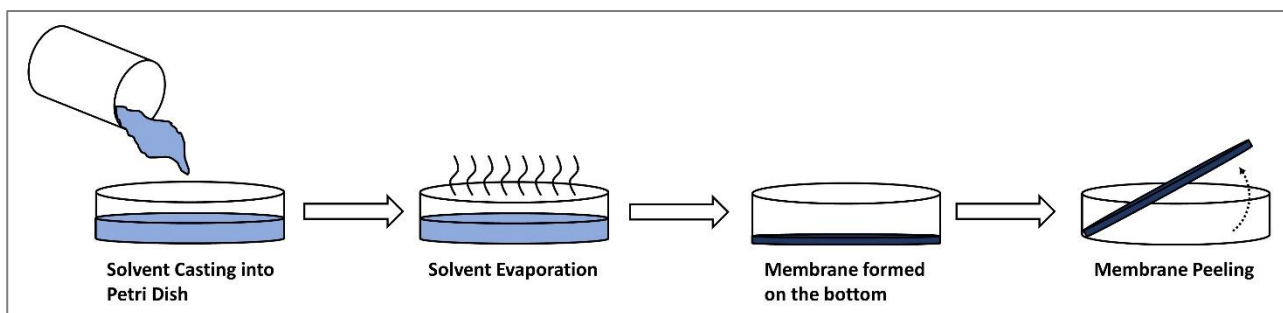


Figure 47: Solvent Casting Scheme

3.3.2 Spin Coating

One of the purposes of NANOMEMC² project was to prepare thin membranes, microns or less, since only these dimensions can lead to a possible application.

To realize such membranes Spin Coating was employed to realize thin supported membranes, because, even if it is not easy to scale-up, such technique is highly automatized, thus allowing precise control of all the parameters and remarkable reproducibility. Moreover, the experiment can be optimized by tune different parameters: solution concentration, solution amount, type of dispense, rounds per minute (rpm), spinning program.

The spin coater used was a WS-400B-6NPP/Lite model from Laurell Technologies Corporation.

The support was still PDMS (450±50 nm) coated on a PAN non-woven fabric (190±5 µm thick), and the total support area of spin coating was 35-40 cm².

Since the top layer, PDMS, is highly hydrophobic, the spin coating has been carried out with the modified Benzoyl-P2533, at the same conversion of the other BP2533 membranes tested 70 mol%, solubilized in chloroform 1 wt% (15 mg/ml).

In this way, for a given Δp , it was possible to extrapolate the thin layer thickness by using the following Equation 26, that can be obtained from the previously defined Equation 1 in Section 1.2.1.

$$L (\mu m) = \frac{P (Barrer)}{\varphi (GPU)} \quad (26)$$

Since such material resulted to be particularly sticky and substantially hydrophobic, it was the perfect candidate among the materials available to form a continuous thin film attached to the PDMS substrate.

To obtain 2 different thicknesses, two protocols have been used, with the same coating program and solution concentration (15 mg BP2533/ml CHCl₃), changing the amount of solution dropped. In both protocols, four consecutive coatings have been performed in order to properly cover the whole surface.

The “static dispense” [191] spin coating technique was used in both cases, which means that all the chosen polymeric solution was first dropped on the support’s center with the spinner fixed, then the program, specifically optimized for this case, was started with rising rpm, as displayed in Table 8 below.

Table 8: Spin Coating optimized program used for both protocols (static dispense, room temperature).

| Step | 1 | 2 | 3 | 4 | 5 | 6 | 7 | 8 | 9 |
|----------|-----|-----|-----|-----|-----|-----|------|-----|-----|
| rpm | 150 | 300 | 500 | 600 | 700 | 800 | 1000 | 500 | 300 |
| Time (s) | 5 | 5 | 10 | 10 | 10 | 10 | 15 | 5 | 5 |

- Protocol 1: low amount of solution was dropped in the center (1 ml) which then was spread by the centrifuge force of the spin forming a thin polymer layer, and the excess of solution was pushed away.
- Protocol 2: high amount of solution was dropped (5 ml) with about all the support surface initially covered, and the centrifuge force removed the excess solvent leaving a thin polymer layer.

In this way, protocol 1 produced the thinnest layers of this work, while the protocol 2 a bit thicker, the latter developed to be sure of covering the overall surface with no defects.

Apart from the solution amount and spreading, the two protocols share every other parameter: rpm, time, number of accelerating steps, temperature and the number of coating per membrane: every spin-coated membrane has been produced with 4 consecutive spin coatings.

Static dispense technique is displayed in Figure 48.

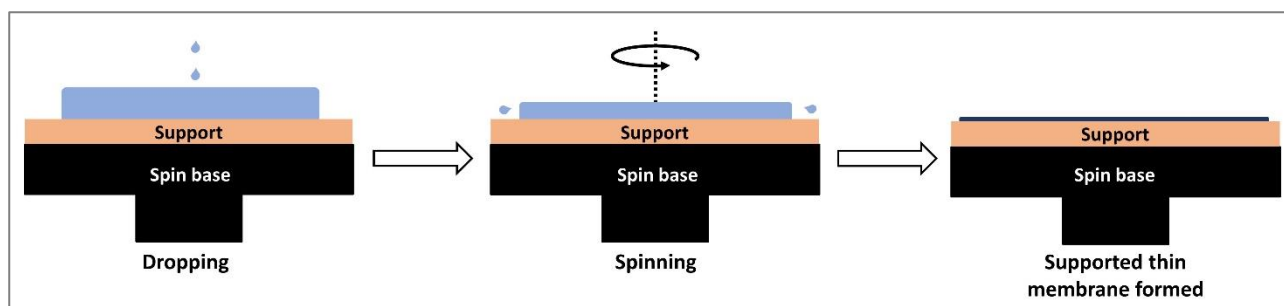


Figure 48: Spin Coating Static Dispense Scheme

3.3.3 Membrane Masking

After being realized, with any of the methods explained in the previous sections, to be safely handled and tested all the membranes have been previously “masked”, that is covered and glued with an aluminum tape foil provided with a hole. The epoxy resin glue was placed at the aluminum-membrane to seal it thus preventing any gas to bypass between the membrane and the aluminum.

The testing membranes were round shaped, with a diameter of 46 mm, the aluminum tape foils were round as well with the same diameter, and the round hole in its center was 20 mm diameter, with a permeation area of 314 mm², minus a small surface occupied by the epoxy resin on the edge, thus the real area was determined through the freeware “ImageJ” [192].

A scheme of a masked membrane mounted into the permeation cell is displayed in Figure 49 and an example of area determination with ImageJ in Figure 50.

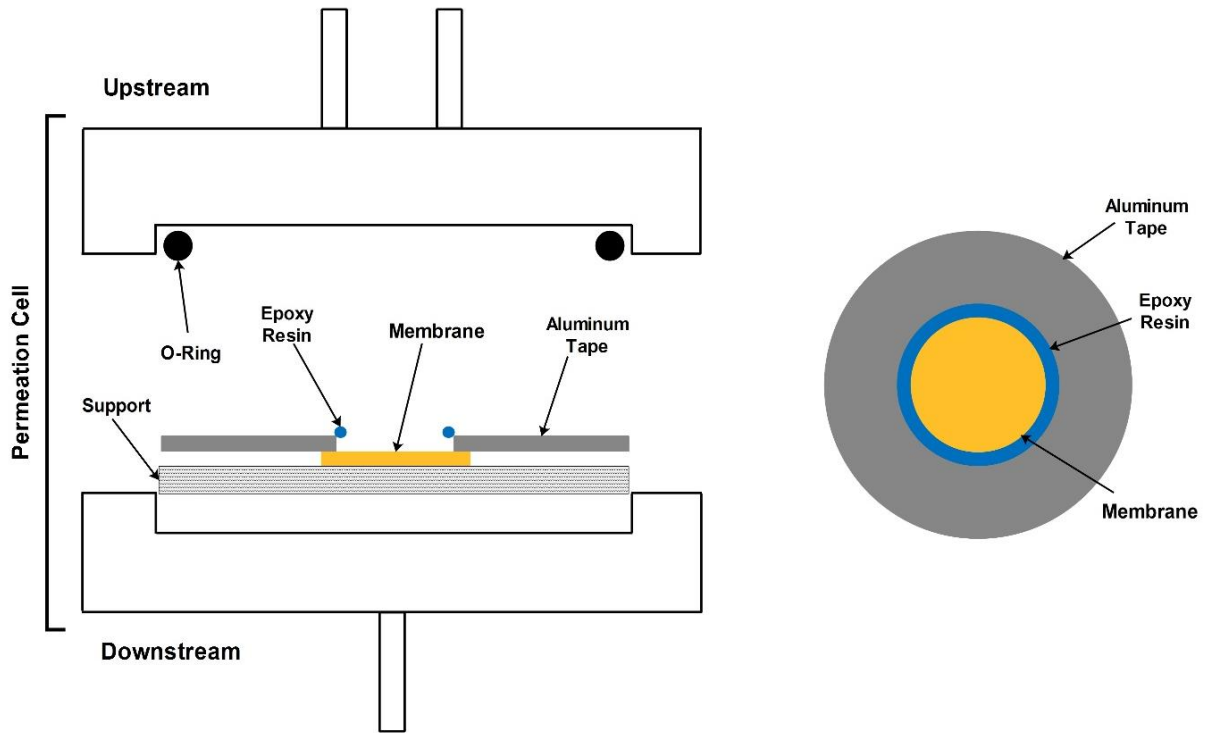


Figure 49: Schematic positioning of the membrane into the cell (left), and schematic view from above (right)

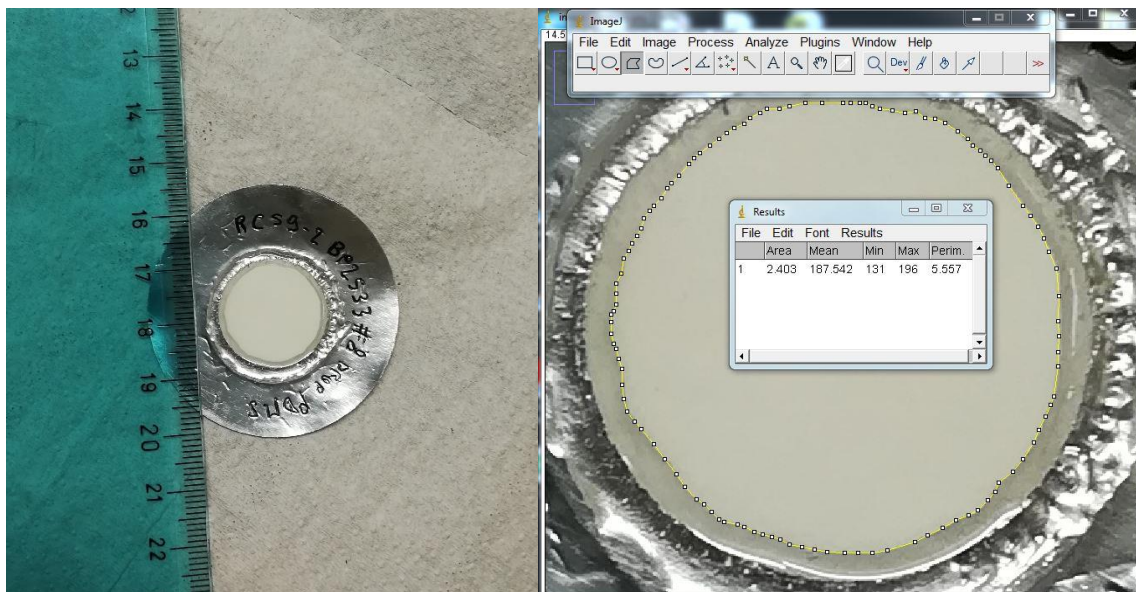


Figure 50: Example of ImageJ software for membrane's area determination

3.4 Gas Permeation Characterization

In this chapter the setup and technique used to conduct gas permeation test will be discussed. During the Doctorate different systems has been used to that aim all operating in a similar way, so that for simplicity this thesis will refer only to the one displayed in the following Figure 51, located in DICAM Chemical Engineering Department, which permits to conduct both static dry and dynamic humid permeation test. The base concept of permeation through the membrane in these experiments is displayed in Figure 52.

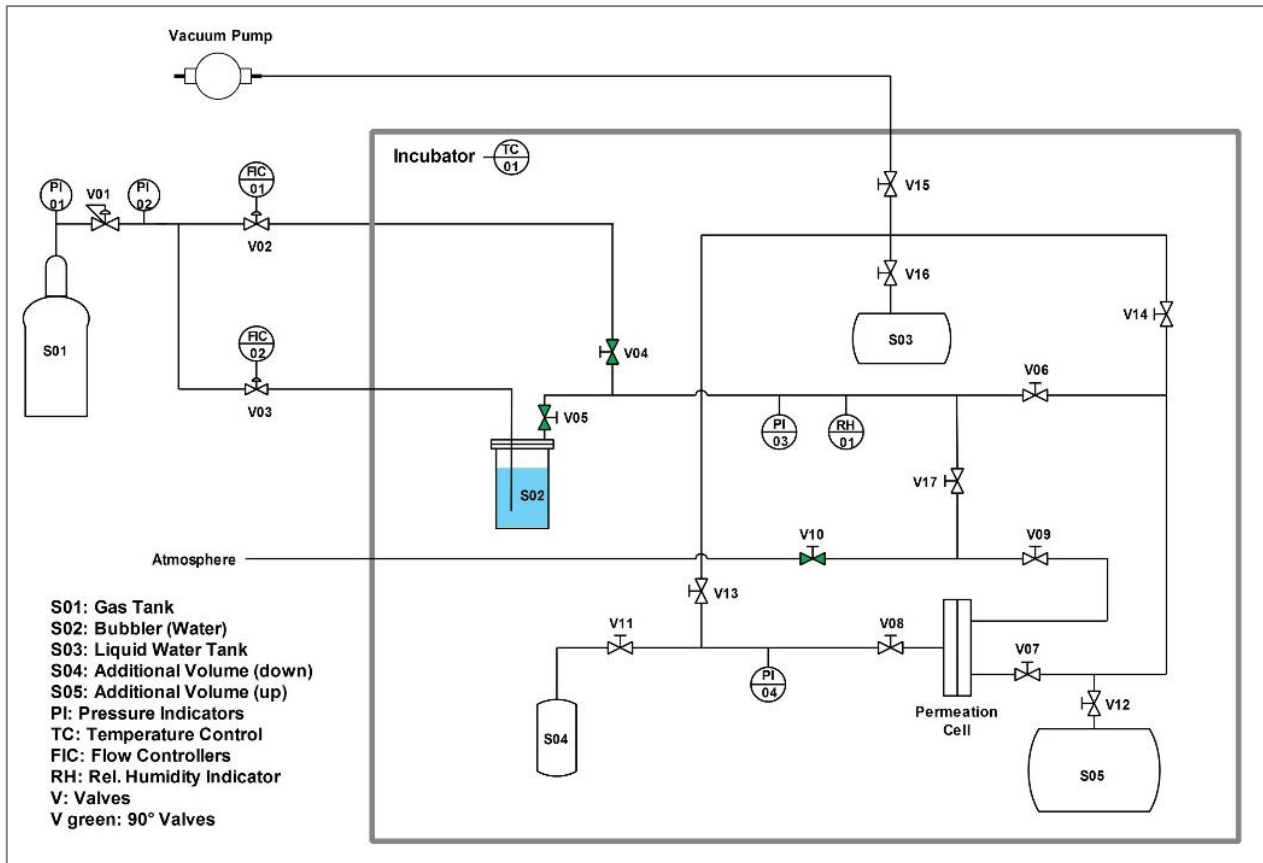


Figure 51: Gas Permeation System used for both Humid and Dry test

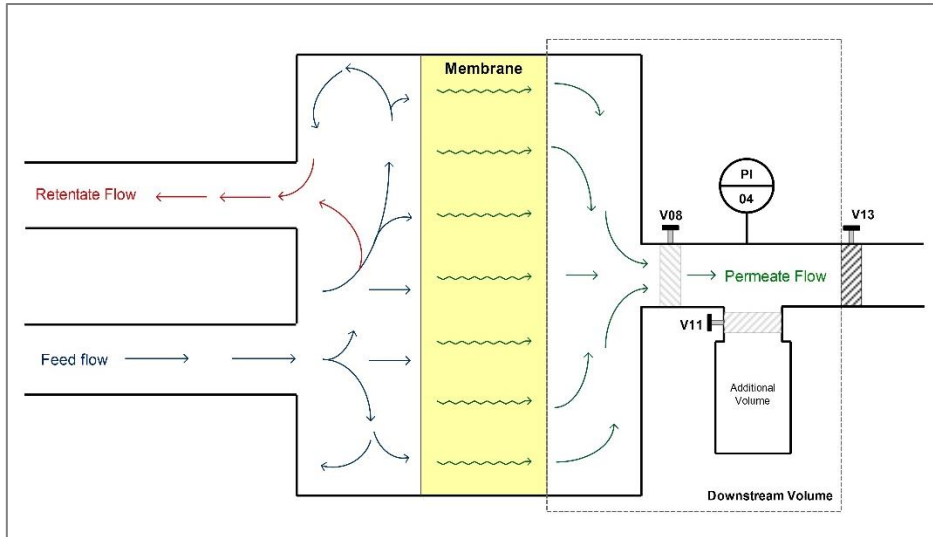


Figure 52: Gas permeation Scheme – focus on cell

All the apparatus is kept inside a thermostatic chamber, provided with an internal additional fan to have a homogeneous temperature in every part of the system.

The permeability is calculated through a barometric technique widely used in gas permeation membrane field [63,77,153,161,193–195]. This technique allows to test one gas at once, so that the selectivity is calculated by the ratio of two different permeabilities measured separately, thus obtaining the so called “ideal selectivity”, as previously discussed in Section 1.2.1.

The main concept is the same for both static dry and dynamic humid test: a gradient of pressure is created between upstream and downstream side of the permeation cell, the former containing the gas to be tested at a certain pressure while the latter initially under vacuum. During tests the gas permeating through the membrane, increases the pressure in the known downstream volume (confined by the cell and V13 in the Figure 51 and 52) allowing the calculation of permeated flow. The rise of pressure can be indeed correlated to the flux through a suitable equation of state and then to the permeability, that can be calculated through Equation 27 once the slope of increment of pressure over time (dp/dt) reaches the steady state, as shown in Figure 53.

$$Permeability = \left(\frac{dp_1}{dt}\right)_{t \rightarrow \infty} \frac{V}{RT} \frac{L}{A} \frac{1}{(p_2 - p_1)} \quad (27)$$

Where V is the downstream volume, L the membrane’s thickness, A the permeation area, T the temperature, $p_2 - p_1$ the pressure gradient between upstream and downstream compartment and R the gas constant.

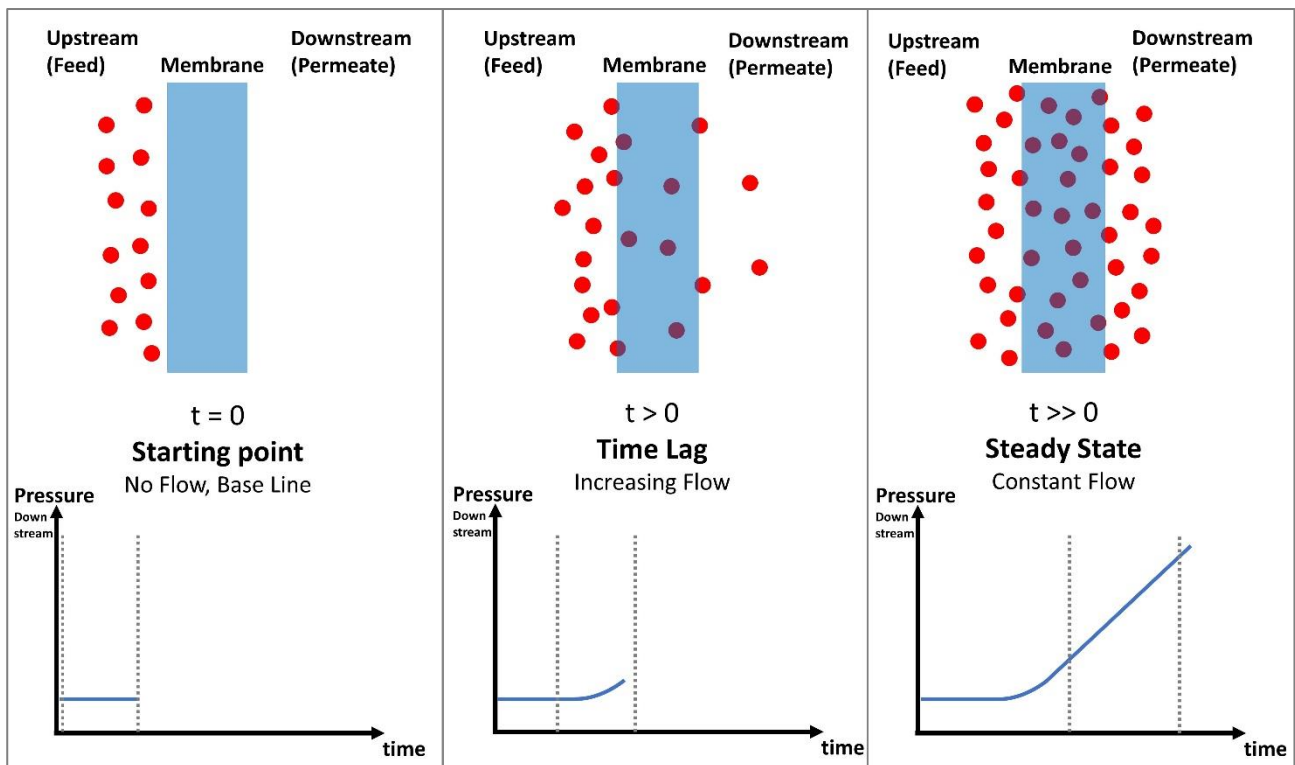


Figure 53: Ideal downstream pressure trend in gas separation membranes through barometric technique

3.4.1 Static Test – Dry

Static dry experiments were carried out for membranes that didn't require humidity to exploit their permeation properties, so Pebax[®]2533 based and its modified version Benzoyl-P2533.

In this case, since no water is needed, the bubbler and water tank were kept isolated, so V03, V05 and V16 in Figure 51 were always closed.

After mounting the cell, high vacuum was pulled from both downstream and upstream over night in order to remove all the residual gas and/or vapor still absorbed into the membrane or support. This was done by opening V07, V08, V13, V14 and V15 while the vacuum pump was on.

After the sample degassing was completed, the cell was isolated by closing V07, V09 and V13, and a certain amount of gas pressure (usually around 1 bar) was charged into upstream volume, big tank S05 included, which was then isolated as well closing V06.

After the gas charge, the system was kept in standby for 20 minutes, in order to heat up the new gas inside, and data acquisition was started to check and estimate possible leaks.

Lastly, to carry on the actual permeation test, V07 was opened, making the gas stored in upstream volume flow against the membrane and filling all the remain volume (up to V09).

In this static condition, the gas can permeate reaching the downstream side, increasing its pressure and allowing the permeability measurements through Equation 27.

It is worthwhile to notice that due to the volume of S05 (about 5 liters) , the volume in upstream was significantly higher than the downstream volume (in the order of 90 cm³) thus the gas flowing downstream did not affect the pressure upstream, which remained substantially constant maintaining the permeation driving force constant and simplifying the data processing. For the same reason, all the static dry tests were terminated before the downstream pressure was reaching 100 mbar.

3.4.2 Dynamic Test – Humid

As already mentioned, the permeation system described allowed to perform experiments with controlled humidity, which is a crucial parameter for facilitated transport materials, in this case PVAn, cNFC and Arginine. In this case the test was conducted in dynamic conditions with the humid gas flowing in the upstream side of the membrane to void possible polarization concentration phenomena. To allow the calculation of pure gas permeability in presence of water vapor a humidity equilibration has to be carried out, on both the feed flow and the membrane itself, in order to have an increment of pressure in downstream due to the target gas only; if the water activity is the same on both sides of the membrane, indeed, it does not migrate in any direction and remains in equilibrium throughout the tests.

Membrane Humidity Equilibration

For the membrane's side equilibration, an indirect method has been used, exploiting the water vapor pressure: after the sample degassing, carried out as for dry tests, and with the sample kept under vacuum, the water tank S06, containing DI water, was connected to the system (opening V16), so that the water vapor could fill the volume until the desired relative humidity, RH, was reached. This parameter, defined in Equation 24, can be calculated, since the water vapor saturation pressure is obtained through the Antoine law (Equation 23).

Feed Humidity Equilibration

The humidity equilibration of the feed flow was conducted with a direct method instead: through the electrovalves V02 and V03 it was possible to tune the amount of dry gas (from V02) and humid gas, humidified by passing through the water filled bubbler S02 (from V03). Then the two streams were merged in one before reaching the hygrometer RH01 (Chilled Mirror Hygrometer Dewtrak II, from Edgetech Instruments), which measured and displayed directly the humidity percentage of the outlet gas. To reach the proper ratio of dry vs humid flow, few minutes were required, and in this time the flow were not led to the membrane but out of the system, through the bypass (V17), with V06 and V09 closed.

Once both membrane and feed flow were equilibrated to the same RH, data acquisition was started, and it was possible to feed the gas to the membrane, closing the bypass V17, and opening V06 and V09.

4) Results and Discussion: Polyvinylamine and Nanocellulose

In this chapter all results about facilitated transport membranes made of PVAm, Nanocellulose (and Arginine) will be discussed, that is:

- the Lupamin purification to obtain PVAm,
- the blending and dispersion of the three compounds (PVAm/cNFC/Arg),
- the water absorption experiments
- the humid gas permeability test,
- the controlled crosslinking with glutaraldehyde.

Purification, blending and crosslinking will be discussed along with their FTIR results.

4.1 Purification of Lupamin[®]9095 - Polyvinylamine

The Lupamin[®]9095 purification protocol explained in Section 3.1.1 resulted in a success, providing two different degree of purified polyvinylamine, based on the step of the protocol itself.

One, called “PVAm Low Grade” (PVAm-LG) was the product obtained after the first precipitation in ethanol, still containing a certain amount of salt; the other was called “PVAm High Grade” (PVAm-HG), obtained at the end of the whole protocol, resulting in basically pure polymer.

Lupamin[®]9095 and purified PVAm films (PVAm-LG and PVAm-HG) were analyzed by IR spectroscopy to assess the efficiency of the purification process, with the related FTIR results displayed in Figure 54.

The peaks at 770, 1350 and 1570 cm^{-1} are referred to the presence of the sodium formate salt (by comparison with the NIST's IR spectra [196]) [197,198]. They are well visible in the commercial Lupamin[®]9095 spectrum but lose intensity in the purified PVAm spectra. In particular PVAm-LG shows depressed absorbance at the mentioned wavelengths with respect to Lupamin[®]9095, but the peaks are still present, suggesting a significant, but not complete purification. In PVAm-HG films, on the other hand, the characteristic signals of the salt are almost completely absent (except for the one at 770 cm^{-1}), indicating an excellent purification of the polymer. It is worth to notice that an intensification of the characteristic polymer signals (880 cm^{-1} N–H wagging, 1380 and 1440 cm^{-1} C–H bending/rocking, 1660 cm^{-1} N–H bending, 2920 cm^{-1} C–H stretching, 3150-3400 cm^{-1} broad peak N–H stretching) is observed in these materials, which also corresponds to a better degree of purification.

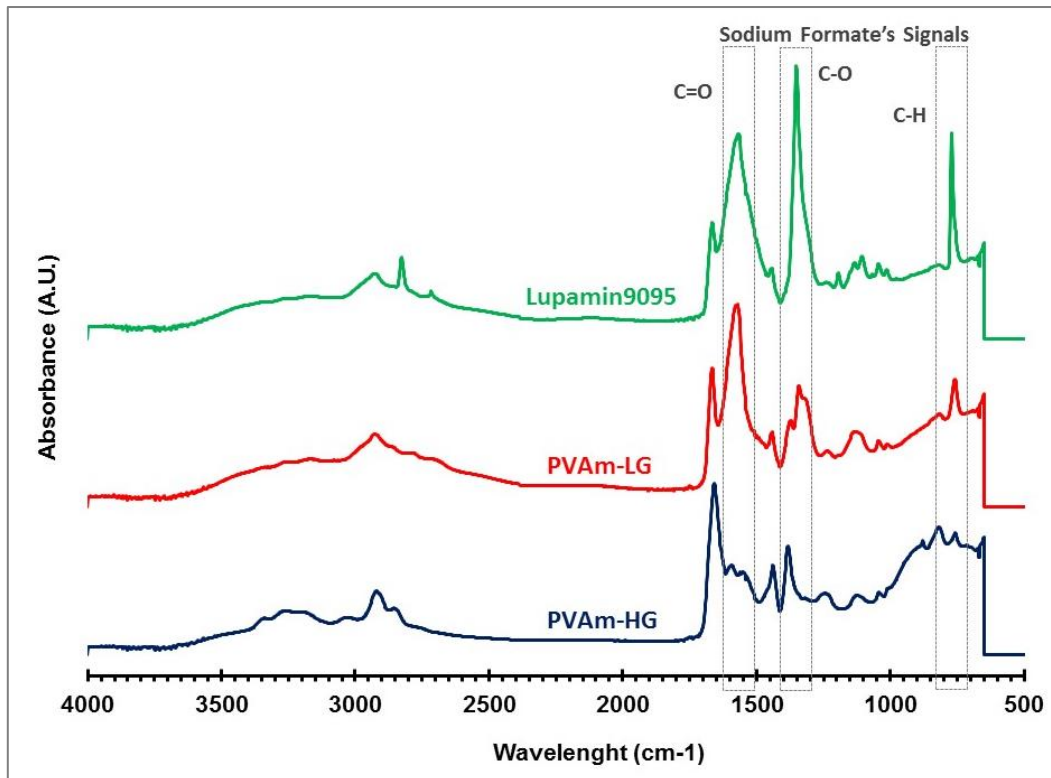


Figure 54: FTIR-ATR spectra of commercial Lupamin®9095 and purified PVAm with different degree of purification.

Concerning the polymer peaks, then, an interesting change in the different spectra is the shift of the peak related to N-H stretching before and after the resin treatment (PVAm-HG); this one moves from 3100 to 3300 cm^{-1} , which is quite reasonably associated to the neutralization of amine group from the R-NH_3^+ to the R-NH_2 form, as also confirmed by the results obtained by Annenkov et al [102]. This neutralizing effect is caused by the use of the hydroxylated resin, which exchange hydroxyl anions in solution while retaining salt anions.

To have also a more practical perception of the purification, in Figure 55 three membranes are displayed made respectively of Lupamin®9095, PVAm-LG and PVAm-HG.

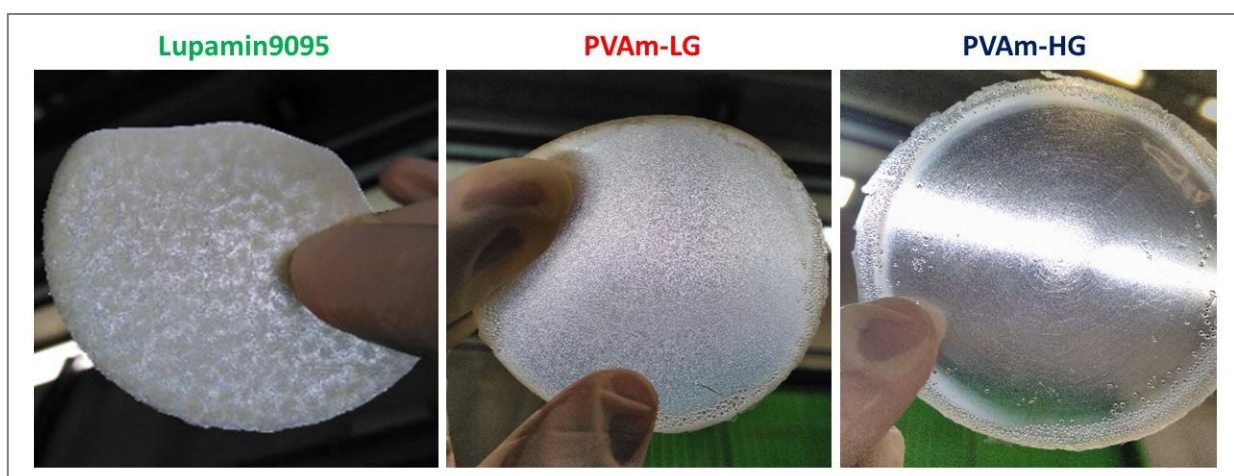


Figure 55: Solvent Casting membranes made of Lupamin®9095, PVAm-LG and PVAm-HG

As already mentioned, since PVAm-LG was already pure enough to form stable blends but far easier to be produced and in higher amount, it has been the most often used PVAm-material.

4.2 Dispersion and Blending

Initially, three different composition of PVAm and cNFC have been blended, respectively 50/50, 35/65 and 20/80 in wt%.

The respectively FTIR results are shown in Figure 56, along with a sample of pure cNFC with a surface charge of 3600 $\mu\text{equiv/mol}$ and the PVAm-LG used for the blend.

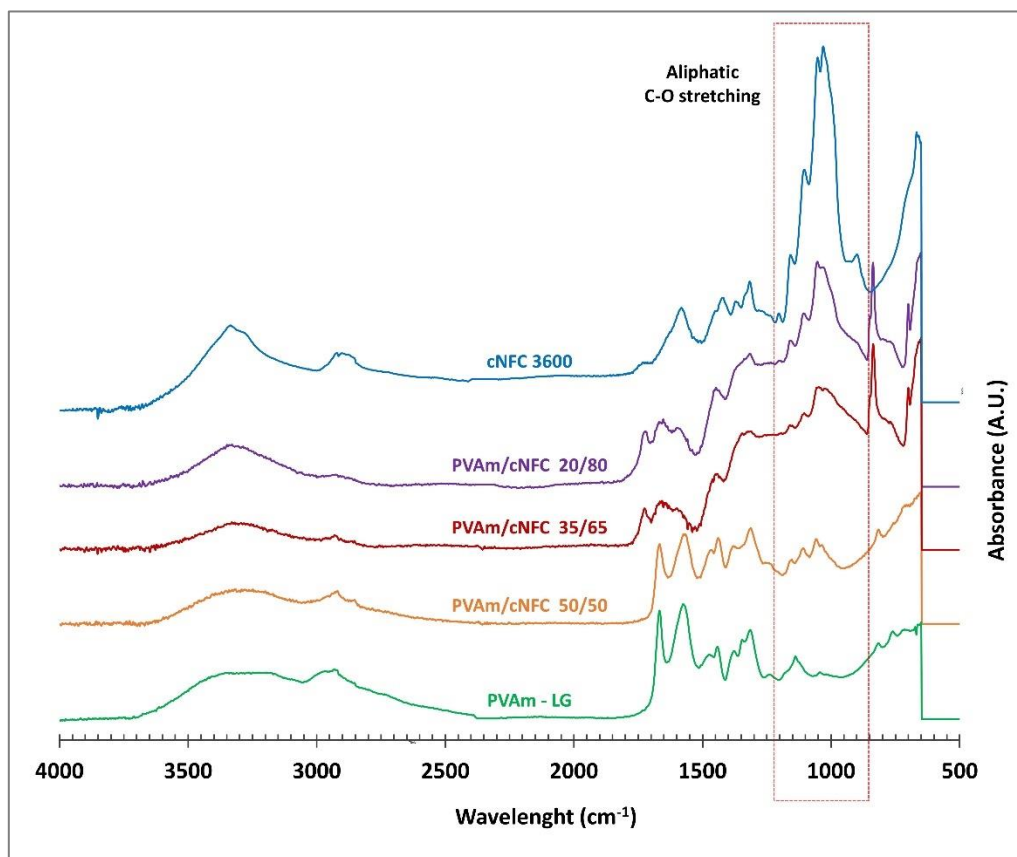


Figure 56: FTIR of different compositions of PVAm/cNFC blends

In the figure it can be seen that by increasing the concentration of the cNFC in Lupamin new characteristic cellulose peaks appears in the blends, the most clear is the one at around 1000 cm^{-1} , corresponding to the C-O stretching of the cNFC. This one, indeed, is not superimposed to any PVAm peaks and clearly increases with the content of cNFC providing its typical shape of the spectra between 800 and 1200 cm^{-1} .

Among the different composition tested the best combination resulted to be the 50/50 blend, in terms of both homogeneity and water absorption capability (described in the next section); thus, to this half cNFC half PVAm blend, two different loadings of arginine have been added: 25 wt% and 45 wt%.

In this case as well, the three components blends have been investigated via FTIR, as shown in Figure 57, along with pure L-Arginine and the 50/50 only.

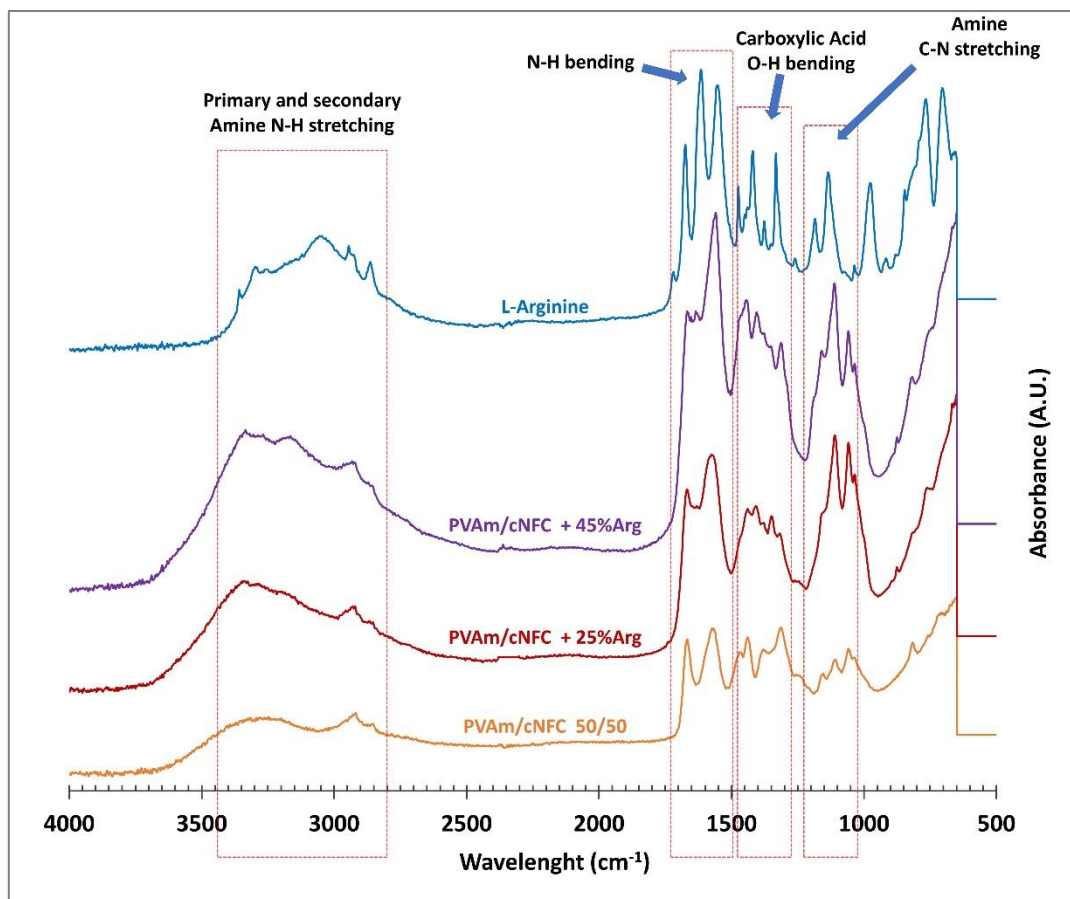


Figure 57: FTIR of three components PVAm/cNFC/Arg blends

In this case, the FTIR spectra is highly affected by the presence of arginine, especially in the 45 wt% loaded: primary and secondary N-H peaks from 2800 to 3400 cm^{-1} are visible, as well as other nitrogen-based signals, like N-H bending at 1500-1750 cm^{-1} and C-N stretching at 1100-1200 cm^{-1} . A set of carboxylic acid signals from arginine can be appreciated as well, between 1500 and 1250 cm^{-1} .

Overall, all the blend resulted very homogeneous and aesthetically very similar to each other, with both two and three components and compositions. As an example, a three composition of PVAm/cNFC loaded with 45 wt% Arg is displayed in Figure 58.



Figure 58: Sample of three component membrane, made of PVAm/cNFC 50/50 + 45wt% Arg

4.3 Water Absorption

Water absorption test, through quartz microbalance, have been initially conducted on the first three double-blends PVAm/cNFC, to investigate the water intake based on their ratio (50/50, 35/65 and 20/80 wt%). The results are displayed in Figure 59.

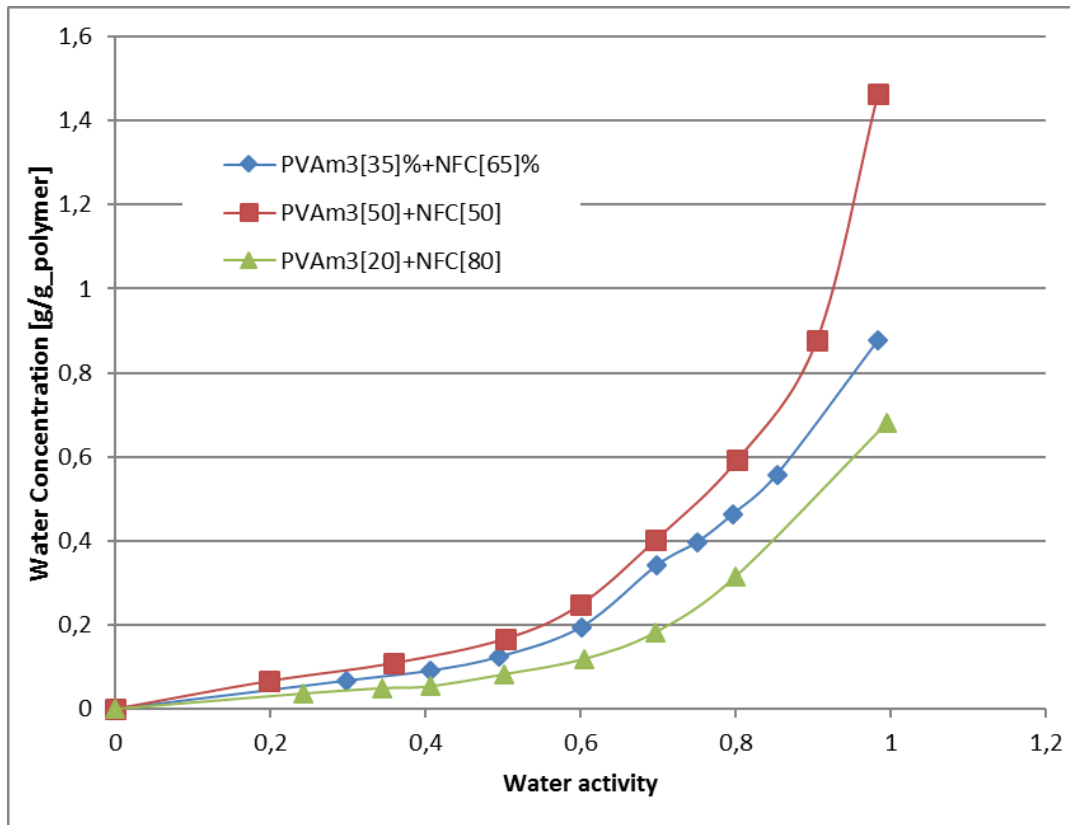


Figure 59: Water Absorption results of different PVAm/cNFC blends

The three curves clearly show that the water uptake is mostly driven by the polyvinylamine amount: the higher is PVAm content, the higher is the water absorbed.

The maximum is indeed achieved by the 50/50 blend, where the water absorbed in term of $\text{mass}_{\text{water}}/\text{mass}_{\text{polymer}}$ reach a value of 1,47 in saturation conditions (100 RH%). Thus, since water plays a key role in facilitated transport of CO₂ through amines, the PVAm/cNFC 50/50 blend have been chosen as base, to be added with arginine.

Arginine was then added to the blend in two different amounts: 25 wt% (PVAm/cNFC/Arg = 37,5/37,5/25) and 45 wt% (PVAm/cNFC/Arg = 27,5/27,5/45), and water absorption test were conducted on these samples as well, as showed in Figure 60.

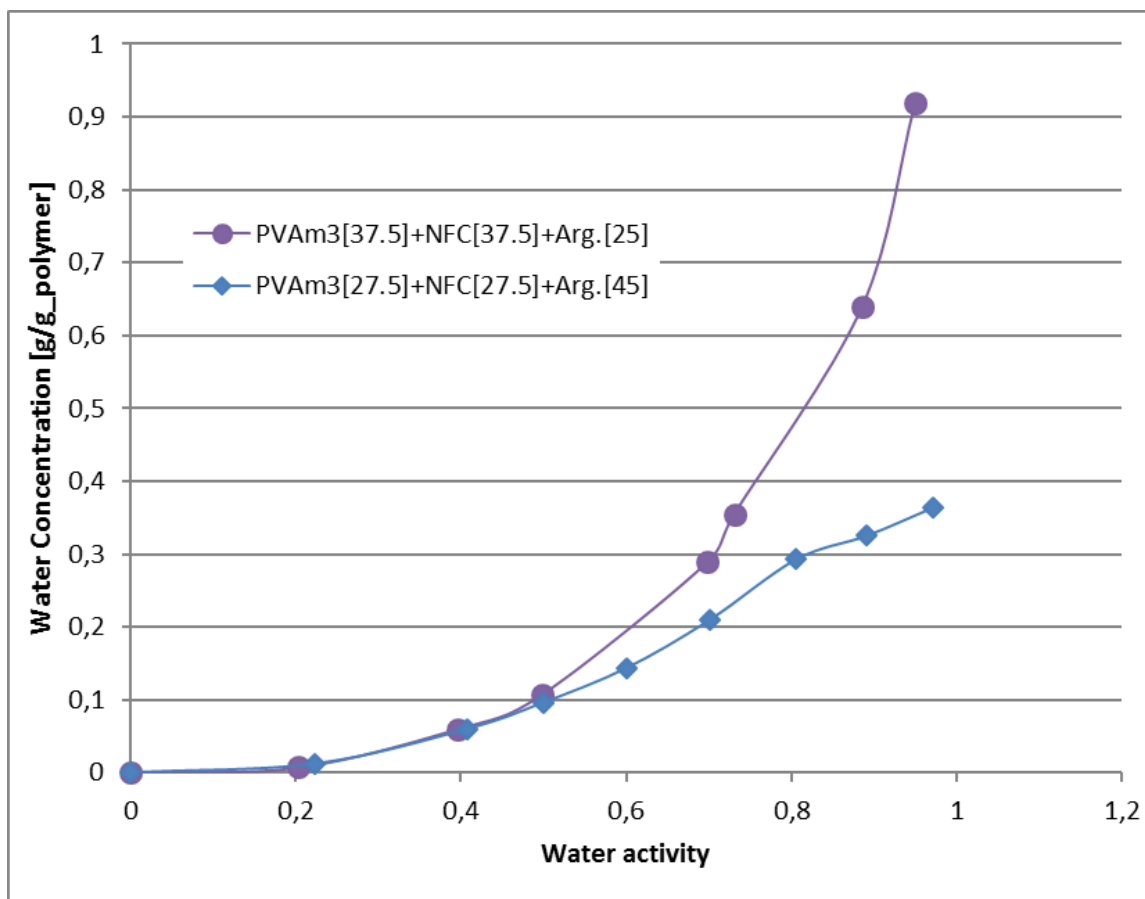


Figure 60: Water Absorption results of the three component PVAm/cNFC/Arg blends

Although L-Arginine is a hydrophilic compound, the water absorption results demonstrated that the water intake is still mainly driven by the PVAm content: comparing the two blends, indeed, the one with higher amount of arginine, 45 wt% (and 27,5 wt% PVAm) reached a $\text{mass}_{\text{water}}/\text{mass}_{\text{polymer}}$ of just about 0,37 at saturation conditions (100 RH%), while the other one, with 25 wt% Arg (and 37,5 wt% PVAm) reached a value of 0,92 at the same conditions.

Such behavior is in line with that already observed in a previous work, where, in a blend of nanocellulose and PVAm, the water intake increased with the content of PVAm [77]. Also from previous work, it was confirmed that Arginine's water intake is comparable with the cNFC ones [62], so far lower than the PVAm's.

In any case, all the three component blends have been investigated with humid permeation experiments, along with the base 50/50 double component one.

4.4 Humid Permeability Test

Three blends have been carried out permeation test on: PVAm/cNFC 50/50, PVAm/cNFC/Arg 37,5/37,5/25, and PVAm/cNFC/Arg 27,5/27,5/45.

Permeation conditions were always humid, at 75 and 100 RH%, at 35°C. Plus a set of data obtained at 100 RH% but 50°C.

The permeability results are summarized in Figure 61.

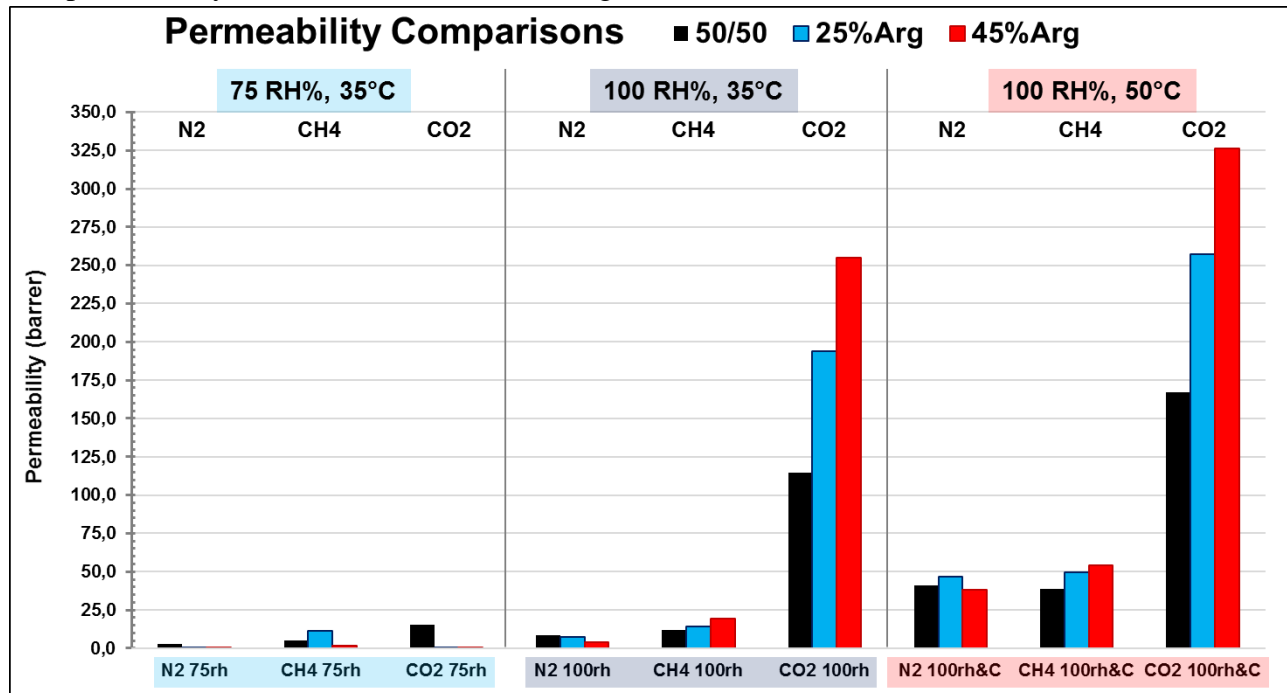


Figure 61: Summary of CO₂, N₂ and CH₄ Permeabilities of 50/50 PVAm/cNFC, +25wt% Arg and +45wt% Arg blends

From the chart it's possible to notice an extremely low permeability for all gases in every blend, when humidity is 75 RH%, showing once again the importance of water to activate the facilitated transport of CO₂.

Keeping temperature fixed at 35°C, but conducting the same experiments at 100 RH%, an increment of permeability is observed for all three gases, but especially for CO₂, which shows an increase of more than about order of magnitude definitely higher than that observed for both N₂ and CH₄. Among the three blends, then, the highest increment and gap difference is clearly the three components loaded with 45 wt% Arg for which the CO₂ permeability increased from about 0,3 to 271 Barrer going from 75 to 100% RH.

Keeping fixed the water saturation, 100 RH%, and increasing the temperature at 50°C resulted in a further increment of CO₂ permeability, especially for the 45 wt% Arg loaded sample where it increased from 271 to 326 Barrer, with an increment of 20%.

These trends can be discussed more in detail by using the Robeson plots for both CO₂/N₂ and CO₂/CH₄, showed in Figure 62.

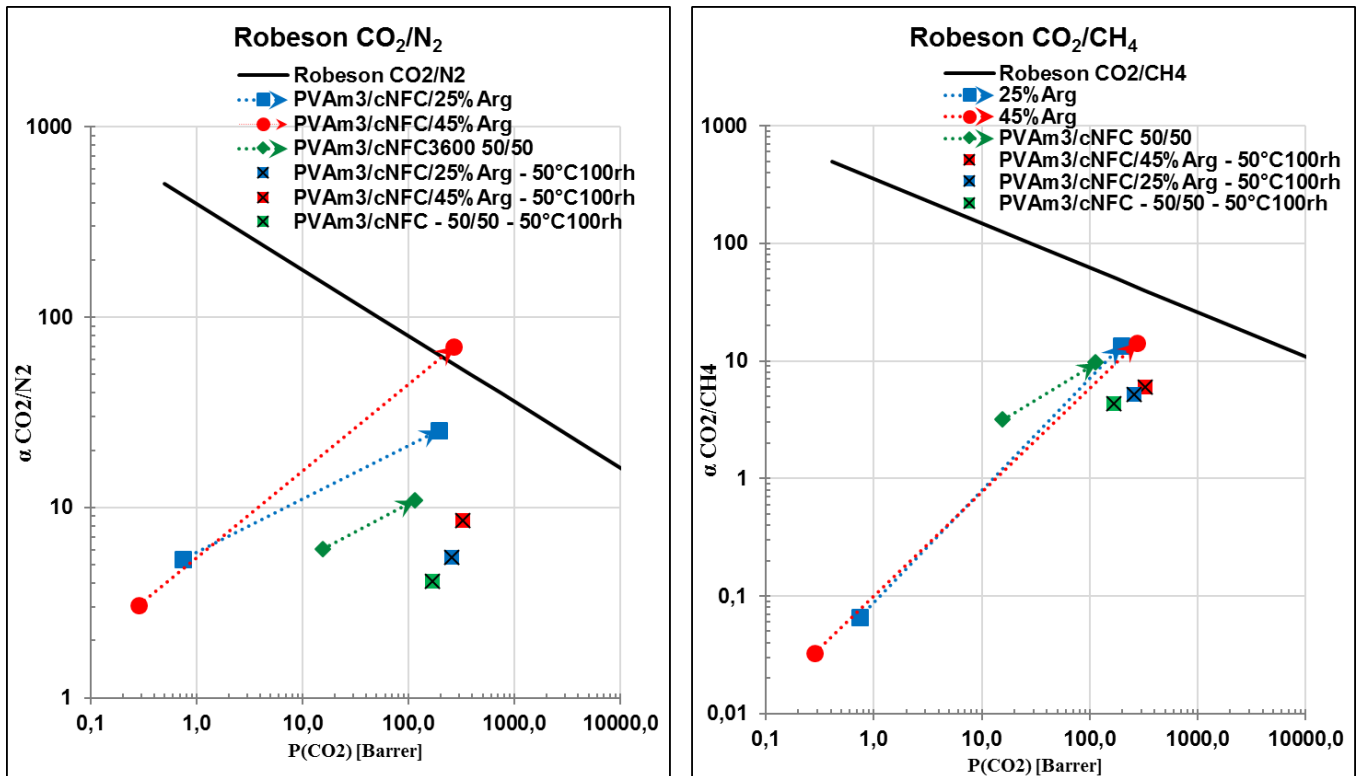


Figure 62: CO₂/N₂ and CO₂/CH₄ Robeson plots for the blend tested

In both the Robeson Plots presented, the colors refer to different blends, the arrows direction indicate the increment of humidity (starting point 75 RH%, final arrow point 100 RH%, both at 35°C), and the single squares with “X” represent the 100 RH% test conducted at 50°C.

It’s possible to notice that the permselective trend of the 35°C tests are the same for both Robesons: both permeability and selectivity increase with the increment of humidity, from 75 RH% to 100 RH%. The main difference between the two plots is that in the CO₂/N₂ one also the trend between the different blends is clearer: permeability but especially selectivity increases with the increment of arginine content. For the CO₂/CH₄ plot, on the other hand, even if a similar behavior is visible, all the three blends are relatively close to each other, and the +25% Arg and +45% Arg are almost overlapped. In general, therefore arginine seems to definitely improve the CO₂ transport in the membrane especially with respect to nitrogen, while in the case of methane the effect is less clear likely because the slightly higher solubility of this gas with respect to N₂.

The observed behavior leads to another clear difference between the two charts, more related to performances: for the CO₂/N₂ Robeson, indeed the blend loaded with 45 wt% Arg resulted to cross the upper bound, when tested at 100 RH% and 35°C, with a CO₂ permeability of 271 Barrer and CO₂/N₂ selectivity of 70. For the CO₂/CH₄ Robeson, instead, none of the blend tested was able to cross the upper bound, mostly due to the relative low selectivity obtained, with the highest around 14.

The test conducted at 100 RH% and 50°C resulted in a slight increment of CO₂ permeability compared to the one made at 35°C, reaching indeed 326 Barrer for the 45 wt% Arg loaded, but with a quite big drop of both CO₂/N₂ and CO₂/CH₄ selectivity, from 70 to 8 the former, and from 14 to 6 the latter, moving these points away from the upper bounds with respect to data at 35°C.

Such result is somewhat unexpected as facilitated transport should still be active at 50°C and literature results indicate that higher temperature increases both selectivity and permeability. The present data

therefore suggests that during high temperature tests the membrane structure was modified creating defects (i.e. by swelling) leading to a selectivity reduction. In this presence of defects indeed the facilitated transport results less effective, even if notable, and all gases permeated in higher amount, not only CO₂, causing an overall loss of selectivity.

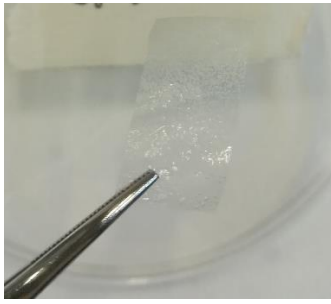



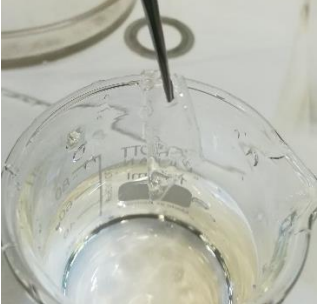
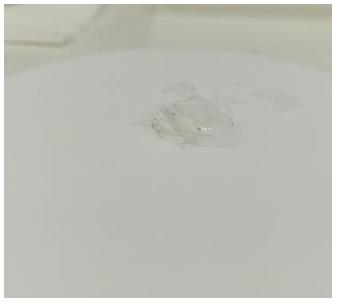

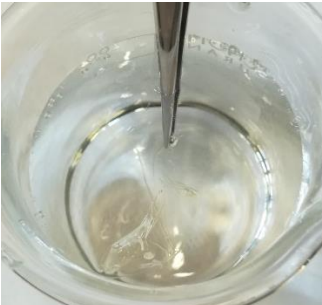

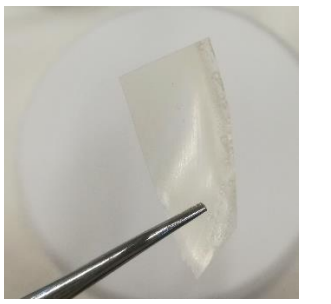


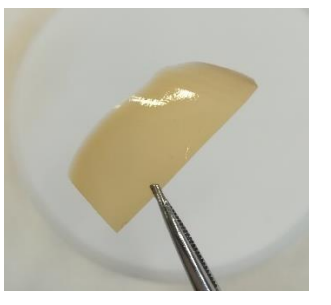
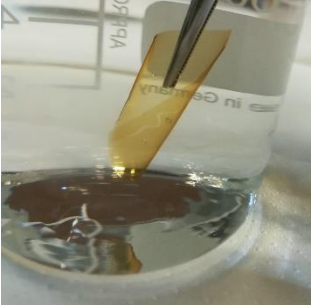

4.5 Controlled Crosslinking

4.5.1 Fast Dipping Test

The fast dipping test was carried out to see the different behavior of the material when exposed to liquid water for a short time. Five membrane-like samples have been investigated in this way: PVAm (LG), PVAm + 1 mol% GA (Glutaraldehyde), PVAm + 5 mol% GA, PVAm + 10 mol% GA and PVAm + 20 mol% GA.

The results are purely graphic, and are shown in Table 9.

Table 9: Crosslinked PVAm fast dipping test results

| Material | Before | Meanwhile | After |
|------------------|---|--|---|
| PVAm-LG |  |  |  |
| + 1 % GA |  |  |  |
| + 5 % GA |  |  |  |
| + 10 % GA |  |  |  |
| + 20 % GA |  |  |  |

As shown by the pictures, the pristine PVAm-LG cannot withstand even few seconds in water, as it instantly swells and deform into a 3D hydrogel structure, which cannot be considered a membrane

anymore. The sample with 1 mol% of GA retained its 2D-like membrane shape, but got extremely brittle and easy to be broken when bended or stretched.

From the 5 mol% GA and above, after the dipping it was still possible to handle and even manually stretch or bend the membrane without breaking it, as shown in Figure 63, thus confirming the increased mechanical stability of the membrane when GA crosslinking reached the adequate amount of PVAm chains. By analyzing the PVAm-GA reticulation product in Figure 43, It's possible to deduce that, with 5 mol% GA and assuming the totally completion of the reaction, around 20% of the PVAm amine groups were crosslinked.

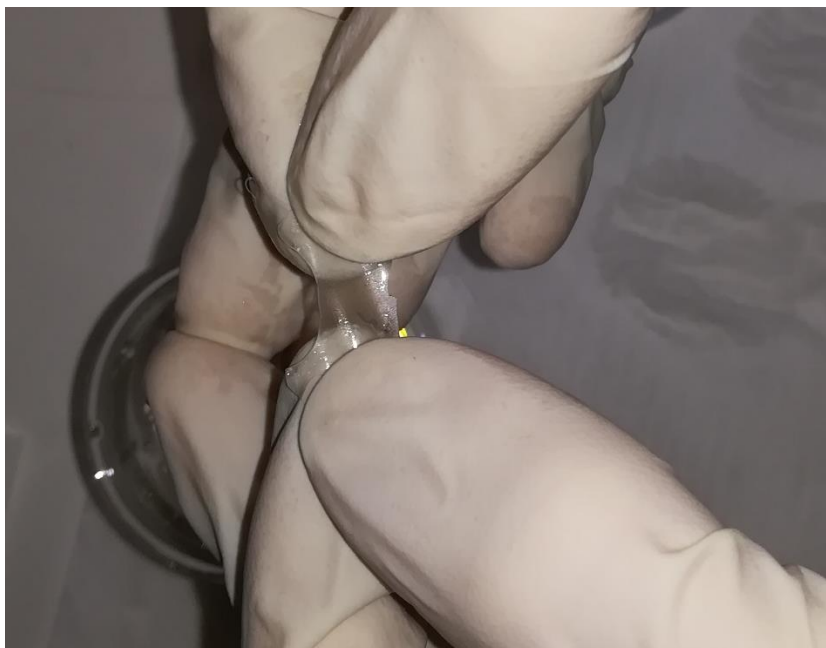


Figure 63: Manually stretched PVAm-LG + 5 mol% GA after being dipped in water

4.5.2 Long Dipping Test and Weight Loss

The previous results were somewhat confirmed by the other dipping tests carried on. Other samples of the same five materials have been kept into an excess of water at 35°C for 60 hours, then their leftover was dried and weighted properly, with results showed in Figure 64.

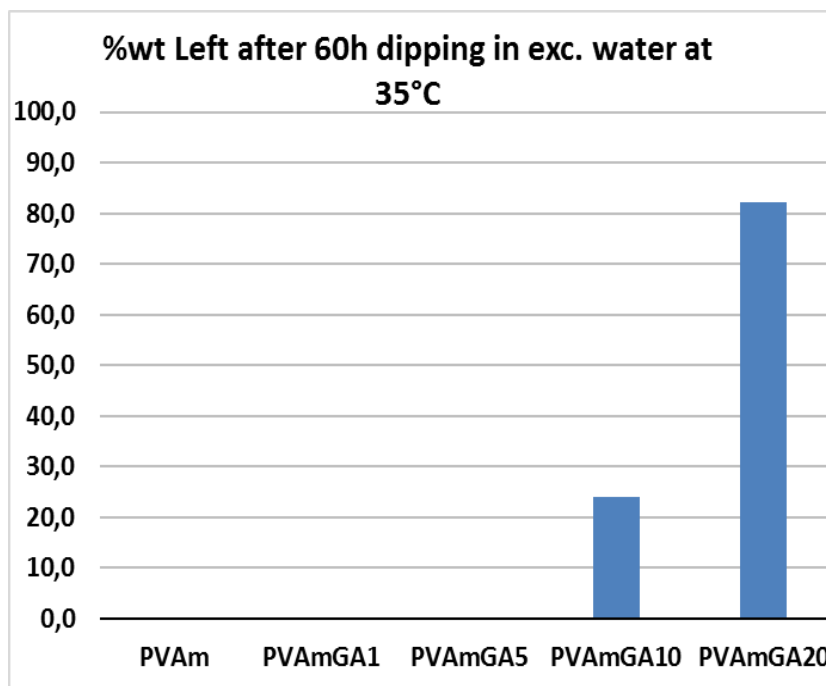


Figure 64: wt% remained after Long Dipping Test

As displayed in the chart, PVAm, PVAm + 1 mol% GA and PVAm + 5 mol% GA were all solubilized, or in any case not recoverable for the weight.

The 5 mol% GA film resulted greatly swollen of at least 2 to 4 times its initial surface, and extremely damaged with the membrane's structure substantially compromised. The 10 mol% GA was swelled but still intact and possible to be weight, resulting in a 24 wt% of the total initial mass.

However, the 20 mol% GA seemed the very same to the naked eye: no swelling, no surface extended, physically remained basically the same, with a remaining mass of 82 wt%.

Even if these results seem not particularly positive, it's mandatory to note that the experiment was conducted in extremely harsh conditions: membranes for gas separation, in humid condition, may face some drops or micro-drops of water, they're not kept into liquid water directly.

Thus, it's safe to say that both the 10 and 20 mol% GA crosslinked PVAm, and very likely also the one at 5% crosslinking, should form compact membranes able to withstand humid test, and perhaps even at temperature higher than 35°C. The addition of nanocellulose in this concern would increase even more the stability of the materials.

Unfortunately, due to the lockdown following the Covid19 pandemic, the work on these materials could not be completed and the permeation tests, necessary to understand the real potential of the membranes could not be carried out. The crosslinking indeed is well known to stabilize the membranes but also to reduce the water sorption and the gas permeation, thus endangering the overall permselectivity of the materials.

As a possible future work research project, it could be interesting to continue with the study of the controlled crosslinking and its optimizations in term of mechanical and swelling resistance compared to permselective properties. In this way, a hydrophilic but far more resistant backbone matrix would be generated, to be loaded with a number of filler and/or carriers for selective gas transport.

5) Results and Discussion: Pebax®2533 and Graphene Oxide

In this chapter all the results related to Pebax®2533 and GO-based materials (GO, PGO and PEAGO) will be discussed: fillers-matrix blending, chemical analysis and gas permeation experiments.

5.1 GO Dispersion and Blending

For GO, water worked perfectly as solvent producing a limpid dispersion that appeared like an homogenous solution. On the other hand, even after extensive mixing and sonication, GO could not be dispersed in ethanol or buthanol which always produced turbid solution with high amount of precipitate (Figure 65)

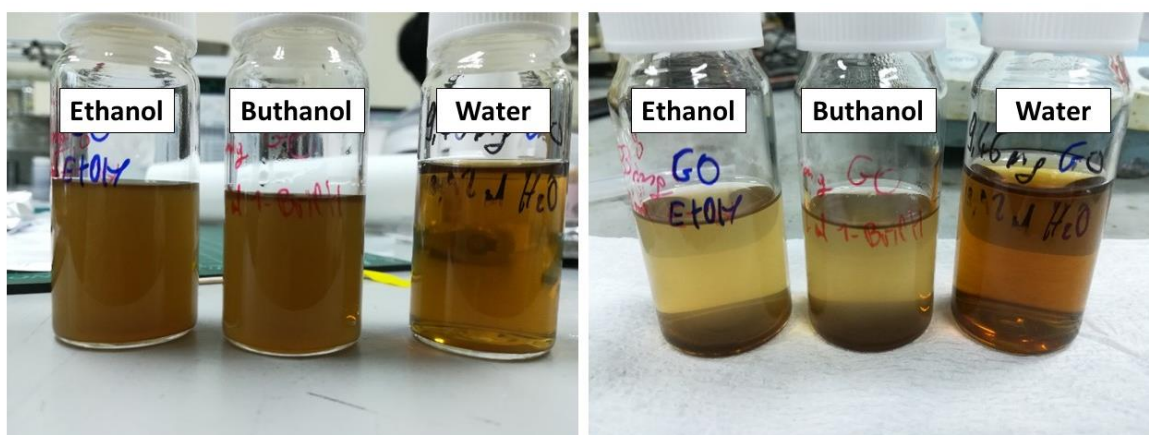


Figure 65: GO dispersions in EtOH, ButOH and Water soon after sonication (left) and after 24 h rest (right).

As explained in Section 3.1.4, being Pebax not soluble in water but only in ethanol, the blending protocol was carried out by slowly adding the water GO dispersion to the hot stirred Pebax®2533 ethanol solution. This procedure allowed, in all cases, to obtain an homogeneous mixture and, by casting, very smooth membranes with no sign of agglomerates even at the highest loading inspected, 1 wt% GO, as shown in Figures 66a-c.

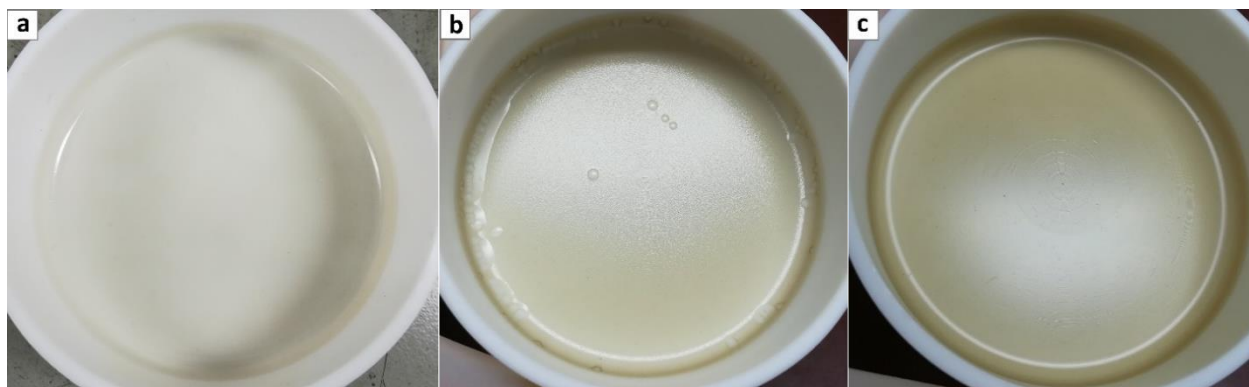


Figure 66: Pebax®2533 + Graphene Oxide Composite Membranes Casted; loadings a) 0.1 wt%, b) 0.5 wt%, c) 1 wt%

Unfortunately for the two other GO types considered the dispersion in Pebax[®]2533 resulted more difficult and for both PGO and PEAGO only the 0.02 wt% loaded films were obtained with good homogeneity and no presence of GO aggregates (see Figures 67a-b) while increasing concentration always led to aggregation and heterogenous films as shown in Figure 67c.

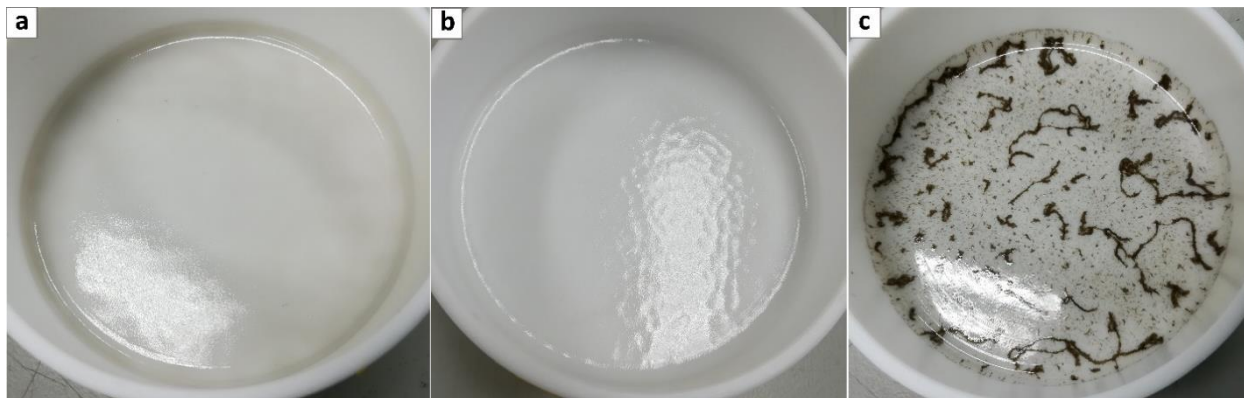


Figure 67: Figure 4: Pebax[®]2533 loaded with 0.02 wt% PGO (a), 0.02 wt% PEAGO (b) and PGO 0.1wt% (c)

Such fact was not considered an issue, since, as it will be explained below, the permeation results showed that with higher loadings the overall permselective properties of CO₂/N₂ transport decrease. For this reason, it was decided not to try to further optimize the protocol to obtain membrane with also with higher loading of modified GO.

The thickness of different tested membranes ranged from 75 to 100 μm, and every membrane resulted very homogeneous, with a variation in thickness of less than 2% on each sample.

5.2 FTIR

In this section FTIR has been mostly used to qualitatively verify the functionalization reaction on GO to obtain PEAGO: among the three materials used, this was indeed the less common in Professor Park's group, while Graphene, Graphene Oxide and PGO were daily produced in Hanyang Chemical Engineering laboratory and already present in literature, for example in a recent paper of Moghadam et al [199].

The spectra comparison is shown in Figure 68:

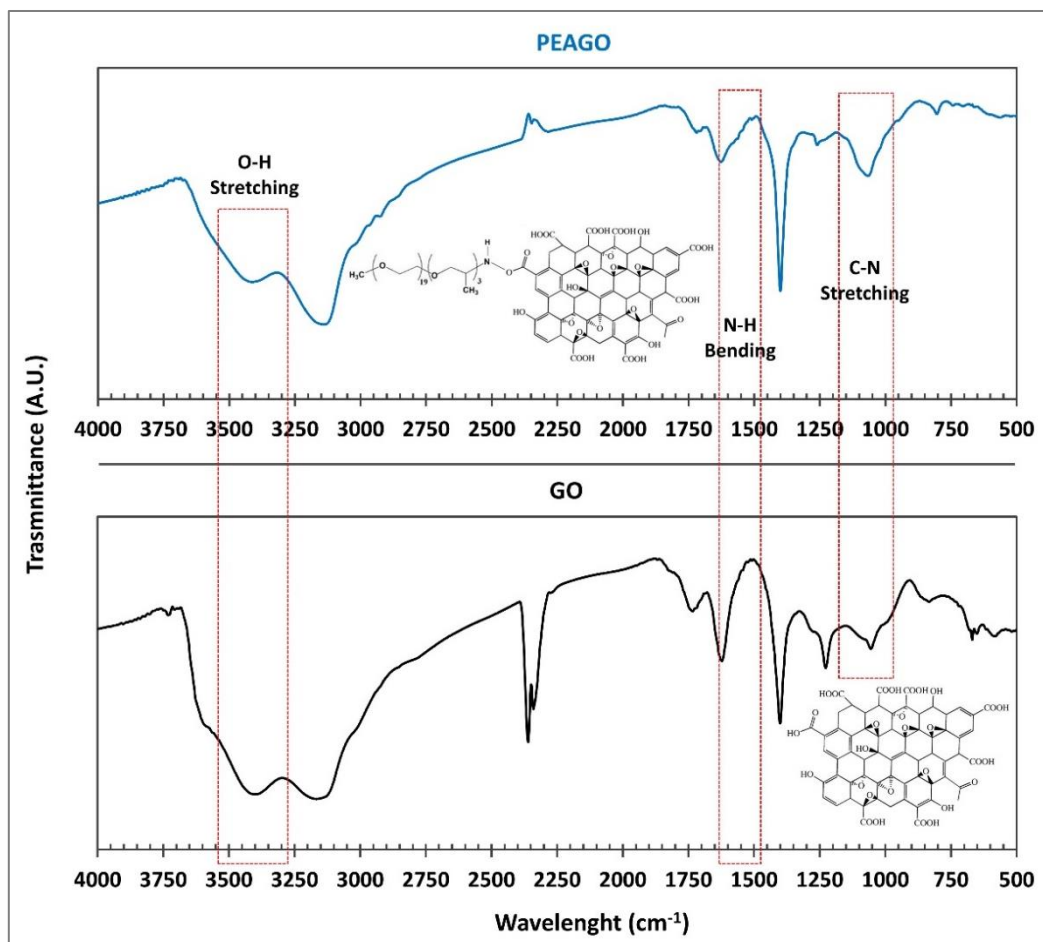


Figure 68: FTIR comparison of GO with PEAGO

It is possible to notice few little differences between GO and PEAGO spectra: first the reduction of signal at 3400 cm^{-1} , which indicate the decreasing of O-H content caused by the amino acid bond formed ; a very small almost not-visible shoulder peak at 1570 cm^{-1} , probably related to the weak N-H bending ; and lastly the increment and enlargement of the signal at 1050 cm^{-1} , most likely due to the C-N stretching.

Changes in signals weren't that impressive, still, experimental differences resulted evident: PEAGO produced had darker color, as well as different dispersion behavior in solvents.

Moreover, it has to be noted that the amount of nitrogen bonds had to be relatively low compared to the carbon bonds, since also the grafter specie, PEA, possess nitrogen only in the terminal functional group of the overall polymer.

Overall, even if a fairly high amount of PEA has been grafted, it did not bring enough heterogeneity into the structure to influence FT-IR spectra that much.

In the same way, FTIR investigation of composites have been carried out, with the result of the pristine Pebax[®]2533 compared with the highest loaded material, P2533 + 1 wt% GO, displayed in Figure 69:

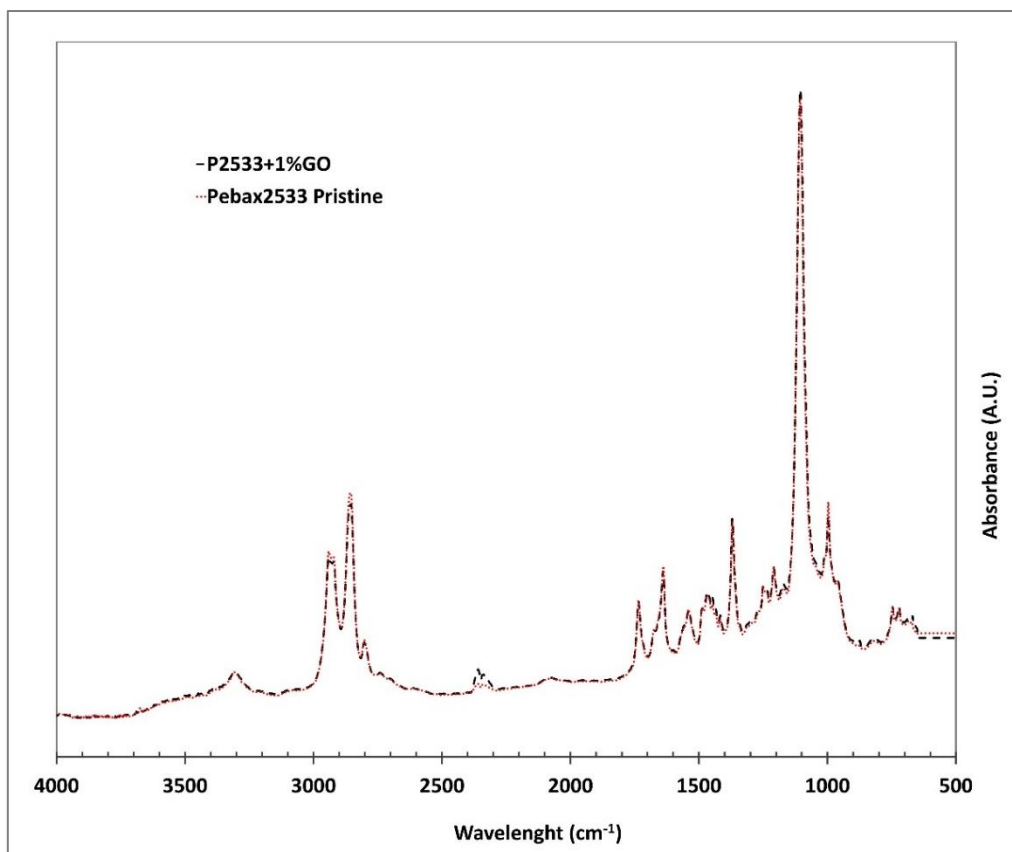


Figure 69: FTIR comparison of Pebax®2533 pristine with 1 wt% GO loaded

From the FTIR comparison, it seemed that even the highest Graphene Oxide loaded composite material (1 wt%) did not affect the analysis at all: the two spectra overlapped almost perfectly. Thus, all the other composite samples have not been analyzed through this technique.

5.3 XPS

Since the FTIR analysis was not clearly conclusive, XPS characterization has been carried out as well on PEA GO to verify the yield of the grafting reaction. The results are showed in Figure 70:

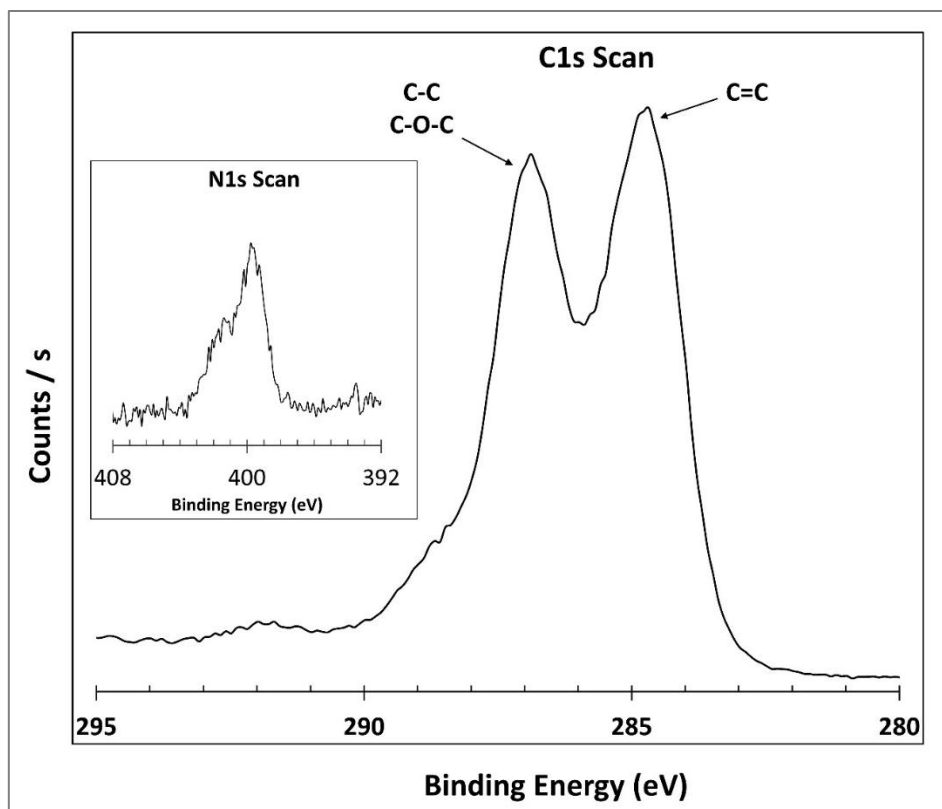


Figure 70: PEAGO XPS C1s and N1s results

From the XPS analysis, a small amount of nitrogen 1s was found into the structure, while almost negligible changes were present in the C1s region, which is consistent with the type of molecule grafted: as said above PEA already carries a low amount of nitrogen itself, so a high amount of this atom is not expected after the reaction with a nitrogen-less material like GO. XPS confirmed the nitrogen presence and therefore ensured the success of the reaction with a conversion similar to the one obtained from Yoo et al. [148] which, indeed, presented very similar XPS results.

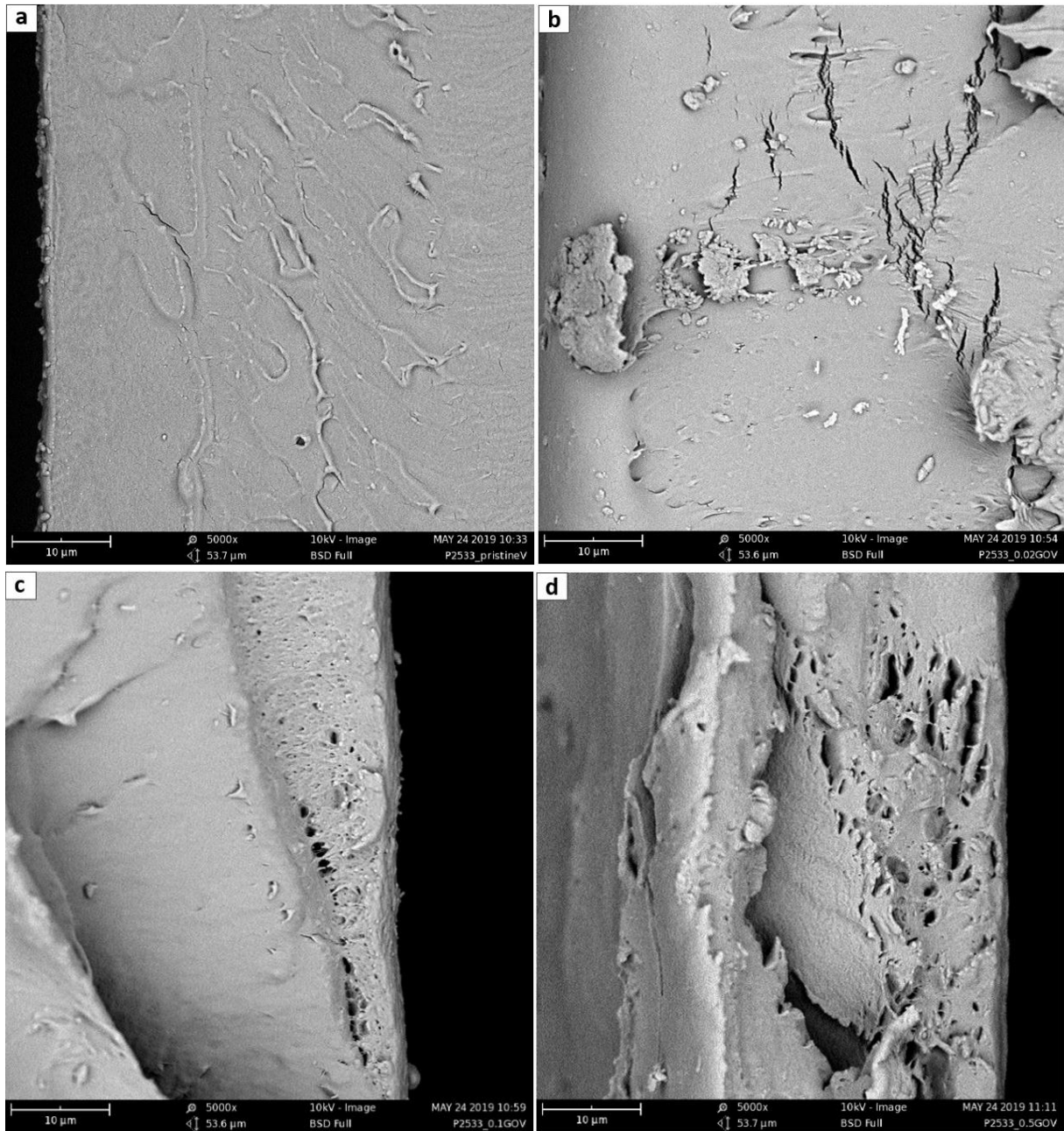
5.4 SEM

To investigate the composite membranes morphology and how it affected the gas transport results, SEM has been carried out on every membrane tested in permeation.

Through the SEM images presented below, it has been possible to view the membranes' microstructures, which may be helpful to understand material properties, including the permeation behavior.

Considering the fracture sections, reported in Figure 71, it is possible to notice from that the neat polymer fracture (71-a) is the smoothest, while the amount of imperfections increases with the rise of the GO content (71-b,c,d,e). Indeed, while neat Pebax shows a very homogeneous structure, the fractured surface of the different Mixed Matrix Membranes always present cracks likely related to nanometric defects, close to the polymer/GO interface, which were amplified during the fracture. Such defects and cracks clearly increase and become more pronounced by increasing the amount of

the filler with the 71-d and -e images, referring respectively to 0.5 and 1% GO loading, that suggest the presence of layered structure on the membrane surface induced by the presence of the filler. Considering the differences between different type of GO considered, it is worthwhile to notice that comparing images SEM-b, -f and -g, which refer to GO, PGO and PEAGO with 0.02%wt loading, the latter results have less cracks, suggesting a better interaction between the filler and the polymeric matrix.



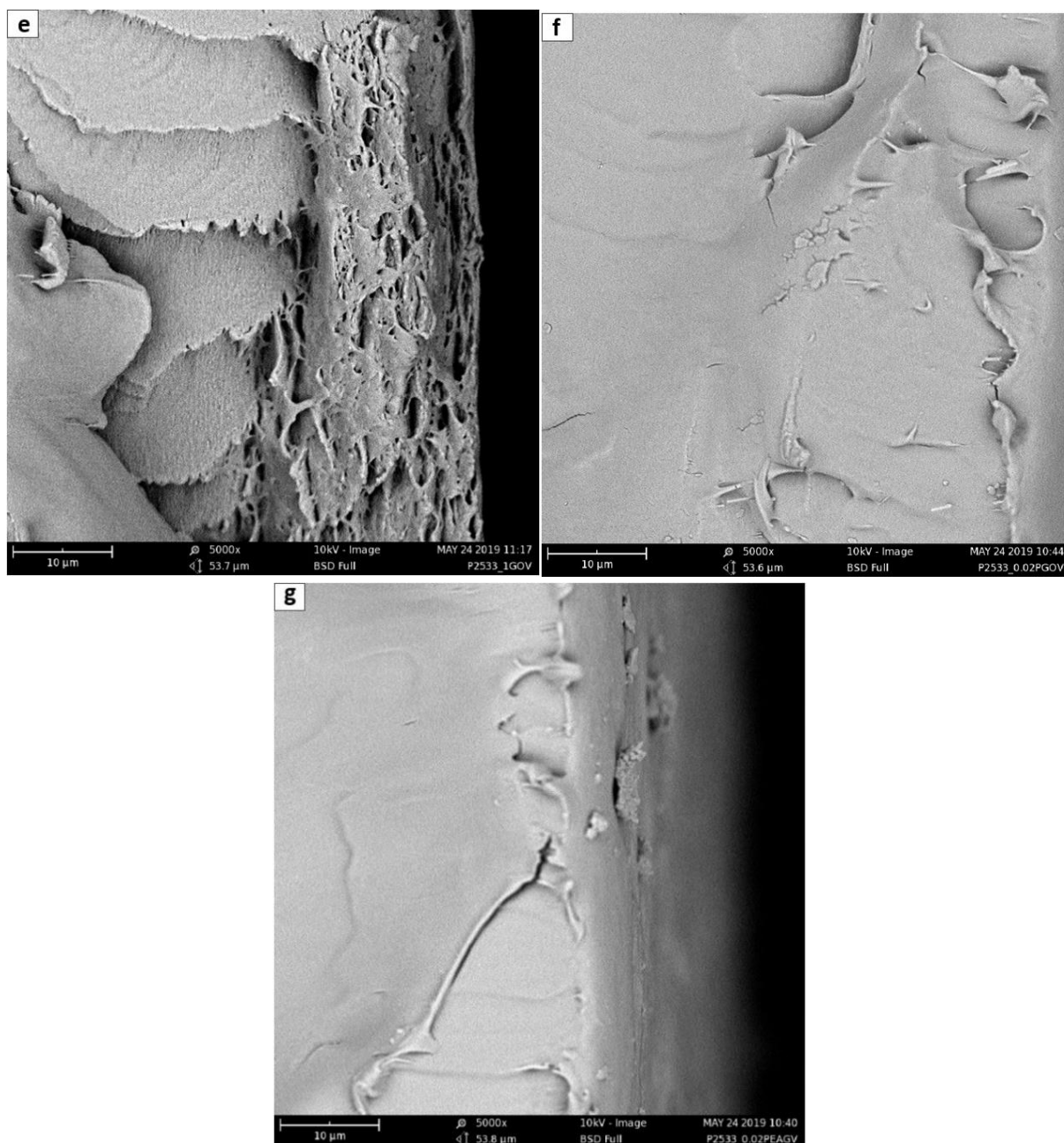


Figure 71: fracture sections 5000x SEM images of a) neat Pebax®2533 ; b) + 0.02 wt% GO ; c) + 0.1 wt% GO ; d) + 0.5 wt% GO ; e) + 1 wt% GO ; f) + 0.02 wt% PGO ; g) + 0.02 wt% PEAGO.

SEM analysis of the membrane surfaces did not give the same amount of information as the images obtained for the different composites are indeed very similar and are not showed in detail. In general, however, they provide indirect information about platelet dimension as on membrane surface, as shown in Figure 72, it is sometime possible to see the presence of the biggest agglomerated GO flakes, partially covered by the polymer; this graphene flakes present high aspect ratio with lateral dimension in the order of 10-70 μm , although with the GO synthesis method described in Section 3.1.3 it is possible to obtain a wide range of GO size, from hundreds of nanometers to some micrometers, as demonstrated by Cho et al. [200].

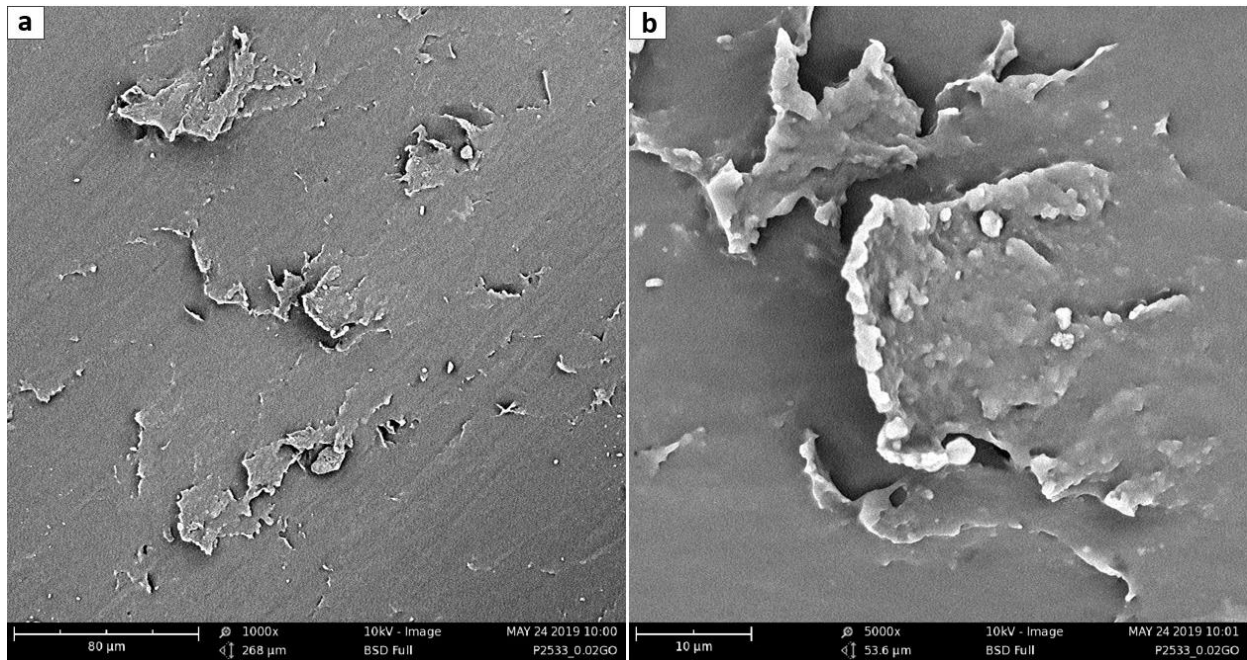


Figure 72: SEM of GO sheets trapped in Pebax®2533 matrix 1000x (a) and 5000x (b).

5.5 DSC

DSC analysis was conducted through the four cycles explained in Section 3.2.3, and below are listed the full spectra of the 4th cycle of heating (Figure 73) and, of the 3rd cycle of cooling (Figure 74), both with shifted lines for the sake of clarity.

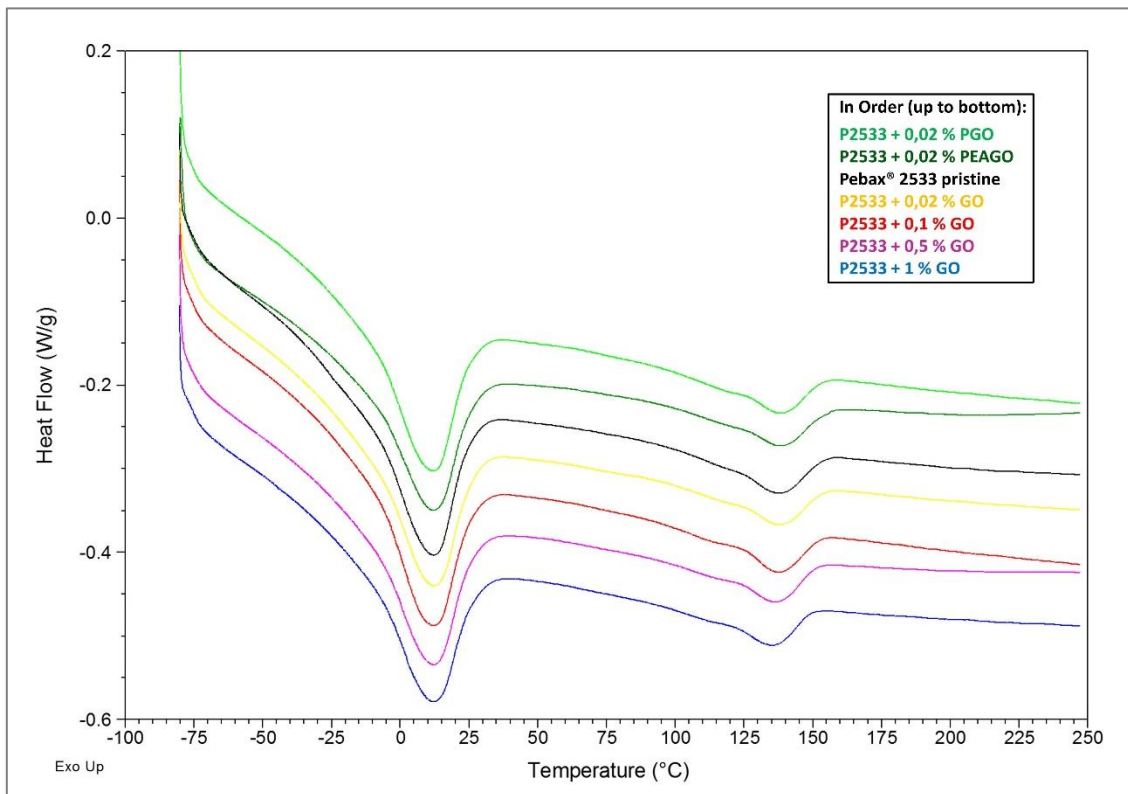


Figure 73: DSC results – 4th cycle, heating

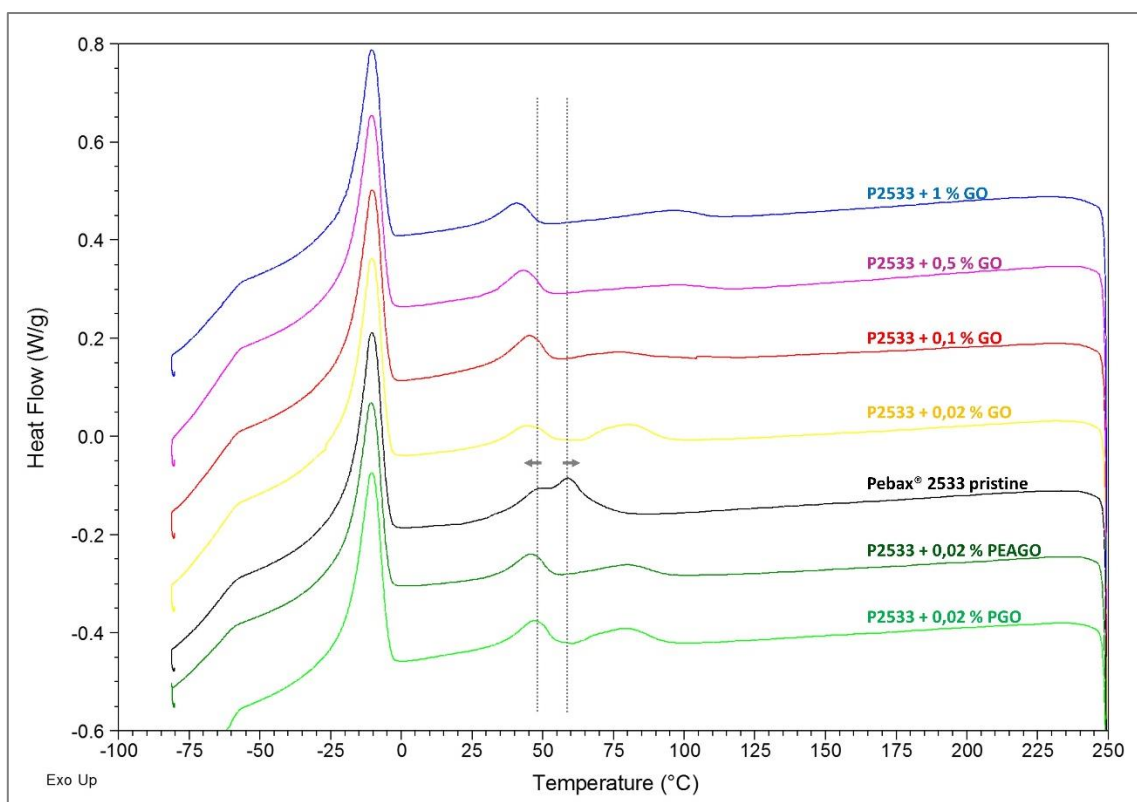


Figure 74: DSC results – 3rd cycle, cooling

In the heating cycle (Figure 73) it results clear that all the inspected materials substantially present the same behavior. The two melting peaks (at about 130°C for the polyamide-12 block and at about 10°C for polytetramethyleneoxide (PTMO) domains) are indeed very similar in all the different spectra, both for position and intensity. It seems, therefore, that the presence of GO nanofillers did not affect the amount or distribution of crystals within the copolymers.

However, looking at the cooling cycle (Figure 74), some differences are clear. Indeed, while the crystallization peak of PTMO (at about -10°C) remained substantially unaltered in every sample, the crystallization signal of Nylon, made up of two partially overlapped peaks at about 50 and 60°C, was subjected to a slight but noticeable change. The two peaks indeed shifted respectively toward lower and higher temperatures, thus becoming more and more separated as the filler loading was increased. The shift was then independent of the chemical nature of the materials as in Pebax[®]2533 loaded with 0.02% GO, two peaks moved at 45 and 80°C in almost the same positions observed respectively for the PEAGO and PGO composites with the same filler loading.

Such results suggest that the filler was mainly dispersed into the Nylon moiety, affecting its crystallization process. Nylon crystals indeed started to form at lower temperatures with respect to the unloaded polymer (as the GO was acting as nucleating agent) and completed their growth at higher temperature likely due to the increased rigidity of the loaded material, which slowed down the overall process. The platelet, however, did not compromise the completion of the crystallization, nor the structure of the crystals since, as stated above, the melting signals (Figure 73) remained substantially unchanged.

5.6 Permeation

Figure 75 shows the results of the permeation tests in the Pebax[®]2355 MMMs obtained with different loading of GO. The addition of Graphene Oxide seems to substantially decrease the permeability for both CO₂ and N₂. Indeed from 0.02 wt% GO to 1 wt% the Pebax-based MMMs show lower and lower permeability with a decrease from 365 to 51 Barrer for CO₂ and from 15 to 2 Barrer for nitrogen. The only exception in the observed trend is possibly represented by the composite with the lower loading, which indeed showed a very limited increase for CO₂ permeability (371 Barrer with respect to the 365 Barrer measured for pristine Pebax). Similar behavior was already observed also in a previous work made by Lee et al. that were able to improve the permselective properties of polymer matrix Pebax[®]1657 loaded with “ZPGO” (that is ZIF-8 grown on Porous graphene oxide), by employing such low filler concentration [201]. In the present case, however, the difference observed is too limited, within 2 %, to conclude that the observed increase is real and not due to an experimental uncertainty, which was also in the order of 2 %, considering thickness variation in the membranes and uncertainty in the experimental tests.

The observed decrease in permeability at “high” loading, on the other hand, was somewhat expected as GO platelets tend to increase the tortuosity of the diffusion path within the membrane, as schematized in Figure 76, due to their high aspect ratio and their low intrinsic permeability [63]. This type of effect seems also confirmed by the SEM images previously analyzed, where layered structures were clearly visible when the Graphene Oxide concentration increased within the matrix.

By comparing the CO₂ and nitrogen permeability, membrane selectivity can be obtained which is also presented in Figure 75 as a black line. Interestingly this parameter resulted substantially unaffected by the addition of the filler, somewhat in contrast with the expected behavior since GO is usually considered to be selective towards CO₂ and already proved to be able to improve polymer selectivity when used to obtain mixed matrix membranes [146,177–182].

In the present case, instead, no substantial changes in CO₂/N₂ selectivity were observed, as this parameter indeed remained very close to 24 for all the materials tested, so that GO seemed to behave as an impermeable filler which reduced the permeability merely because of tortuosity effects without affecting the permselective behavior of the polymer.

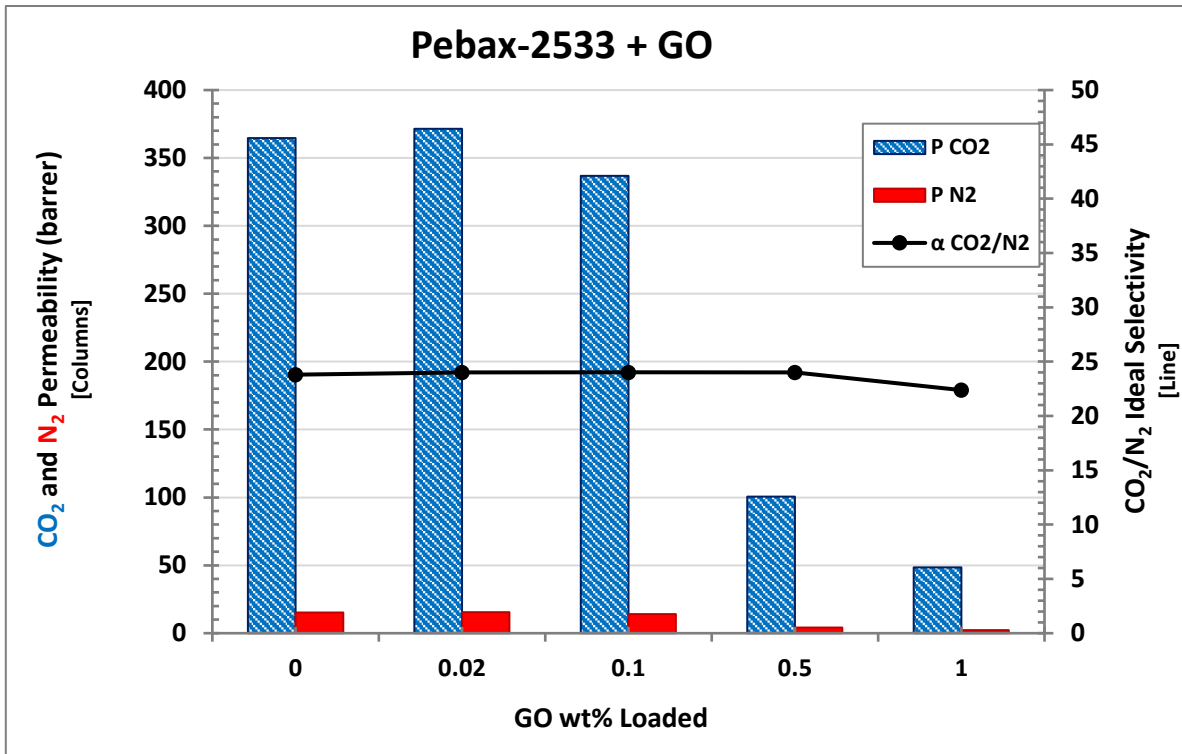


Figure 75: CO₂/N₂ Permeability and Ideal Selectivity of Pebax[®]2533 with different GO loadings

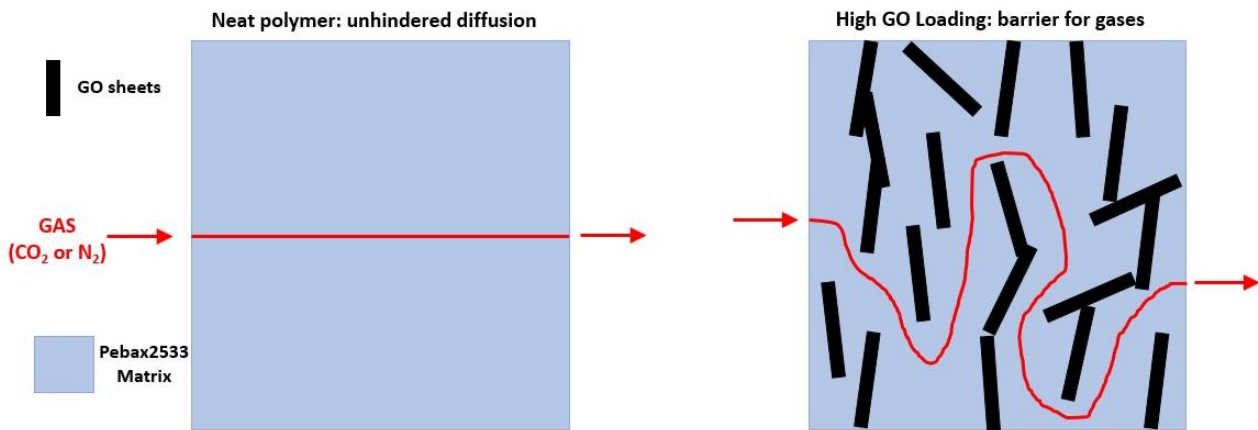


Figure 76: Graphene Oxide barrier behavior concept.

In order to test different GO-based fillers behavior, Pebax[®]2533 membrane also mixed with PEAGO and PGO have been tested, all of them compared with 0.02 wt% loading which, based on GO analyses, resulted in being the most promising in terms of permselective properties. The results are shown in Figure 77 where the permeability of CO₂ and N₂ in PGO and PEAGO nanofiller are reported together with those already discussed of pristine Pebax and 0.02 wt% GO membrane that are repeated for the sake of clarity.

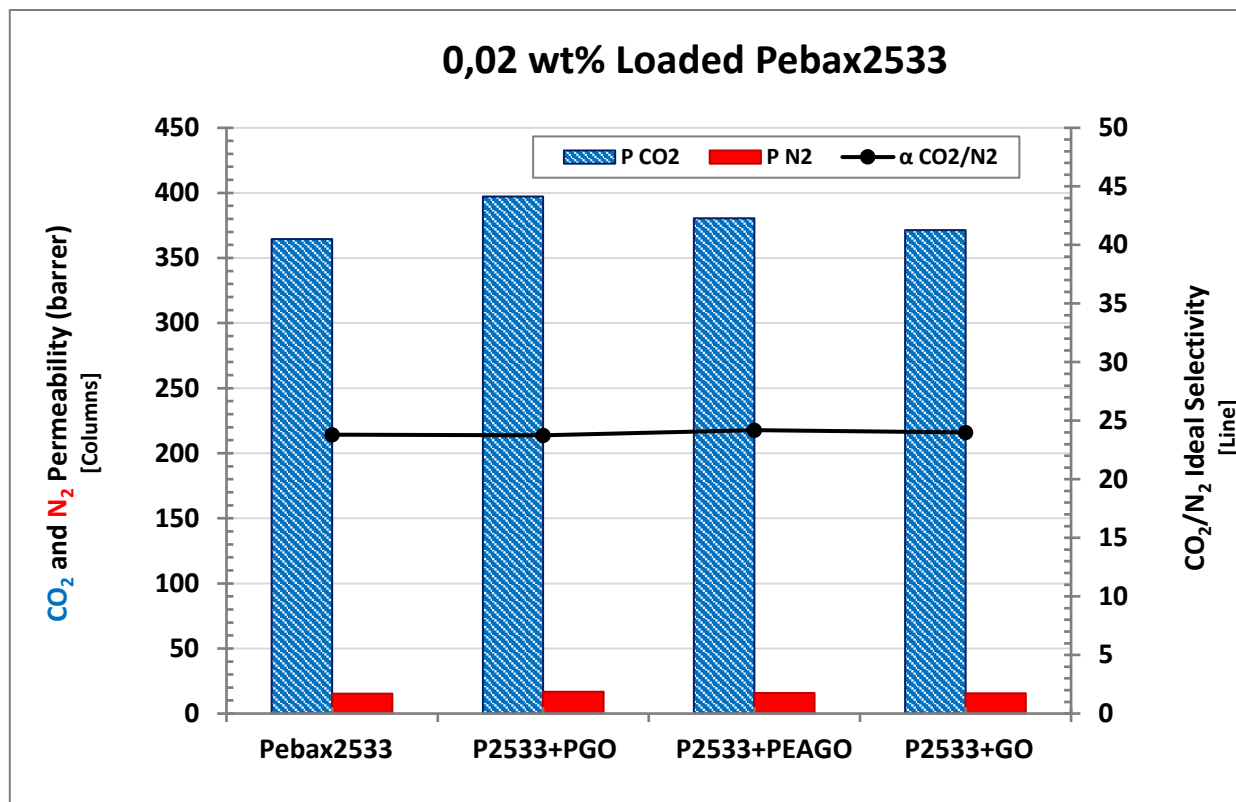


Figure 77: CO₂ Permeability of Pebax®2533 filled with 0.02 wt% of different GO-based materials.

Interestingly both PEAGO and PGO slightly improved permselective properties with respect to the base polymer with differences between 4 and 8 % (that is higher than the recognized experimental error). CO₂ permeability in particular reached the value of 380 Barrer in PEAGO loaded sample, and increased even more in PGO loaded Pebax, where it reached 397 Barrer. CO₂/N₂ selectivity, on the other hand, resulted still unaltered remaining very close to 24 also for the last two samples inspected. Such an increase in permeability without any effect on selectivity cannot be explained by gas platelet interaction which would favor CO₂ with respect to nitrogen, so that it seems to be related to the presence of a lower density region (possibly related to poor interfacial adhesion or less efficient polymer packing) at the polymer–filler interface where the permeating gases, both CO₂ and N₂, can permeate at a higher rate, thus reducing the time to cross the membranes without altering the relative selectivity, as already suggested by various authors [65,101,202–204]. A schematic concept of this hypothesis is displayed in Figure 78.

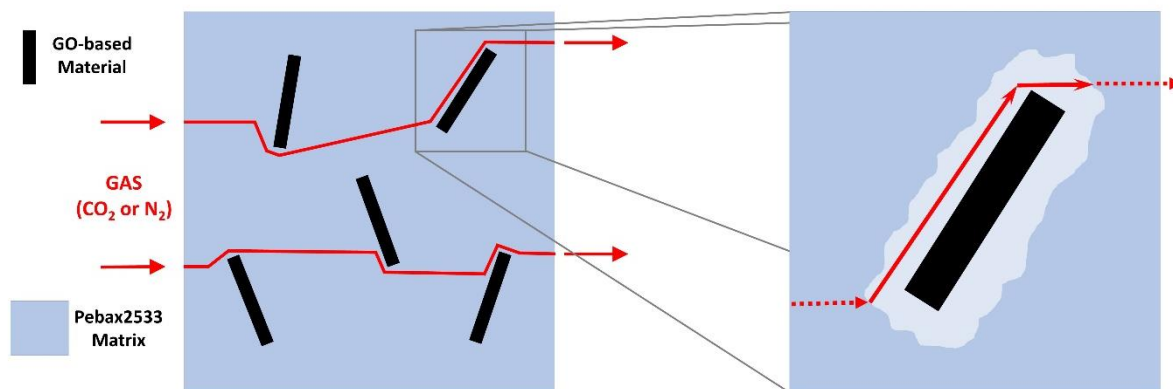


Figure 78: GO materials – Pebax Interface voids concept.

From this point of view, the performance differences among the three GO materials at the same low concentration (0.02 wt%) are probably related to the dispersion of the different types of GO in the matrix, which influences both the increase in tortuosity and the properties of the interfacial region. These two processes indeed have opposite effects on permeability, and their balance gives the final materials properties. In the present case, the observed behavior could be explained by considering that, very likely, two modified GOs have lower aspect ratio with respect to the pristine one, due to the additional harsh treatment that the original materials had to undergo to be modified.

Porous graphene oxide is indeed well known to have reduced area compared the pristine GO and also a higher amount of defects, which makes the nanofiller intrinsically more permeable: Lee et al. [201] demonstrated the formation of pores upon GO, and most likely, such treatment was also able to partially fracture the sheets themselves. On the other hand, fragmentation of GO platelet during PEAGO synthesis can likely be related to the presence of intensive mixing and sonication, which could produce mechanical stresses able to break GO and PEAGO sheets, as demonstrated also by Baig et al. [205].

The difference between PGO and PEAGO could be related to the presence of ether-based polymer chains grafted to the latter, which can lead to a better interaction with the Pebax matrix, slightly decreasing the interfacial voids compared to PGO and thus causing a smaller effect on permeability.

Finally, the limited changes observed among different materials can be related to the fact that, as suggested by DSC results, the fillers were preferentially dispersed in the Nylon moiety, which was less abundant and also less involved in gas permeation compared to PTMO; the features of the latter phase, which is also the main one responsible for the CO₂/N₂ selectivity, indeed remained substantially constant in the DSC chart. Thus, by analyzing both DSC and the interface theory previously explained, the obtained permeation results turned out to be consistent.

In general, however, even if slight improvements have actually been obtained, especially with the addition of PGO, the overall permeation properties of the Pebax[®]2533-modified GO were not good enough to overcome current state-of-the-art materials, and remained below the 2008 Robeson's upper bound which, for a CO₂ permeability of 400 Barrer, demands a selectivity with respect to nitrogen above 50 to be overcome [57]. On the other hand, the results show the possibility to obtain homogeneous dispersion of nanofiller in the polymeric matrix, thus opening the path for further optimization aimed at increasing not only permeability but also CO₂ selectivity of the obtained MMMs.

To clearer summarize permeation results, they are all listed in following Table 10, along with variation in percentages

Table 10: Summary and variation in percentage of permeation results.

| Membrane | CO ₂ Permeability (Barrer) | CO ₂ Permeability Variation% | N ₂ Permeability (Barrer) | N ₂ Permeability Variation% | CO ₂ /N ₂ Selectivity | CO ₂ /N ₂ Variation% |
|-------------------------|---------------------------------------|---|--------------------------------------|--|---|--|
| Pebax [®] 2533 | 364.61 | \ | 15.32 | \ | 23.80 | \ |
| + 0.02 % GO | 371.39 | 1.86 | 15.47 | 1.01 | 24.00 | 0.84 |
| + 0.1 % GO | 336.80 | -7.63 | 14.02 | -8.47 | 24.02 | 0.92 |
| + 0.5 % GO | 100.61 | -72.41 | 4.19 | -72.65 | 24.01 | 0.88 |
| + 1 % GO | 48.58 | -86.68 | 2.17 | -85.83 | 22.38 | -5.97 |
| + 0.02 % PGO | 397.35 | 8.98 | 16.73 | 9.19 | 23.75 | -0.19 |
| + 0.02 % PEAGO | 380.44 | 4.34 | 15.73 | 2.65 | 24.19 | 1.64 |

6) Results and Discussion: Benzoyl-P2533

In this chapter all the results, of the modified material “Benzoyl-P2533” (BP2533) will be discussed: after discussing the physical changes due to the reaction, chemical analysis will be analyzed in order to investigate the substitution degree, both qualitatively and quantitatively.

Lastly, gas permeation test will be illustrated, and divided in two sections: one regarding the permeability test, conducted on thick membranes obtained through solvent casting technique; and another about the permeance test, conducted on thin coated membranes too thin to evaluate the thickness.

6.1 Product Physical Change

Physical behavior of the Benzoyl-P2533 definitely changed with respect to the pristine polymer: the product of the most aggressive protocols (#3, #4, #5 and #6) resulted to be elastic, as well as sticky to different types of surfaces, metal, glass, PE.

Such more rubber-like behavior is probably due to the loss of hard Nylon segments which were not be able to crystallize nor to make hydrogen bond after the reaction.

For these reasons it has not been possible to make permeation test on the fully substituted material, since it was almost impossible to be handled. In solvent casting technique, the thick membrane obtained has to be manually peeled, positioned and masked, but being extremely sticky and elastic, BP2533 fully substituted was not possible to be manually prepared to make a thick self-standing membrane for laboratory scale permeation test. This represent one example where an automatized industrial-scale procedure would be actually far more feasible and ease to be carried out compared to the lab-scale one.

Thus, the 70 mol% substituted has been used for permeation test, both thick membranes from solvent casting, and also spin coated for to make a direct comparison. Such material resulted indeed particularly suitable for coating technique.

Before the permeation tests however to verify the reaction achievement and the substitution degree, thorough chemical characterizations of the materials have been conducted, as shown in the next sections.

6.2 FTIR

The results of FTIR tests are reported in Figure 79, where the spectra of the polymers obtained through the six protocols are shown together with the one of the neat Pebax[®]2533. In the spectra of the pristine polymer very clear peaks can be observed as the one at 3300 cm⁻¹ related to N-H stretching, the doublet with peaks at 2925 and 2850 cm⁻¹ related to C-H stretching, and the one at 1100 cm⁻¹ related to C-O stretching.

In the different BP2533 spectra several new peaks appear, while other tends to vanish, with different intensity depending on the reaction protocol considered. The most clear and visible modification is surely the reduction of the N-H peak previously mentioned due to the progressive substitution of the secondary amine in the pristine polymer with the benzoyl group. In addition to that, new peaks are

visible at 1690 cm^{-1} , most likely related to the amide $\text{C}=\text{O}$ bond of the new carboxyl attached to the nitrogen and at 700 cm^{-1} and 800 cm^{-1} , related to the aromatic $\text{C}-\text{H}$ bending out of the benzene ring plane [198]. All the mentioned signals have been confirmed by the IR spectra of Benzoyl Chloride from NIST [206] therefore confirming the success of the substitution reaction in the different protocols.

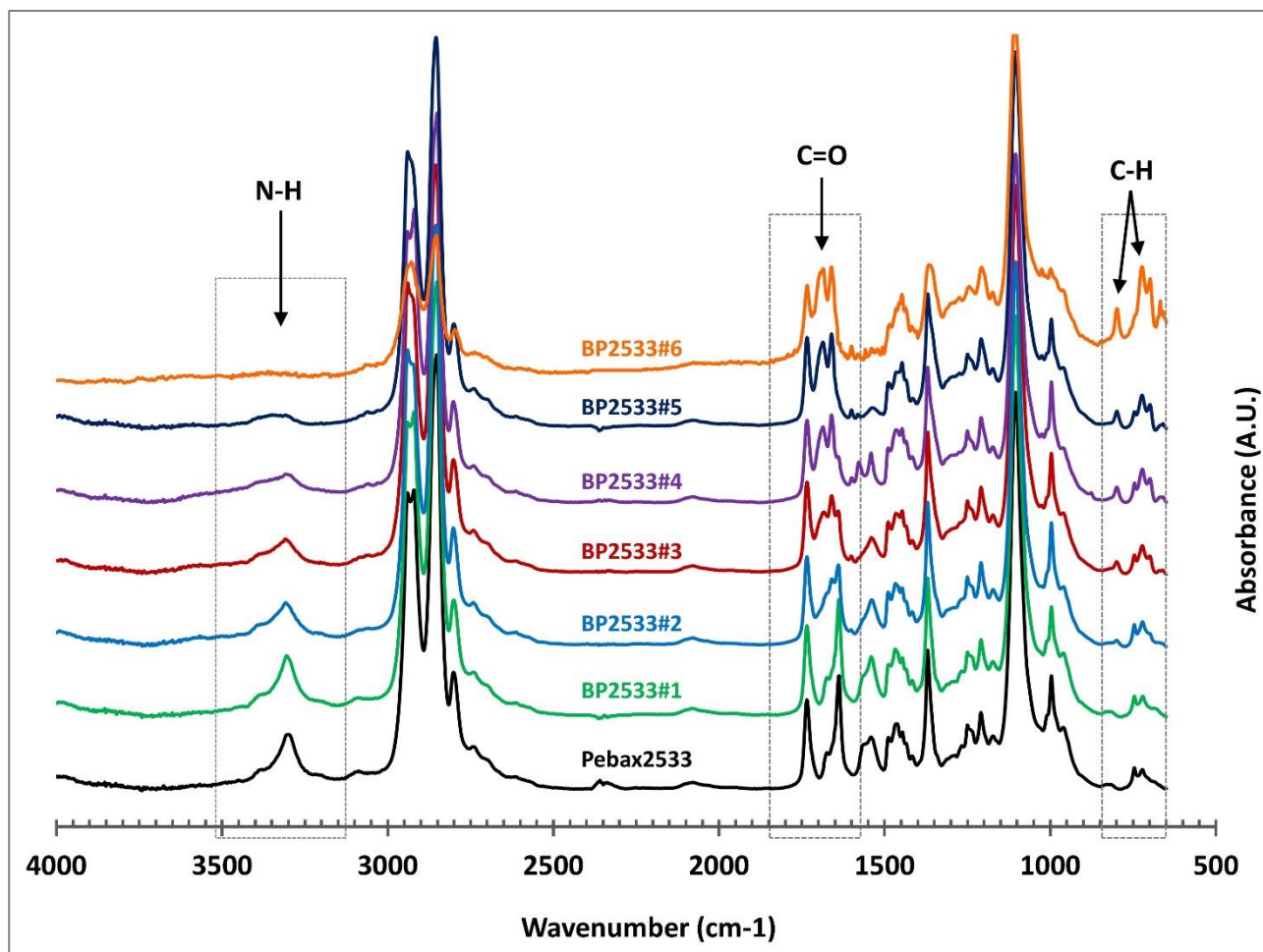


Figure 79: Different BP2533 protocols FTIR results

In particular observing the different spectra it is already possible to obtain qualitative information about which protocol has led to a higher yield of the reaction. As an example, BP2533#1 spectra, the mildest protocol among the six, appeared to be almost the same as the one of the neat materials thus suggesting that no or very little group have been substituted during the reaction.

The signal of $\text{N}-\text{H}$, on the other had clearly decreases in all the other products and overall, its intensity appears to follow the order $\text{P2533} = \text{BP2533\#1} > \text{BP2533\#2} > \text{BP2533\#3} > \text{BP2533\#4} > \text{BP2533\#5} > \text{BP2533\#6}$, showing that the reaction yield increases going from batch 1 to batch 6 following, as expected, the increase of concentration of the benzoyl chloride in the reaction environment and the increase of the reaction temperature and/or time. In particular the $\text{N}-\text{H}$ related signal (at 3300 cm^{-1}), which is already rather small in BP2533#4 and #5, seems to vanish in BP2533#6, which should be therefore very close to complete substitution.

6.3 $^1\text{H-NMR}$

To verify the quantitative yield of substitution, $^1\text{H-NMR}$ analysis has been conducted, and as example Pebax[®]2533 neat and a high substituted product BP2533#5 are shown in Figure 80 and 81, reporting the full spectra plus the zoom in the aromatic range (from about 7 to 8 ppm):

First of all, as further confirmation of the well achieved reaction, in the aromatic range of the spectra it is possible to see three signals, which is in line with the structure of the group inserted: the ortho and meta hydrogens of the benzene, indeed, are symmetric, forming overall one signal each, while the third signal is related to the para hydrogen.

On the quantitative side, the total five aromatic hydrogens have been taken into account to integrate the signal (Figure 82, $\text{H}^{(20)}$, $\text{H}^{(21)}$, $\text{H}^{(22)}$, $\text{H}^{(23)}$, $\text{H}^{(24)}$) since they occurred close to each other and with low intensity, which makes sense considering that the reported mass ratio is 80/20 PTMO/Nylon, with the theoretical mole ratio even lower: about 91/9 PTMO/Nylon.

Such sum of signals has been compared with the signal of the four outer hydrogens of the polytetramethylene oxide block (Figure 82, $\text{H}^{(14)}$ and $\text{H}^{(17)}$), visible at 3,50 ppm, that form a very intense single signal, due to the symmetry. These have been preferred because the signal is cleaner and without interferences or shoulders, compared to the other four inner hydrogens, which integrates at 1,60 ppm.

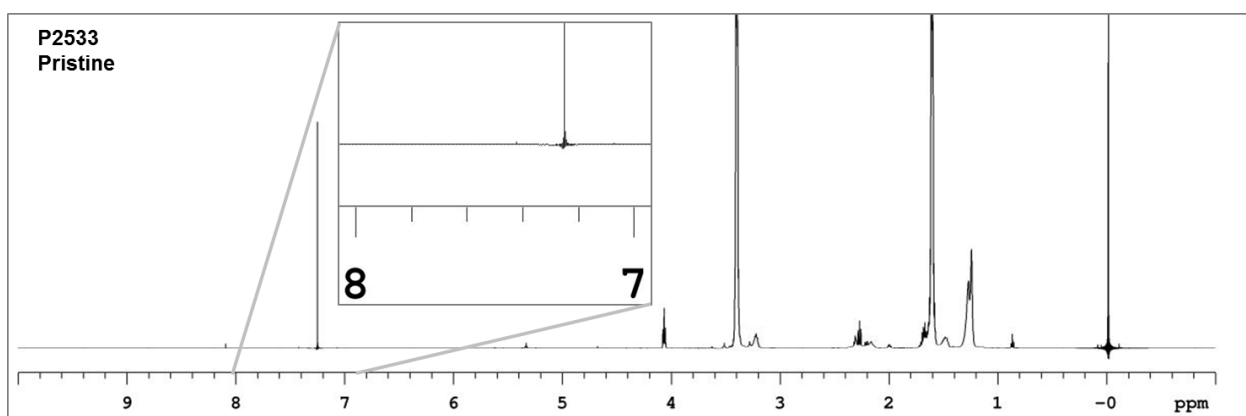


Figure 80: Pebax[®]2533 pristine $^1\text{H-NMR}$ spectra, with zoom in aromatic range

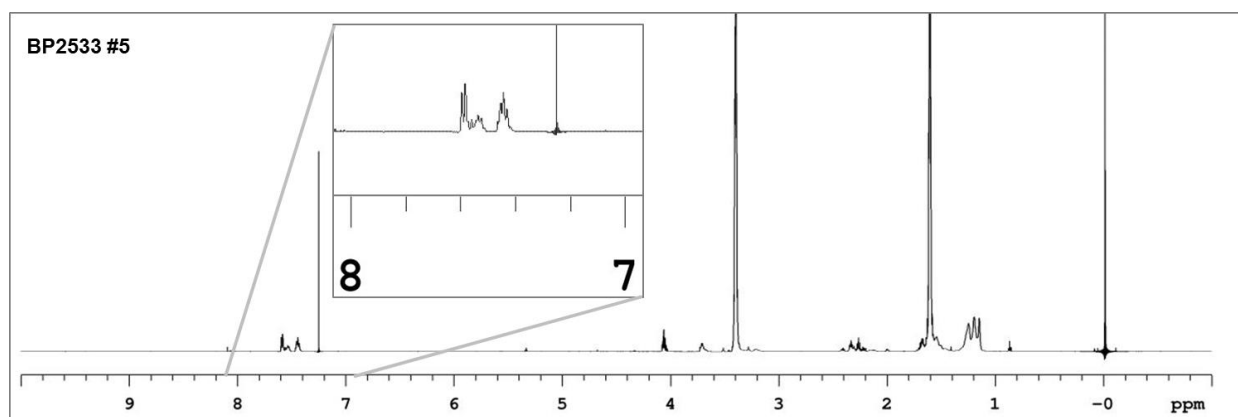


Figure 81: Benzoyl-P2533 #5 (70% substitution degree) $^1\text{H-NMR}$ spectra, with zoom in aromatic range

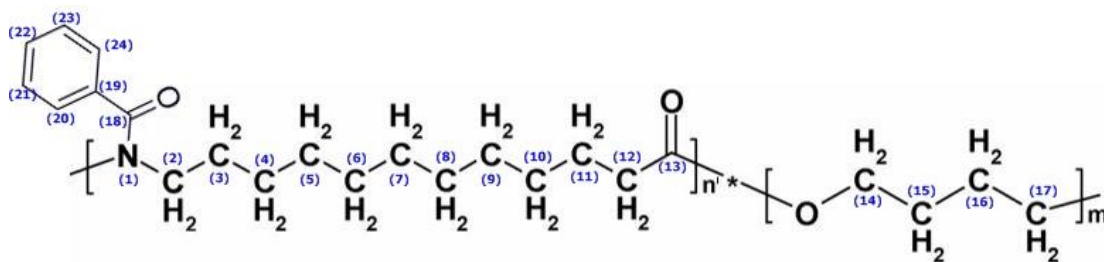


Figure 82: Benzoyl-P2533 structure, with numbered atom for reference

Table 11: Summary of BP2533 molar substitution degree % 1H-NMR results

| Material | ppm H CH ₂ PTMO (H ^{15,16}) | ppm H Ar Nylon (H ^{20,21,22,23,24}) | Molar Substitution degree % |
|-------------------------|--|---|-----------------------------|
| Pebax [®] 2333 | / | / | / |
| BP2533#1 | / | n.d. | 0 |
| BP2533#2 | 3,40 | 7,40-7,65 | 25,33 |
| BP2533#3 | 3,40 | 7,40-7,65 | 41,67 |
| BP2533#4 | 3,40 | 7,40-7,65 | 65,73 |
| BP2533#5 | 3,40 | 7,40-7,65 | 67,57 |
| BP2533#6 | 3,40 | 7,40-7,65 | 98,62 |

From the integration, it was then possible to calculate the reaction yield which is reported in Table 11 for the different materials. It is possible to notice that the substitutions obtained resulted to be in line with the FTIR spectra evaluations: for the mildest protocol #1, no aromatic signal have been detected; while for the others, all of them follow the N-H signal's intensity of the FTIR spectra previously presented in Figure 79, with the molar substitution resulted in this order:

BP2533#1 < BP2533#2 < BP2533#3 < BP2533#4 < BP2533#5 < BP2533#6

The last three protocols showed the highest substitution yield: #4 and #5 resulted 65,7% and 67,6% respectively, while #6, as already hypothesized, resulted basically fully substituted, with a yield of 98,6%.

Using Figure 83, displaying the Pebax materials structure provided by Arkema [155], as molecular weight reference calculation, the experimental mass ratio resulted very similar to the reported one: 78,6 wt% Polyamide12 and 21,4 wt% PTMO (instead of 80/20), for the analyzed Pebax[®]2533.

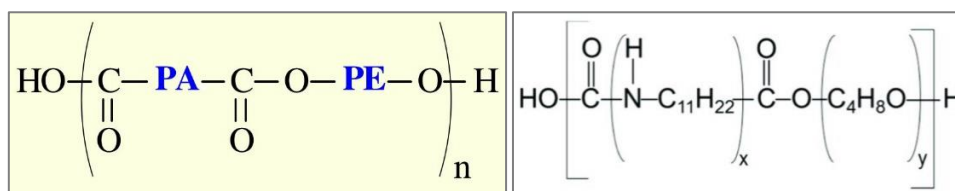


Figure 83: Pebax materials structure (left) [155], and Pebax[®]2533 structure (right)

6.4 TGA

To investigate thermal properties of the materials obtained, and to verify the presence of low molecular weight impurities such like residual solvents or reagents, TGA was conducted, on the different samples with results shown in Figure 84.

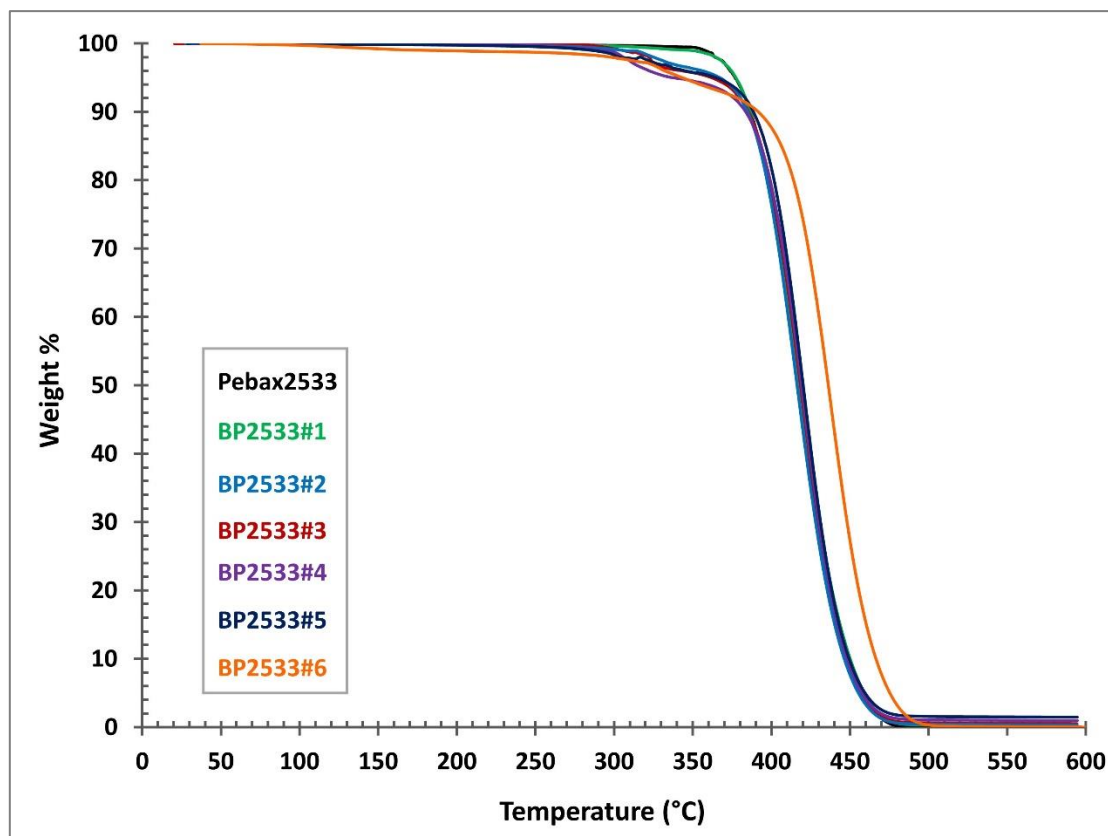


Figure 84: TGA results

From Figure 84 It is possible to notice that Pebax[®]2533, along with the protocol #1 (0 mol% substitution material), start to degrade at 360°C.

The substituted part degrades at lower temperatures, around 275°C, and such weight loss is consistent with the substitution degree: higher substituted samples, from #1 to #6, showed higher weight loss between 275 and 360°C, with 0 wt% loss for sample #1, to 7 wt% for sample #6.

It's also interesting to notice that the fully substituted sample #6 exhibits a notable change in the polymer main chain degradation from 360°C, having it shifted of about 20°C higher, easily notable especially during the degradation after 400°C.

For the final possible applications, such material proved to not have particular thermal limitations for the most common polymeric membrane separation processes, that are usually far below 200°C.

6.5 DSC

To check the thermal properties and evaluate the degree of crystallinity of the two polymeric blocks, DSC analysis have been conducted. In Figure 85 are displayed 3° cooling and 4° heating cycles of all the product investigated:

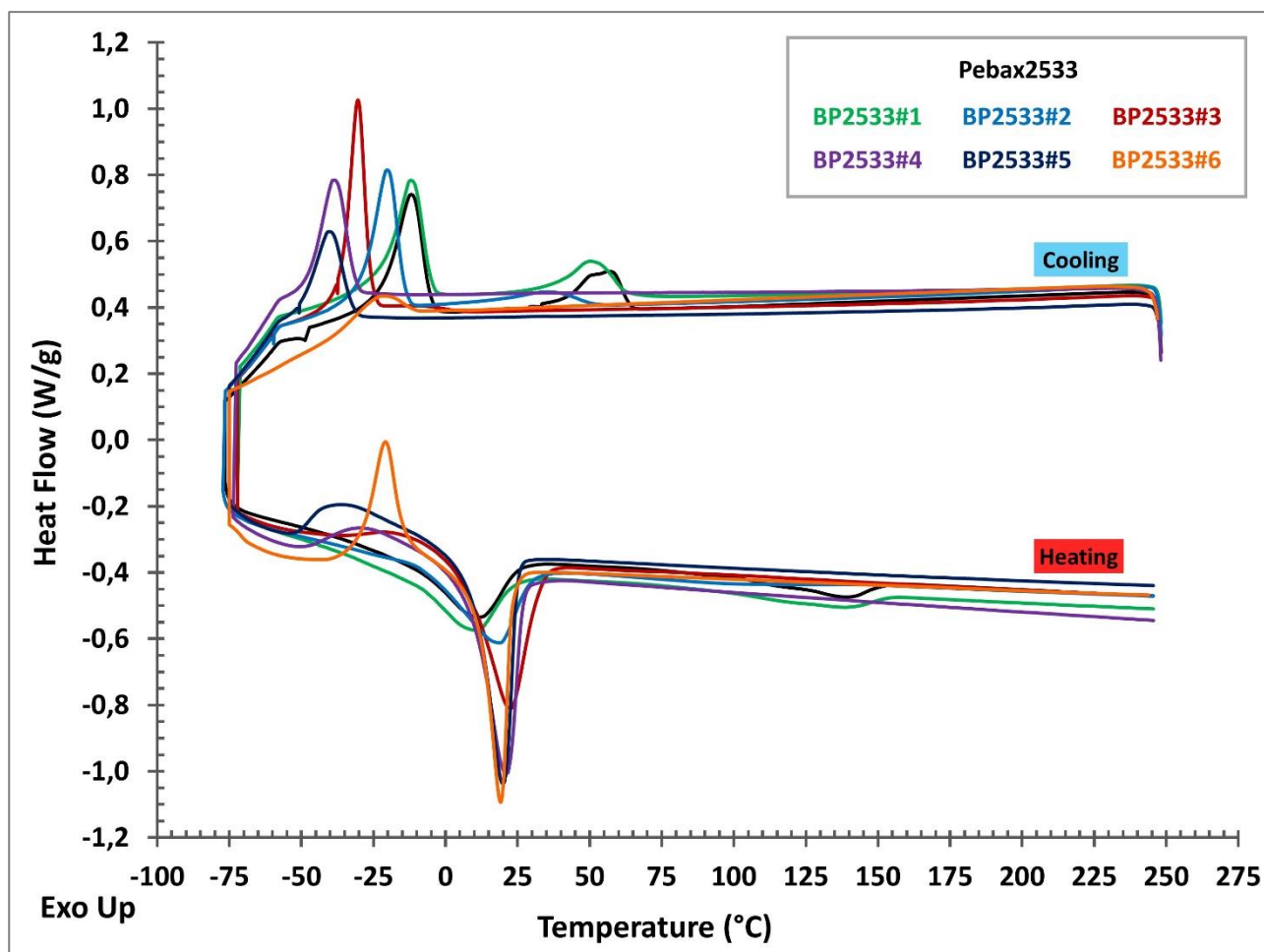


Figure 85: DSC Results

In Figure 85, for the pristine Pebax[®]2533 it's possible to observe, as attend, the crystallization and fusion peaks for both Nylon12 (about 55°C and 140°C, respectively) and PTMO blocks (about -10°C and 10°C, respectively).

Thus, the melting point of Nylon12 resulted lower than how reported in literature, usually around 180°C [207–211].

Such difference is most likely due to the molar weight, which is particularly low as already pointed out before, and also because the overall amount of nylon in the material is low as well.

Nylon12 crystallization and fusion signals are visible only in the pristine material and protocol #1 samples, while from protocol #2 (with a molar substitution of 25%) and above, basically no Nylon

fusion peak occurred. This behavior is due to the insertion of the benzoyl group that, by decreasing the structural order, prevents the crystallization of the polyamide macromolecular chains.

Another peculiar trend is that the crystallization signals fall at lower temperatures when the substitution of benzoyl occur (from sample #2 and above), and such materials complete their very crystallization in the successive cycle 4 of heating.

Such slowing down of the crystallization process with the increment of the substitution may be due to the hindering group inserted, decreasing the polymer chains' mobility so that they required more time to arrange in crystals. Another reason may be the loss of Nylon12 hydrogen bonds, which by reducing the free volume acted as a nucleating agent for the PTMO block. Such phenomena increase the free volume available of the macromolecular chain of PTMO that require more time to be reorganized in phase crystals.

Indeed, the crystallization of PTMO required longer time with the increment of the substitution: from protocol #3 and above crystallization signals appeared also in the fourth cycle, (heating), at the same temperature of the third cycle (cooling), meaning that during the cooling step they crystallized but not totally, then they finished the process in the following cycle, phenomena that did not occur with the pristine material or low substituted ones (#1 and #2), while instead is extremely emphasized in the full substituted sample #6.

The increment of PTMO crystallization with the substitution, from 19% for the pristine to a maximum of almost 35%, is due to the overall increment of free volume disposable for such moiety, that can rearrange more freely without the physical block of the Nylon12 crystals or hydrogen bonds, reaching higher crystallization degree. It seems that such behavior affected the crystallization until a substitution degree of around 40% (protocol #3), where a 32% crystallinity is already gain, and from this point to the fully substituted material (#6) it increases of less than 3%.

To calculate the integrals of the peaks, signals of 4° cycle of heating have been chosen, while the melting heat references employed were 209,3 J/g for 100% crystalline Nylon12 [212], and 167,0 J/g [213] for 100% crystalline PTMO.

The percentage amount of crystal phases was calculated by the following Equation 28:

$$Crystallinity_i\% = \frac{\Delta H_i^{m_{exp}}}{\Delta H_i^{m_0} \cdot y_i} \cdot 100 \quad (28)$$

Where i is one of the two moieties (Nylon12 or PTMO), $\Delta H_i^{m_{exp}}$ was the melting enthalpy obtained experimentally, $\Delta H_i^{m_0}$ the mantling enthalpy of a 100% crystalline compound i , y_i was the mass fraction in the polymer obtained from NMR (0,214 for Nylon12 and 0,786 for PTMO).

Detailed results of the elaboration are listed in Table 12 below:

Table 12: DSC integral results

| Sample | T peak PTMO (°C) | ΔH peak PTMO (J/g) | T peak Nylon (°C) | ΔH peak Nylon (J/g) | Ratio Peak P/Ny | Cryst degree PTMO (%) | Cryst degree Nylon (%) |
|--|------------------|--------------------|-------------------|---------------------|-----------------|-----------------------|------------------------|
| Pebax[®] 2533 Pristine | 11,3 | 25,3 | 138,2 | 8,3 | 0,33 | 19,3 | 18,6 |
| Benzoyl P2533 #1 | 10,1 | 24,0 | 137,4 | 8,3 | 0,34 | 18,3 | 18,5 |
| Benzoyl P2533 #2 | 18,6 | 27,7 | - | - | - | 21,1 | - |
| Benzoyl P2533 #3 | 22,6 | 42,4 | - | - | - | 32,3 | - |
| Benzoyl P2533 #4 | 21,1 | 43,4 | - | - | - | 33,0 | - |
| Benzoyl P2533 #5 | 19,9 | 42,7 | - | - | - | 32,6 | - |
| Benzoyl P2533 #6 | 19,1 | 45,8 | - | - | - | 34,9 | - |

6.6 Permeability – Gas Transport Characterization

Gas transport characterization have been conducted using CO₂, N₂, CH₄, He and O₂, in single gas permeation experiments as described in Section 3.4.

Due to its stickiness and difficulty to be handled, it has been impossible to make testable self-standing fully substituted BP2533#6 membranes, thus, a compromise between substitution and feasibility have been chosen: the materials tested were Pebax[®]2533 pristine as reference, and BP2533 obtained using a protocol #5, with a molar substitution of about 70%.

In Figure 86 the overall permeability results of tested gases are shown, while in Figure 87 the ideal selectivity to CO₂ is reported.

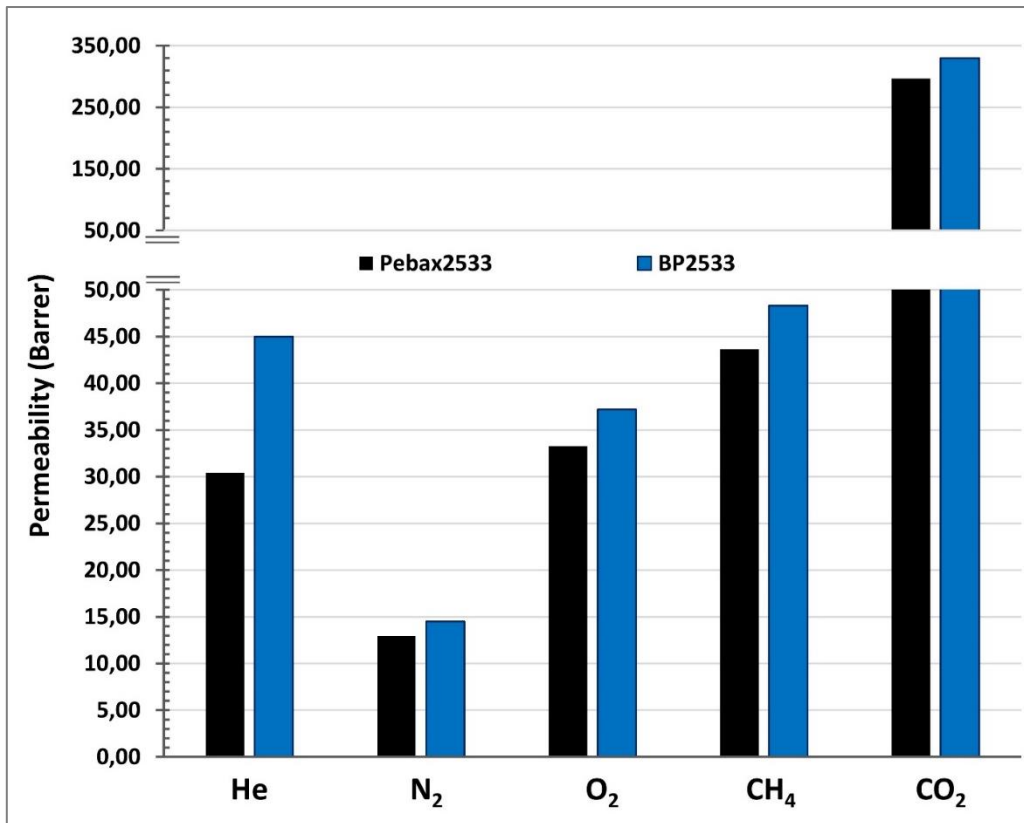


Figure 86: Pebax®2533 and Benzoyl-P2533 (70 mol%) Permeability results

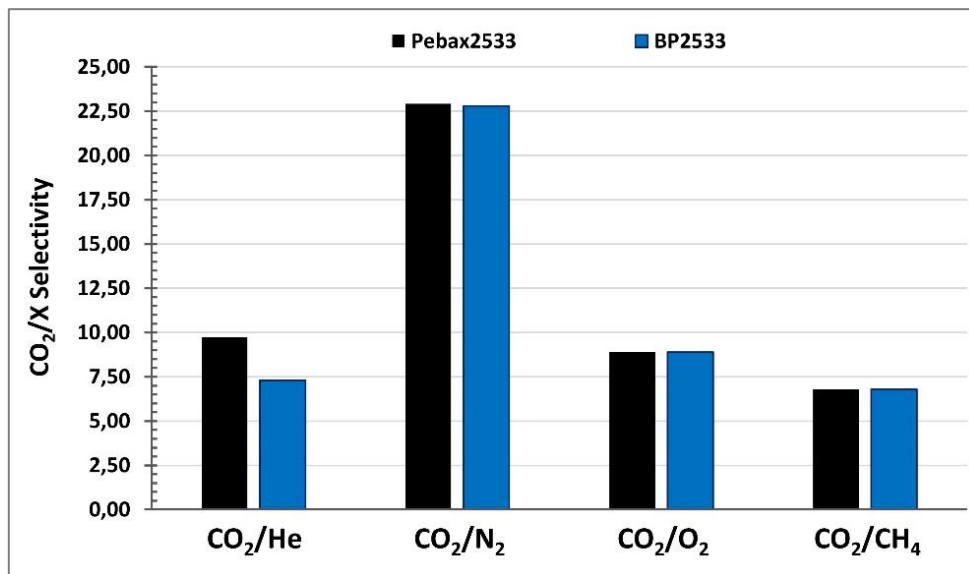


Figure 87: Pebax®2533 and Benzoyl-P2533 (70 mol%) Selectivity results

For clarity, gas permeation results of Figure 86 and 87 are more precisely listed in Table 13, along with the percentual variation of permeability and CO₂/X selectivity between the neat Pebax®2533 and BP2533 70% substituted, and the gases' boiling points and kinetic diameters:

Table 13: Pebax®2533 and Benzoyl P2533#5 (70 mol%) gas permeation summary

| Gas | Pebax®2533 | | | | | Benzoyl-P2533 (70% conv.) | | | | |
|--------------------------------|-----------------|----------------|-----------------|----------------|-------|---------------------------|----------------|-----------------|----------------|--------|
| | CO ₂ | N ₂ | CH ₄ | O ₂ | He | CO ₂ | N ₂ | CH ₄ | O ₂ | He |
| Permeability (Barrer) | 296,61 | 12,94 | 43,64 | 33,28 | 30,43 | 329,80 | 14,47 | 48,34 | 37,19 | 45,00 |
| Selectivity CO ₂ /X | 1 | 22,92 | 6,80 | 8,91 | 9,75 | \ | 22,79 | 6,82 | 8,87 | 7,33 |
| Permeability Variation% | \ | \ | \ | \ | \ | + 11,2 | + 11,8 | + 10,8 | + 11,7 | + 47,9 |
| CO ₂ /X Selec.Var.% | \ | \ | \ | \ | \ | \ | -0,5 | + 0,4 | -0,5 | -24,8 |
| Boiling Point (K) | 195 | 77 | 112 | 90 | 4 | 195 | 77 | 112 | 90 | 4 |
| Kinetic Diam. (pm) | 330 | 364 | 380 | 346 | 260 | 330 | 364 | 380 | 346 | 260 |

From the permeation results obtained, it is clear that the modification of the polymer increased the overall permeability of the system: the increment was about 11-12 % for all gases except helium, where the permeability jumped by 48 %.

All gases except helium shared also the same selectivity behavior with respect to CO₂, which remained basically constant for all of them, oscillating between -0,5 % and + 0,4 %, while for helium it decreased of a fair 25 %.

Such behavior is probably due to the higher mobility provided to the overall copolymer, that, after the modification, possess less crystallinity and had no rigid amides blocks anymore, which can favorite diffusion processes.

After the modification, helium's permeability increased more than any other gas, leading to a decrement of CO₂/He selectivity, and this may be caused by its higher dependence by diffusivity process, being the gas with smallest kinetic diameter.

In Table 13, for all gases are reported the respective boiling points and kinetic diameter as well. Analyzing such data, it's possible to notice that the permeability of all gases (except helium) increase with the increment of their boiling point, for both neat Pebax®2533 and the modified one. this is not the case for the comparison with kinetic diameters, where no trends are appreciable.

Considering the solution diffusion mechanism and permeability dependence on both thermodynamic and kinetics factor, this result seems to indicate that the solubility parameter is dominant for these materials, in respect to the diffusivity one. In this concern the fact that Helium results to be outside the trends followed by all other gases, generally showing higher permeability than want expected, can be easily explained by the fact that it is definitely smaller than any other gas, so that in that case it is likely that the diffusivity factor counts as well in the determination of the overall flux across the membrane.

Considering the results obtained in the precedent Chapter 5 with GO-materials, it is licit to hypnotize that, combining both PGO at 0,02 wt% loading into BP2533, it could be possible to obtain a high

CO₂ permeability material, up to 20% higher than pristine Pebax[®]2533 (reaching around 350 Barrer), with CO₂/N₂ selectivity of 23 and very low filler loading (just 0,02 wt%).

Unfortunately, due to Covid19 pandemic, such investigation was not carried out and the focus remained on the characterization of the pure new material, but the BP2533 compatibilization with GO-materials and other fillers remains an interesting starting point for future works.

6.7 Permeance - Thin Coated Membranes

The two spin coating programs described in Section 3.3.2, and performed by static dispense with other parameter identical apart from the volume of solution used, resulted extremely reproducible. Also in this case, the material employed has been of BP2533 70 mol%, that as said above, already proved to be optimal for making stable coated films.

To verify the coating effectiveness, CO₂ and N₂ were tested, in order to compare the selectivity with the thick membranes, verifying in this way the integrity or not of the thin film.

The results are summarized in Table 14.

Table 14: BP2533 70 mol% permeance results

| Volume per Coating (ml) | CO ₂ Permeance (GPU) | CO ₂ /N ₂ Selectivity | Estimated Thickness (μm) |
|-------------------------|---------------------------------|---|--------------------------|
| 1 | 270 | 23,0 | 1,2 |
| 5 | 100 | 23,0 | 3,4 |

Since the thick membranes made of Benzoyl-P2533 70 mol% obtained through solvent casting had a selectivity of basically 23, it is safe to say that the coverage provided by the spin coating has been not only complete, but also without any defect.

The thickness estimated have been calculated with large approximation through the previously discussed Equation 26, using as known permeability the one obtained from the thick solvent casting membranes and neglecting the resistance of the PDMS support thanks to its definitely higher permeance (in the order of 2000 GPU)

The thickness resulted to be relatively “high”, over the micron, mostly due to the 4 consecutive coatings performed and to the solution concentration (15 mg BP2533/ml CHCl₃).

However, it is safe to say that, with the very same material, far thinner coated layer could be obtained, by making 1 or 2 coatings instead of 4, and decreasing the concentration of the polymeric solution dispensed.

Unfortunately, due to Covid19 pandemic, the work suffered a drastic slowdown and also a complete stop for a certain period, thus such thin coating investigation got interrupted.

Conclusions

During this Project, different materials have been employed to realize CO₂ separation membranes, exploiting a number of technical strategies to improve their performances: facilitated transport mechanism, fillers to make mixed matrix membranes, or the modification of the matrix itself. Chemical, physical and gas permeation characterizations were carried on the membranes, in order to achieve a full characterization of their structure, morphology and permeation properties. The latter were carried out through barometric-based single gas experiments.

The three-component FTM membranes included PVAm, cNFC and Arginine, and the blending process resulted extremely efficient, by exploiting the homogenizer Ika Ultra Turrax T18 Digital, obtaining homogeneous composite materials.

The permeation tests were tested in humid conditions at 75 and 100 RH% in order to exploit the CO₂ facilitated transport, at 35°C and 1 bar feed. Also 100 RH% and 50°C tests were carried out. For this type of membranes, CO₂, N₂ and CH₄ were used, due to the final application targets of post combustion carbon capture and natural gas sweetening.

The permeation data resulted in line with the expectations: the permselective properties increased with the increment of humidity, and especially the sample containing 45 wt% of Arginine, into a matrix made of PVAm/cNFC 50/50 in weight, crossed the 2008 CO₂/N₂ Robeson Plot at 100RH% and 35°C, with a CO₂ permeability of 271 Barrer and CO₂/N₂ selectivity of 70.

The test conducted at 50°C and 100RH% resulted in higher CO₂ permeability for all the material tested, i.e. from 271 to 326 Barrer for the 45 wt% Arginine loaded, with an increment of about 20%. But at the same time both CO₂/N₂ and CO₂/CH₄ selectivity dropped, from 70 to 8 for CO₂/N₂, and from 14 to 6 for CO₂/CH₄. Similar trend was observed also for the other samples. Such behavior proved that the blends used, even with the stable precipitate formed when mixing PVAm and cNFC, do not resist at 50°C. Therefore, a controlled crosslinking of PVAm with glutaraldehyde was investigated, obtaining a reinforced 3D matrix far more stable even in liquid water.

For the Pebax[®]2533 loaded with GO-based materials, the blending process was driven by the use of a double-solvent blending approach, instead of the high-power homogenization, still producing extremely homogeneous composites.

The application target was post combustion carbon capture, thus CO₂ and N₂ gas were tested, at 35°C, 1 bar feed and dry conditions to be more reproducible and comparable with literature data.

Permeation test conducted on Pebax loaded with different amount of neat GO showed that such material can be applicable only at low concentrations, in this case 0,02 wt% was the best among the tested, due to a slight increment of CO₂ permeability (2%), while no effect on selectivity. Higher concentration of GO provided indeed an increment of barrier effect and drop of permeability.

PEAGO and PGO were used as filler at 0,02 wt% as well, showing a similar behavior of not affecting CO₂/N₂ selectivity, but increasing a bit further the CO₂ permeability of the composite membranes, of 4% and 8% respectively. DSC analysis confirmed that the fillers tend to locate into the Nylon12 moiety of the copolymer, suggesting that this was the reason why no effect on selectivity occurred, since is the ether PTMO moiety that lead the gas permeation.

The matrix Pebax[®]2533 have been also successfully modified by grafting a benzoyl group upon the nitrogen of the Nylon12 moiety, obtaining the product named “Benzoyl-P2533” (BP2533). The modified material was first fully characterized with FTIR, NMR and DSC.

The ¹H-NMR results proved the success of such modification, function of the different protocol carried out, which was already suggested by FTIR results.

Interesting results about the crystallinity of the system emerged from DSC analysis: it showed that with a substitution degree of just 25 mol%, the Nylon moiety is not able to crystallize anymore, while in the pristine material reached the 20% of crystallinity. The crystallization of PTMO instead remained constant at about 19% until the conversion reached 40%, from where its crystallinity jumped to 32%, and reaching 35% at full substitution. Such result indicated the increment of mobility of the overall co-polymer with the new structure, that allow the PTMO side to rearrange and crystallize in higher amount. The Nylon side, instead, with a so big hindering group, was totally unable to crystallize.

Being a new material, a wide gas permeation characterization was carried out as well, using five different gas: CO₂, N₂, CH₄, O₂, and He. The condition chosen were the same for the Pebax-GO composite membranes: 35°C, 1 bar feed. For these tests, a 70 mol% substituted BP2533 were used, since it resulted to be a compromise between high substitution degree and handling. The fully converted membranes indeed were too sticky and elastic to be manually handled after solvent casting for permeation characterization test.

The permeation results indicated that the new material possess a fair 10% higher permeability compared to the pristine Pebax[®]2533, with no effect on selectivity at all, for all gases tested, basically increasing the overall CO₂ permselective properties of the material.

The only exception was helium, which showed an increment of almost 50% for BP2533, and thus a slightly smaller selectivity with respect to CO₂ if compared to the pristine Pebax[®]2533.

In conclusion, during this doctorate different way to improve gas permeation membranes have been investigated, using all the materials provided by the Project NANOMEMC² members, obtaining not ground-breaking but undoubtedly interesting results.

The research activity on the topic treated in this thesis indeed are far from being completed and many further work may be possible: for FTM, by implementing the controlled crosslinked PVAm with mobile carriers or other fillers, in order to have hydrophilic and highly water intaking matrix but extremely more resistant to water and high temperatures.

For solution-diffusion materials, it could be virtually possible to prepare a polymeric mixed matrix membrane made of BP2533 loaded with extremely low concentration of PGO or other fillers, obtaining an extremely high permeable dense material. Considering the results obtained in this work for GO and BP2533 separately, by combine them, permeability could rise of almost 20% compared to the pristine Pebax[®]2533, obtaining an interesting very low-loaded MMM as starting-point for membrane making, with the possibility to add even different nano-materials.

Indeed, since a standalone BP2533 characterization was successfully achieved, both chemically and in term of gas permselectivity, an investigation of the compatibility of Graphene, Graphene Oxide and also other filler materials with this new polymer could be an intriguing topic for future works.

Acknowledgements

The author would like to thank Prof. Marco Giacinti Baschetti for his supervision during the years of the PhD program.

A thanks also to Prof. Loris Giorgini, for his support during the whole work in matter of chemical characterizations.

The author wishes to thank Prof. Ho Bum Park, for the period abroad spent in his group of Energy Engineering at Hanyang University, Seoul, South Korea.

A special thanks also to the Bachelor and Master students that participated to this work: Matteo Perelli, Melissa Phipps, Elham Firouznia, Baptiste Guillaume Rerolle.

References

1. Dudley, B. *BP Statistical Review of World Energy 2019 | 68th edition*; 2019;
2. Tzimas, E.; Georgakaki, A. A long-term view of fossil-fuelled power generation in Europe. *Energy Policy* **2010**, *38*, 4252–4264.
3. Nasa.gov Carbon Dioxide Concentration 2020 Available online: <https://climate.nasa.gov/vital-signs/carbon-dioxide/> (accessed on Jul 28, 2020).
4. Team, T.I.C.W. *Climate Change 2014 Synthesis Report*; ISBN 9789291691432.
5. Church, J.A.; Gregory, J.M. Sea level change. *Encycl. Ocean Sci.* **2019**, 493–499.
6. Goudie, A.S. Desertification. *Encycl. Environ. Heal.* **2019**, 46–51.
7. Seneviratne, S.I.; Nicholls, N.; Easterling, D.; Goodess, C.M.; Kanae, S.; Kossin, J.; Luo, Y.; Marengo, J.; Mc Innes, K.; Rahimi, M.; et al. Changes in climate extremes and their impacts on the natural physical environment. *Manag. Risks Extrem. Events Disasters to Adv. Clim. Chang. Adapt. Spec. Rep. Intergov. Panel Clim. Chang.* **2012**, *9781107025*, 109–230.
8. Chen, J.; Wang, Z.; Tam, C.Y.; Lau, N.C.; Lau, D.S.D.; Mok, H.Y. Impacts of climate change on tropical cyclones and induced storm surges in the Pearl River Delta region using pseudo-global-warming method. *Sci. Rep.* **2020**, *10*, 1–10.
9. Holden, W.N.; Marshall, S.J. *Climate change and typhoons in the Philippines: Extreme weather events in the anthropocene*; Elsevier Inc., 2018; ISBN 9780128120576.
10. IPCC — Intergovernmental Panel on Climate Change *Global warming of 1.5 °C*; IPCC: Geneva, Switzerland, 2018, Ed.; ISBN 9789291691517.
11. Rogelj, J.; Shindell, D.; Jiang, K.; Fifita, S. IPCC 2018, cap2. *Glob. Warm. 1.5°C. An IPCC Spec. Rep. [...] 2018*, *2*.
12. Krinner, G.; Germany, F.; Shongwe, M.; Africa, S.; France, S.B.; Uk, B.B.B.B.; Germany, V.B.; Uk, O.B.; France, C.B.; Uk, R.C.; et al. Long-term climate change: Projections, commitments and irreversibility. *Clim. Chang. 2013 Phys. Sci. Basis Work. Gr. I Contrib. to Fifth Assess. Rep. Intergov. Panel Clim. Chang.* **2013**, *9781107057*, 1029–1136.
13. Meehl, G.A.; Stocker, T.F.; Collins, W.D.; Friedlingstein, P.; Gaye, A.T.; Gregory, J.M.; Kitoh, A.; Knutti, R.; Murphy, J.M.; Noda, A.; et al. Global Climate Projections. *Clim. Chang. 2007 Phys. Sci. Basis. Contrib. Work. Gr. I to Fourth Assess. Rep. Intergov. Panel Clim. Chang.* **2007**.
14. Mearns, L.O.; Hulme, M. Climate Scenario Development. *Clim. Chang. 2001 Phys. Sci. Basis. Contrib. Work. Gr. I to Third Assess. Rep. Intergov. Panel Clim. Chang.* **2001**, 739–768.
15. Tyszczyk, R.; Smith, J. Culture and climate change scenarios: the role and potential of the arts and humanities in responding to the ‘1.5 degrees target.’ *Curr. Opin. Environ. Sustain.* **2018**, *31*, 56–64.
16. Leung, D.Y.C.; Caramanna, G.; Maroto-valer, M.M. An overview of current status of carbon dioxide capture and storage technologies. *Renew. Sustain. Energy Rev.* **2014**, *39*, 426–443.
17. Gibbins, J.; Chalmers, H. Carbon capture and storage. *Energy Policy* **2008**, *36*, 4317–4322.
18. Koytsoumpa, E.I.; Bergins, C.; Kakaras, E. The CO2 economy: Review of CO2 capture and reuse technologies. *J. Supercrit. Fluids* **2018**, *132*, 3–16.
19. Carpenter, S.M.; Long, H.A. *Integration of carbon capture in IGCC systems*; Elsevier Ltd, 2017; ISBN 9780081001851.
20. Capture, C. CHAPTER 7 Carbon Capture and Storage. **2015**.
21. Figueroa, J.D.; Fout, T.; Plasynski, S.; McIlvried, H.; Srivastava, R.D. Advances in CO2 capture technology-The U.S. Department of Energy’s Carbon Sequestration Program. *Int. J. Greenh. Gas Control* **2008**, *2*, 9–20.
22. Wang, Y.; Zhao, L.; Otto, A.; Robinius, M.; Stolten, D. A Review of Post-combustion CO2 Capture Technologies from Coal-fired Power Plants. *Energy Procedia* **2017**, *114*, 650–665.

23. Jansen, D.; Gazzani, M.; Manzolini, G.; Dijk, E. Van; Carbo, M. Pre-combustion CO₂ capture. *Int. J. Greenh. Gas Control* **2015**, *40*, 167–187.
24. Stanger, R.; Wall, T.; Spörl, R.; Paneru, M.; Grathwohl, S.; Weidmann, M.; Scheffknecht, G.; McDonald, D.; Myöhänen, K.; Ritvanen, J.; et al. Oxyfuel combustion for CO₂ capture in power plants. *Int. J. Greenh. Gas Control* **2015**, *40*, 55–125.
25. Rafiq, S.; Deng, L.; Hägg, M.-B. Role of Facilitated Transport Membranes and Composite Membranes for Efficient CO₂ Capture - A review. *ChemBioEng Rev.* **2016**, 68–85.
26. Khalilpour, R.; Mumford, K.; Zhai, H.; Abbas, A.; Stevens, G.; Rubin, E.S. Membrane-based carbon capture from flue gas: A review. *J. Clean. Prod.* **2015**, *103*, 286–300.
27. Bernhardsen, I.M.; Knuutila, H.K. A review of potential amine solvents for CO₂ absorption process: Absorption capacity, cyclic capacity and pKa. *Int. J. Greenh. Gas Control* **2017**, *61*, 27–48.
28. Isa, F.; Rozali, N.E.M.; Suleman, H.; Maulud, A.; Shariff, A.M. An overview on control strategies for CO₂ capture using absorption/stripping system. *Chem. Eng. Res. Des.* **2019**, *147*, 319–337.
29. Modak, A.; Jana, S. Advancement in porous adsorbents for post-combustion CO₂ capture. *Microporous Mesoporous Mater.* **2019**, *276*, 107–132.
30. Smyrnioti, M.; Tampaxis, C.; Steriotis, T.; Ioannides, T. Study of CO₂ adsorption on a commercial CuO/ZnO/Al₂O₃ catalyst. *Catal. Today* **2019**, 1–8.
31. Han, Y.; Ho, W.S.W. Recent advances in polymeric membranes for CO₂ capture. *Chinese J. Chem. Eng.* **2018**, *26*, 2238–2254.
32. Han, Y.; Ho, W.S.. Recent advances in polymeric membranes for CO₂ capture. *Chinese J. Chem. Eng.* **2018**, *26*, 2238–2254.
33. Babar, M.; Azmi, M.; Ali, A.; Shah, A.; Shafiq, U.; Mukhtar, A.; Nasir, S.; Maqsood, K.; Mellon, N.; Shariff, A.M. Thermodynamic data for cryogenic carbon dioxide capture from natural gas: A review. *Cryogenics (Guildf).* **2019**, *102*, 85–104.
34. Song, C.; Liu, Q.; Deng, S.; Li, H.; Kitamura, Y. Cryogenic-based CO₂ capture technologies : State-of-the-art developments and current challenges. *Renew. Sustain. Energy Rev.* **2019**, *101*, 265–278.
35. Olajire, A.A. A review of mineral carbonation technology in sequestration of CO₂. *J. Pet. Sci. Eng.* **2013**, *109*, 364–392.
36. Narahariseti, P.K.; Yeo, T.Y.; Bu, J. New classification of CO₂ mineralization processes and economic evaluation. *Renew. Sustain. Energy Rev.* **2019**, *99*, 220–233.
37. Goh, P.S.; Ismail, A.F.; Sanip, S.M.; Ng, B.C.; Aziz, M. Recent advances of inorganic fillers in mixed matrix membrane for gas separation. *Sep. Purif. Technol.* **2011**, *81*, 243–264.
38. Leung, D.Y.C.; Caramanna, G.; Maroto-Valer, M.M. An overview of current status of carbon dioxide capture and storage technologies. *Renew. Sustain. Energy Rev.* **2014**, *39*, 426–443.
39. David, J.; Herzog, H. The Cost of Carbon Capture. *Energy* **2000**, 13–16.
40. Brouwer, A.S.; van den Broek, M.; Seebregts, A.; Faaij, A. Operational flexibility and economics of power plants in future low-carbon power systems. *Appl. Energy* **2015**, *156*, 107–128.
41. Naims, H. Economics of carbon dioxide capture and utilization—a supply and demand perspective. *Environ. Sci. Pollut. Res.* **2016**, *23*, 22226–22241.
42. Yeo, Z.Y.; Chew, T.L.; Zhu, P.W.; Mohamed, A.R.; Chai, S.P. Conventional processes and membrane technology for carbon dioxide removal from natural gas: A review. *J. Nat. Gas Chem.* **2012**, *21*, 282–298.
43. Adewole, J.K.; Ahmad, A.L.; Ismail, S.; Leo, C.P. Current challenges in membrane separation of CO₂ from natural gas: A review. *Int. J. Greenh. Gas Control* **2013**, *17*, 46–65.
44. Alcheikhhamdon, Y.; Hoorfar, M. Natural gas purification from acid gases using membranes: A review of the history, features, techno-commercial challenges, and process intensification of commercial membranes. *Chem. Eng. Process. Process Intensif.* **2017**, *120*,

- 105–113.
45. J. D. Seader, Ernest J. Henley, D.K.R. *Separation Processes Principles - Chemical and Biochemical Operations*; Third Edit.;
 46. Sreedhar, I.; Vaidhiswaran, R.; Kamani, B.M.; Venugopal, A. Process and engineering trends in membrane based carbon capture. *Renew. Sustain. Energy Rev.* **2017**, *68*, 659–684.
 47. Rowe, B.W.; Freeman, B.D.; Paul, D.R. Influence of previous history on physical aging in thin glassy polymer films as gas separation membranes. *Polymer (Guildf)*. **2010**, *51*, 3784–3792.
 48. Kitchin, M.; Teo, J.; Konstas, K.; Lau, C.H.; Sumbly, C.J.; Thornton, A.W.; Doonan, C.J.; Hill, M.R. AIMS: A new strategy to control physical aging and gas transport in mixed-matrix membranes. *J. Mater. Chem. A* **2015**, *3*, 15241–15247.
 49. Rezakazemi, M.; Sadrzadeh, M.; Matsuura, T. Thermally stable polymers for advanced high-performance gas separation membranes. *Prog. Energy Combust. Sci.* **2018**, *66*, 1–41.
 50. Iulianelli, A.; Drioli, E. Membrane engineering: Latest advancements in gas separation and pre-treatment processes, petrochemical industry and refinery, and future perspectives in emerging applications. *Fuel Process. Technol.* **2020**, *206*, 106464.
 51. Roussanaly, S.; Anantharaman, R.; Lindqvist, K.; Zhai, H.; Rubin, E. Membrane properties required for post-combustion CO₂ capture at coal-fired power plants. *J. Memb. Sci.* **2016**, *511*, 250–264.
 52. R.Ravishankar, J.M.; Jacobs, P. The scientific legacy of the late Richard M. Barrer, FRS. *Microporous Mater.* **1997**, *8*, 283–284.
 53. STERN, S.A. The “Barrer” Permeability Unit. *JOIJRNAL Polym. Sci.* **1968**, *6*, 1933–1934.
 54. Dai, Z.; Ansaloni, L.; Deng, L. Recent advances in multi-layer composite polymeric membranes for CO₂ separation: A review. *Green Energy Environ.* **2016**, *1*, 102–128.
 55. Wijmans, J.G.; Baker, R.W. The solution-diffusion model: a review. *J. Memb. Sci.* **1995**, *107*, 1–21.
 56. Suloff, E. Chapter 4. Permeability, Diffusivity, and Solubility of Gas and Solute Through Polymers. In: Berlin, Heidelberg, 2002.
 57. Robeson, L.M. The upper bound revisited. *J. Memb. Sci.* **2008**, *320*, 390–400.
 58. Comesaña-Gándara, B.; Chen, J.; Bezzu, C.G.; Carta, M.; Rose, I.; Ferrari, M.C.; Esposito, E.; Fuoco, A.; Jansen, J.C.; McKeown, N.B. Redefining the Robeson upper bounds for CO₂/CH₄ and CO₂/N₂ separations using a series of ultrapermeable benzotriptycene-based polymers of intrinsic microporosity. *Energy Environ. Sci.* **2019**, *12*, 2733–2740.
 59. Kozłowski, C.A. Facilitated transport of metal ions through composite and polymer inclusion membranes. *Desalination* **2006**, *198*, 132–140.
 60. Faiz, R.; Li, K. Olefin/paraffin separation using membrane based facilitated transport/chemical absorption techniques. *Chem. Eng. Sci.* **2012**, *73*, 261–284.
 61. Venturi, D.; Ansaloni, L.; Baschetti, M.G. Nanocellulose based facilitated transport membranes for CO₂ separation. *Chem. Eng. Trans.* **2016**, *47*, 349–354.
 62. Venturi, D.; Chrysanthou, A.; Dhuiège, B.; Missoum, K.; Baschetti, M.G. Arginine/Nanocellulose membranes for carbon capture applications. *Nanomaterials* **2019**, *9*, 877.
 63. Casadei, R.; Venturi, D.; Baschetti, M.G.; Giorgini, L.; Maccaferri, E.; Ligi, S. Polyvinylamine membranes containing graphene-based nanofillers for carbon capture applications. *Membranes (Basel)*. **2019**, *9*, 20.
 64. Tomé, L.C.; Guerreiro, D.C.; Teodoro, R.M.; Alves, V.D.; Marrucho, I.M. Effect of polymer molecular weight on the physical properties and CO₂/N₂ separation of pyrrolidinium-based poly (ionic liquid) membranes. *J. Memb. Sci.* **2018**, *549*, 267–274.
 65. Wang, M.; Wang, Z.; Li, N.; Liao, J.; Zhao, S.; Wang, J.; Wang, S. Relationship between polymer-filler interfaces in separation layers and gas transport properties of mixed matrix composite membranes. *J. Memb. Sci.* **2015**, *495*, 252–268.

66. Yuan, S.; Wang, Z.; Qiao, Z.; Wang, M. Improvement of CO₂/N₂ separation characteristics of polyvinylamine by modifying with ethylenediamine. *J. Memb. Sci.* **2011**, *378*, 425–437.
67. Ansaloni, L.; Zhao, Y.; Jung, B.T.; Ramasubramanian, K.; Baschetti, M.G.; Ho, W.S.W. Facilitated transport membranes containing amino-functionalized multi-walled carbon nanotubes for high-pressure CO₂ separations. *J. Memb. Sci.* **2015**, *490*, 18–28.
68. Vakharia, V.; Salim, W.; Wu, D.; Han, Y.; Chen, Y.; Zhao, L.; Ho, W.S.W. Scale-up of amine-containing thin-film composite membranes for CO₂ capture from flue gas. *J. Memb. Sci.* **2018**, *555*, 379–387.
69. Salim, W.; Han, Y.; Vakharia, V.; Wu, D.; Wheeler, D.J.; Ho, W.S.W. Scale-up of amine-containing membranes for hydrogen purification for fuel cells. *J. Memb. Sci.* **2019**, *573*, 465–475.
70. Han, Y.; Salim, W.; Chen, K.K.; Wu, D.; Ho, W.S.W. Field trial of spiral-wound facilitated transport membrane module for CO₂ capture from flue gas. *J. Memb. Sci.* **2019**, *575*, 242–251.
71. Ooi, Z.L.; Tan, P.Y.; Tan, L.S.; Yeap, S.P. Amine-based solvent for CO₂ absorption and its impact on carbon steel corrosion: A perspective review. *Chinese J. Chem. Eng.* **2020**, *28*, 1357–1367.
72. Bernhardsen, I.M.; Knuutila, H.K. A review of potential amine solvents for CO₂ absorption process: Absorption capacity, cyclic capacity and pK_a. *Int. J. Greenh. Gas Control* **2017**, *61*, 27–48.
73. Zhang, H.; Tian, H.; Zhang, J.; Guo, R.; Li, X. Facilitated transport membranes with an amino acid salt for highly efficient CO₂ separation. *Int. J. Greenh. Gas Control* **2018**, *78*, 85–93.
74. El-azzami, L.A.; Grulke, E.A. Carbon dioxide separation from hydrogen and nitrogen Facilitated transport in arginine salt – chitosan membranes. **2009**, *328*, 15–22.
75. Zhao, Y.; Winston Ho, W.S. Steric hindrance effect on amine demonstrated in solid polymer membranes for CO₂ transport. *J. Memb. Sci.* **2012**, *415–416*, 132–138.
76. Kim, T.-J.; Vrålstad, H.; Sandru, M.; Hägg, M.-B. The effect of pH on CO₂-separation from post combustion gas by polyvinylamine based composite membrane. *Energy Procedia* **2013**, *37*, 986–992.
77. Venturi, D.; Grupkovic, D.; Sisti, L.; Baschetti, M.G. Effect of humidity and nanocellulose content on Polyvinylamine-nanocellulose hybrid membranes for CO₂ capture. *J. Memb. Sci.* **2018**, *548*, 263–274.
78. Chaudhari, S.; Kwon, Y.S.; Moon, M.J.; Shon, M.Y.; Nam, S.E.; Park, Y.I. Poly(vinyl alcohol) and poly(vinyl amine) blend membranes for isopropanol dehydration. *J. Appl. Polym. Sci.* **2017**, *134*, 1–8.
79. Gierszewska, M.; Ostrowska-czubenko, J. Chitosan-based membranes with different ionic crosslinking density for pharmaceutical and industrial applications. *Carbohydr. Polym.* **2016**, *153*, 501–511.
80. Lin, Y.; Lin, Y.; Lee, C.; Lin, K.A.; Chung, T.; Tung, K. Synthesis of mechanically robust epoxy cross-linked silica aerogel membranes for CO₂ capture. *J. Taiwan Inst. Chem. Eng.* **2018**, *87*, 117–122.
81. Duan, K.; Li, Y.; Li, L.; Hu, Y.; Wang, X. Pillared graphene as excellent reinforcement for polymer-based nanocomposites. *Mater. Des. J.* **2018**, *147*, 11–18.
82. Wu, J.; Ye, C.; Liu, T.; An, Q.; Song, Y.; Lee, K.; Hung, W.; Gao, C. Synergistic effects of CNT and GO on enhancing mechanical properties and separation performance of polyelectrolyte complex membranes. *Mater. Des.* **2017**, *119*, 38–46.
83. Papageorgiou, D.G.; Kinloch, I.A.; Young, R.J. Mechanical Properties of Graphene and Graphene-based Nanocomposites. *Prog. Mater. Sci.* **2017**, *90*, 75–127.
84. Hao, W.; Wang, M.; Zhou, F.; Luo, H.; Xie, X.; Luo, F.; Cha, R. A review on nanocellulose as a lightweight filler of polyolefin composites. *Carbohydr. Polym.* **2020**, *243*.

85. Dufresne, A. Cellulose nanomaterial reinforced polymer nanocomposites. *Curr. Opin. Colloid Interface Sci.* **2017**, *29*, 1–8.
86. Kargarzadeh, H.; Mariano, M.; Huang, J.; Lin, N.; Ahmad, I.; Dufresne, A.; Thomas, S. Recent developments on nanocellulose reinforced polymer nanocomposites: A review. *Polymer (Guildf)*. **2017**, *132*, 368–393.
87. Chawla, K.K. *COMPOSITE MATERIALS - Science and Engineering*; (USA), S.S., Ed.; Second.; 2007;
88. Romanenko, A.; Suslyayev, V.; Molenda, M.; Świętosławski, M.; Dziembaj, R.; Alejandro, D.; Escárpita, A.; Cárdenas, D.; Elizalde, H.; Probst, O.; et al. *COMPOSITES AND THEIR PROPERTIES Edited by Ning Hu*; 2012; ISBN 9789535107118.
89. Adatoz, E.; Avci, A.K.; Keskin, S. Opportunities and challenges of MOF-based membranes in gas separations. *Sep. Purif. Technol.* **2015**, *152*, 207–237.
90. Younas, M.; Rezakazemi, M.; Daud, M.; Wazir, M.B.; Ahmad, S.; Ullah, N.; Inamuddin; Ramakrishna, S. Recent progress and remaining challenges in post-combustion CO₂ capture using metal-organic frameworks (MOFs). *Prog. Energy Combust. Sci.* **2020**, *80*.
91. Aniruddha, R.; Sreedhar, I.; Reddy, B.M. MOFs in carbon capture-past, present and future. *J. CO₂ Util.* **2020**, *42*, 101297.
92. Kosinov, N.; Gascon, J.; Kapteijn, F.; Hensen, E.J.M. Recent developments in zeolite membranes for gas separation. *J. Memb. Sci.* **2016**, *499*, 65–79.
93. Bastani, D.; Esmaeili, N.; Asadollahi, M. Polymeric mixed matrix membranes containing zeolites as a filler for gas separation applications: A review. *J. Ind. Eng. Chem.* **2013**, *19*, 375–393.
94. Caro, J. Are MOF membranes better in gas separation than those made of zeolites? *Curr. Opin. Chem. Eng.* **2011**, *1*, 77–83.
95. Wang, M.; Wang, Z.; Zhao, S.; Wang, J.; Wang, S. Recent advances on mixed matrix membranes for CO₂ separation. *Chinese J. Chem. Eng.* **2017**, *25*, 1581–1597.
96. Vinoba, M.; Bhagiyalakshmi, M.; Alqaheem, Y.; Alomair, A.A.; Pérez, A.; Rana, M.S. Recent progress of fillers in mixed matrix membranes for CO₂ separation: A review. *Sep. Purif. Technol.* **2017**, *188*, 431–450.
97. Goh, P.S.; Ismail, A.F.; Sanip, S.M.; Ng, B.C.; Aziz, M. Recent advances of inorganic fillers in mixed matrix membrane for gas separation. **2011**, *81*, 243–264.
98. Aroon, M.A.; Ismail, A.F. Performance studies of mixed matrix membranes for gas separation : A review. *Sep. Purif. Technol.* **2010**, *75*, 229–242.
99. Chung, T.; Ying, L.; Li, Y.; Kulprathipanja, S. Mixed matrix membranes (MMMs) comprising organic polymers with dispersed inorganic fillers for gas separation. **2007**, *32*, 483–507.
100. Rezakazemi, M.; Ebadi, A. Progress in Polymer Science State-of-the-art membrane based CO₂ separation using mixed matrix membranes (MMMs): An overview on current status and future directions. *Prog. Polym. Sci.* **2014**, *39*, 817–861.
101. Casadei, R.; Baschetti, M.G.; Yoo, M.J.; Park, H.B.; Giorgini, L. Pebax® 2533/graphene oxide nanocomposite membranes for carbon capture. *Membranes (Basel)*. **2020**, *10*, 1–20.
102. Annenkov, V. V.; Danilovtseva, E.N.; Pal'shin, V.A.; Aseyev, V.O.; Petrov, A.K.; Kozlov, A.S.; Patwardhan, S. V.; Perry, C.C. Poly(vinyl amine)-silica composite nanoparticles: Models of the silicic acid cytoplasmic pool and as a silica precursor for composite materials formation. *Biomacromolecules* **2011**, *12*, 1772–1780.
103. Schmalen, A. Post Polymerization Modification of Poly(vinyl amine) with Functional Epoxides: Multifunctional, Antimicrobial, Protein-like Polymers, PhD. Dissertation, RWTH Aachen University, 2014.
104. ROBERT K. PINSCHMIDT, JR (Institute for Advanced Materials, Nanoscience and Technology, U. of N.C. Polyvinylamine at Last. *Wiley Intersci.* **2010**.
105. BONDSTAR ® POLYVINYLAMINE. 1–3.

106. BASF Carrier System resolves strength problems of corrugating medium Combined use of synthetic dry strength agents.
107. Liu, M.; Zheng, Y.; Shuai, S.; Zhou, Q.; Yu, S.; Gao, C. Thin-film composite membrane formed by interfacial polymerization of polyvinylamine (PVAm) and trimesoyl chloride (TMC) for nanofiltration. *Desalination* **2012**, 288, 98–107.
108. Yu, S.; Ma, M.; Liu, J.; Tao, J.; Liu, M.; Gao, C. Study on polyamide thin-film composite nanofiltration membrane by interfacial polymerization of polyvinylamine (PVAm) and isophthaloyl chloride (IPC). *J. Memb. Sci.* **2011**, 379, 164–173.
109. Jin, L.; Sun, Q.; Xu, Q.; Xu, Y. Adsorptive removal of anionic dyes from aqueous solutions using microgel based on nanocellulose and polyvinylamine. *Bioresour. Technol.* **2015**, 197, 348–355.
110. Huang, Y. Applications of Polyvinylamine in Removal of Heavy Metals from Wastewater by Polymer-Enhanced. **2016**.
111. Huang, Y.; Wu, D.; Wang, X.; Huang, W.; Lawless, D.; Feng, X. Removal of heavy metals from water using polyvinylamine by polymer-enhanced ultrafiltration and flocculation. *Sep. Purif. Technol.* **2016**, 158, 124–136.
112. Huang, Y.; Du, J.R.; Zhang, Y.; Lawless, D.; Feng, X. Removal of mercury (II) from wastewater by polyvinylamine-enhanced ultrafiltration. *Sep. Purif. Technol.* **2015**, 154, 1–10.
113. May-Britt HÄGG, Taek-Joong Kim, B.L. Patent FTM PVAm-CO₂ WO2005089907A1.pdf.
114. Tong, Z.; Ho, W.S.W. New sterically hindered polyvinylamine membranes for CO₂ separation and capture. *J. Memb. Sci.* **2017**, 543, 202–211.
115. Chen, Y.; Ho, W.S.W. High-molecular-weight polyvinylamine/piperazine glycinate membranes for CO₂ capture from flue gas. *J. Memb. Sci.* **2016**, 514, 376–384.
116. Sandru, M.; Kim, T. High molecular fixed-site-carrier PVAm membrane for CO₂ capture. **2009**, 240, 2008–2010.
117. Deng, L.; Kim, T.; Hägg, M. Facilitated transport of CO₂ in novel PVAm/PVA blend membrane. *J. of Membrane Sci.* **2009**, 340, 154–163.
118. Deng, L.; Hägg, M. Carbon nanotube reinforced PVAm / PVA blend FSC nanocomposite membrane for CO₂ / CH₄ separation. *Int. J. Greenh. Gas Control* **2014**, 26, 127–134.
119. Kim T.K., Vralstad H., Sandru M., H.M. Separation performance of PVAm composite membrane for CO₂ capture at various pH levels. *J. Memb. Sci.* **2012**, 428, 218–224.
120. Zhao, S.; Cao, X.; Ma, Z.; Wang, Z.; Qiao, Z.; Wang, J.; Wang, S. Mixed-Matrix Membranes for CO₂/N₂ Separation Comprising a Poly(vinylamine) Matrix and Metal-Organic Frameworks. *Ind. Eng. Chem. Res.* **2015**, 54, 5139–5148.
121. Hussain, A.; Hägg, M.B. A feasibility study of CO₂ capture from flue gas by a facilitated transport membrane. *J. Memb. Sci.* **2010**, 359, 140–148.
122. BASF Lupamin ® 9095 2013.
123. Yu, M. Clicking polyelectrolytes to form a crosslinked hydrogel; their use for surface modification, electrospinning and preparation of nanoparticles, 2011.
124. Trache, D.; Tarchoun, A.F.; Derradji, M.; Hamidon, T.S.; Masruchin, N.; Brosse, N.; Hussin, M.H. *Nanocellulose: From Fundamentals to Advanced Applications*; 2020; Vol. 8; ISBN 0000000230049.
125. Thomas, B.; Raj, M.C.; Athira, B.K.; Rubiyah, H.M.; Joy, J.; Moores, A.; Drisko, G.L.; Sanchez, C. Nanocellulose, a Versatile Green Platform: From Biosources to Materials and Their Applications. *Chem. Rev.* **2018**, 118, 11575–11625.
126. Thomas, P.; Duolikun, T.; Rumjit, N.P.; Moosavi, S.; Lai, C.W.; Bin Johan, M.R.; Fen, L.B. Comprehensive review on nanocellulose: Recent developments, challenges and future prospects. *J. Mech. Behav. Biomed. Mater.* **2020**, 110, 103884.
127. Hurley, B.R.A.; Ouzts, A.; Fischer, J.; Gomes, T. PAPER PRESENTED AT IAPRI WORLD CONFERENCE 2012 Effects of Private and Public Label Packaging on Consumer Purchase Patterns. *Packag. Technol. Sci.* **2013**, 29, 399–412.

128. Ferrer, A.; Pal, L.; Hubbe, M. Nanocellulose in packaging: Advances in barrier layer technologies. *Ind. Crops Prod.* **2017**, *95*, 574–582.
129. Azeredo, H.M.C.; Rosa, M.F.; Mattoso, L.H.C. Nanocellulose in bio-based food packaging applications. *Ind. Crops Prod.* **2017**, *97*, 664–671.
130. Khan, A.; Huq, T.; Khan, R.A.; Riedl, B.; Lacroix, M. Nanocellulose-Based Composites and Bioactive Agents for Food Packaging. *Crit. Rev. Food Sci. Nutr.* **2014**, *54*, 163–174.
131. Bongao, H.C.; Gabatino, R.R.A.; Arias, C.F.H.; Magdaluyo, E.R. Micro/nanocellulose from waste Pili (*Canarium ovatum*) pulp as a potential anti-ageing ingredient for cosmetic formulations. *Mater. Today Proc.* **2020**, *22*, 275–280.
132. Ludwicka, K.; Jedrzejczak-Krzepkowska, M.; Kubiak, K.; Kolodziejczyk, M.; Pankiewicz, T.; Bielecki, S. *Medical and Cosmetic Applications of Bacterial NanoCellulose*; Elsevier B.V., 2016; ISBN 9780444634665.
133. Jorfi, M.; Foster, E.J. Recent advances in nanocellulose for biomedical applications. *J. Appl. Polym. Sci.* **2015**, *132*, 1–19.
134. Taheri, P.; Jahanmardi, R.; Koosha, M.; Abdi, S. Physical, mechanical and wound healing properties of chitosan/gelatin blend films containing tannic acid and/or bacterial nanocellulose. *Int. J. Biol. Macromol.* **2020**, *154*, 421–432.
135. Čolić, M.; Tomić, S.; Bekić, M. Immunological aspects of nanocellulose. *Immunol. Lett.* **2020**, *222*, 80–89.
136. de Olyveira, G.M.; Filho, L.X.; Basmaji, P.; Costa, L.M.M. Bacterial nanocellulose for medicine regenerative. *J. Nanotechnol. Eng. Med.* **2011**, *2*, 1–8.
137. Gatenholm, P.; Klemm, D. Bacterial nanocellulose as a renewable material for biomedical applications. *MRS Bull.* **2010**, *35*, 208–213.
138. Bacakova, L.; Pajorova, J.; Tomkova, M.; Matejka, R.; Broz, A.; Stepanovska, J.; Prazak, S.; Skogberg, A.; Siljander, S.; Kallio, P. Applications of nanocellulose/nanocarbon composites: Focus on biotechnology and medicine. *Nanomaterials* **2020**, *10*, 1–32.
139. Torstensen, J.; Helberg, R.M.L.; Deng, L.; Gregersen, Ø.W.; Syverud, K. PVA/nanocellulose nanocomposite membranes for CO₂ separation from flue gas. *Int. J. Greenh. Gas Control* **2019**, *81*, 93–102.
140. Venturi, D.; Grupkovic, D.; Sisti, L.; Baschetti, M.G. Effect of humidity and nanocellulose content on Polyvinylamine-nanocellulose hybrid membranes for CO₂ capture. *J. Memb. Sci.* **2018**, *548*, 263–274.
141. Ghimire, S.; Flury, M.; Scheenstra, E.J.; Miles, C.A. Nanocomposite membranes with high-charge and size-screened phosphorylated nanocellulose fibrils for CO₂ separation. *Sci. Total Environ.* **2019**, 135577.
142. Rol, F.; Belgacem, M.N.; Gandini, A.; Bras, J. Recent advances in surface-modified cellulose nanofibrils. *Prog. Polym. Sci.* **2019**, *88*, 241–264.
143. Wågberg, L.; Decher, G.; Norgren, M.; Lindström, T.; Ankerfors, M.; Axnäs, K. The build-up of polyelectrolyte multilayers of microfibrillated cellulose and cationic polyelectrolytes. *Langmuir* **2008**, *24*, 784–795.
144. Moghadam, F.; Kamio, E.; Yoshizumi, A.; Matsuyama, H. An amino acid ionic liquid-based tough ion gel membrane for CO₂ capture. *Chem. Commun.* **2015**, *51*, 13658–13661.
145. Weiss, I.M.; Muth, C.; Drumm, R.; Kirchner, H.O.K. Thermal decomposition of the amino acids glycine, cysteine, aspartic acid, asparagine, glutamic acid, glutamine, arginine and histidine. *BMC Biophys.* **2018**, *11*, 1–15.
146. Dong, G.; Hou, J.; Wang, J.; Zhang, Y.; Chen, V.; Liu, J. Enhanced CO₂/N₂ separation by porous reduced graphene oxide / Pebax mixed matrix membranes. *J. Memb. Sci.* **2016**, *520*, 860–868.
147. Yu, C.; Zhang, B.; Yan, F.; Zhao, J.; Li, J.; Li, L.; Li, J. Engineering nano-porous graphene oxide by hydroxyl radicals. *Carbon N. Y.* **2016**, *105*, 291–296.
148. Yoo, M.J.; Kim, H.W.; Yoo, B.M.; Park, H.B. Highly soluble polyetheramine-functionalized

- graphene oxide and reduced graphene oxide both in aqueous and non-aqueous solvents. *Carbon N. Y.* **2014**, *75*, 149–160.
149. Meshkat, S.; Kaliaguine, S.; Rodrigue, D. Enhancing CO₂ separation performance of Pebax® MH-1657 with aromatic carboxylic acids. *Sep. Purif. Technol.* **2019**, *212*, 901–912.
 150. Zheng, W.; Ding, R.; Yang, K.; Dai, Y.; Yan, X.; He, G. ZIF-8 nanoparticles with tunable size for enhanced CO₂ capture of Pebax based MMMs. *Sep. Purif. Technol.* **2019**, *214*, 111–119.
 151. Lee, S.; Chan, S.; Kim, T.; Wook, S.; Soo, Y. Direct molecular interaction of CO₂ with KTFSI dissolved in Pebax 2533 and their use in facilitated CO₂ transport membranes. *J. Memb. Sci.* **2018**, *548*, 358–362.
 152. Wahab, M.S.A.; Sunarti, A.R. Development of PEBAX Based Membrane for Gas Separation : A Review. **2015**, 78–84.
 153. Eun, J.; Ki, S.; Hoon, Y.; Bum, H. Effect of PEG-MEA and graphene oxide additives on the performance of Pebax®1657 mixed matrix membranes for CO₂ separation. *J. Memb. Sci.* **2019**, *572*, 300–308.
 154. Nafisi, V.; Hägg, M.B. Development of dual layer of ZIF-8/PEBAX-2533 mixed matrix membrane for CO₂ capture. *J. Memb. Sci.* **2014**, *459*, 244–255.
 155. Deluca, N. PEBA: TPE materials for high performance applications. In Proceedings of the Annual Technical Conference - ANTEC, Conference Proceedings; Anaheim, CA, USA, 8–10 May 2017; pp. 2343–2393.
 156. Armstrong, S.; Freeman, B.; Hiltner, A.; Baer, E. Gas permeability of melt-processed poly (ether block amide) copolymers and the effects of orientation. *Polymer (Guildf).* **2012**, *53*, 1383–1392.
 157. Copolymer, P.; Clarizia, G.; Bernardo, P.; Gorrasi, G.; Zampino, D.; Id, S.C.C. Influence of the Preparation Method and Photo-Oxidation Treatment on the Thermal and Gas Transport Properties of Dense Films Based on a. **2018**.
 158. Konyukhova, E. V.; Buzin, A.I.; Godovsky, Y.U.K. Melting of polyether block amide (pebax): The effect of stretching. *Thermochim. Acta* **2002**, *391*, 271–277.
 159. Liu, Y.C.; Chen, C.Y.; Lin, G.S.; Chen, C.H.; Wu, K.C.W.; Lin, C.H.; Tung, K.L. Characterization and molecular simulation of Pebax-1657-based mixed matrix membranes incorporating MoS₂ nanosheets for carbon dioxide capture enhancement. *J. Memb. Sci.* **2019**, *582*, 358–366.
 160. Dong, L.; Chen, M.; Li, J.; Shi, D.; Dong, W.; Li, X.; Bai, Y. Metal-organic framework-graphene oxide composites : A facile method to highly improve the CO₂ separation performance of mixed matrix membranes. *J. Memb. Sci.* **2016**, *520*, 801–811.
 161. Sanaeepur, H.; Ahmadi, R.; Ebadi Amooghin, A.; Ghanbari, D. A novel ternary mixed matrix membrane containing glycerol-modified poly(ether-block-amide) (Pebax 1657)/copper nanoparticles for CO₂ separation. *J. Memb. Sci.* **2019**, *573*, 234–246.
 162. Nafisi, V.; Hägg, M.B. Development of nanocomposite membranes containing modified Si nanoparticles in PEBAX-2533 as a block copolymer and 6FDADurene diamine as a glassy polymer. *ACS Appl. Mater. Interfaces* **2014**, *6*, 15643–15652.
 163. Wang, J.; Fang, W.; Luo, J.; Gao, M.; Wan, Y.; Zhang, S.; Zhang, X.; Park, A.H.A. Selective separation of CO₂ using novel mixed matrix membranes based on Pebax and liquid-like nanoparticle organic hybrid materials. *J. Memb. Sci.* **2019**, *584*, 79–88.
 164. Rahman, M.M.; Filiz, V.; Shishatskiy, S.; Abetz, C.; Neumann, S.; Bolmer, S.; Khan, M.M.; Abetz, V. PEBAX® with PEG functionalized POSS as nanocomposite membranes for CO₂ separation. *J. Memb. Sci.* **2013**, *437*, 286–297.
 165. Scofield, J.M.P.; Gurr, P.A.; Kim, J.; Fu, Q.; Kentish, S.E.; Qiao, G.G. Development of novel fluorinated additives for high performance CO₂ separation thin-film composite membranes. *J. Memb. Sci.* **2016**, *499*, 191–200.
 166. K. S. Novoselov, A. K. Geim, S. V. Morozov, D. Jiang, Y. Zhang, S. V. Dubonos, I.V.G. and

- A.A.F. Electric Field Effect in Atomically Thin Carbon Films. **2016**, *306*, 666–669.
167. Singh, V.; Joung, D.; Zhai, L.; Das, S.; Khondaker, S.I.; Seal, S. Graphene based materials: Past, present and future. *Prog. Mater. Sci.* **2011**, *56*, 1178–1271.
 168. Zhong, Y.; Zhen, Z.; Zhu, H. Graphene: Fundamental research and potential applications. *FlatChem* **2017**, *4*, 20–32.
 169. Papageorgiou, D.G.; Kinloch, I.A.; Young, R.J. Mechanical properties of graphene and graphene-based nanocomposites. *Prog. Mater. Sci.* **2017**, *90*, 75–127.
 170. K. N. Geim, A.; Novoselov, K.S. *The Rise of Graphene*; 2007; Vol. 6;.
 171. Yoo, B.M.; Park, H.B. Graphene Membranes. *Ref. Modul. Chem. Mol. Sci. Chem. Eng.* **2017**, *1*, 358–385.
 172. Zhong, Y.; Zhen, Z.; Zhu, H. Graphene: Fundamental research and potential applications. *FlatChem* **2017**, *4*, 20–32.
 173. Dreyer, D.R.; Todd, A.D.; Bielawski, C.W. Harnessing the chemistry of graphene oxide. *Chem. Soc. Rev.* **2014**, *43*, 5288–5301.
 174. Baek, S.J.; Hong, W.G.; Park, M.; Kaiser, A.B.; Kim, H.J.; Kim, B.H.; Park, Y.W. The effect of oxygen functional groups on the electrical transport behavior of a single piece multi-layered graphene oxide. *Synth. Met.* **2014**, *191*, 1–5.
 175. Nika, D.L.; Balandin, A.A. Phonons and thermal transport in graphene and graphene-based materials. *Reports Prog. Phys.* **2017**, *80*.
 176. Cho, Y.H.; Kim, H.W.; Lee, H.D.; Shin, J.E.; Yoo, B.M.; Park, H.B. Water and ion sorption, diffusion, and transport in graphene oxide membranes revisited. *J. Memb. Sci.* **2017**, *544*, 425–435.
 177. Koolivand, H.; Razzaghi-kashani, M.; Karimi, M.; Koolivand, M. Functionalized graphene oxide/polyimide nanocomposites as highly CO₂-selective membranes. *J. Polym. Res.* **2014**, *21*, 1–12.
 178. Wang, D.; Yao, D.; Wang, Y.; Wang, F.; Xin, Y.; Song, S.; Zhang, Z.; Su, F.; Zheng, Y. Carbon nanotubes and graphene oxide-based solvent-free hybrid nanofluids functionalized mixed-matrix membranes for efficient CO₂/N₂ separation. *Sep. Purif. Technol.* **2019**, *221*, 421–432.
 179. Chen, M.; Soyekwo, F.; Zhang, Q.; Hu, C.; Zhu, A.; Liu, Q. Graphene oxide nanosheets to improve permeability and selectivity of PIM-1 membrane for carbon dioxide separation. *J. Ind. Eng. Chem.* **2018**, *63*, 296–302.
 180. Fathizadeh, M.; Li, S.; Yu, M. Ultrathin graphene oxide-based hollow fiber membranes with brush-like CO₂-philic agent for highly efficient CO₂ capture. *Nat. Commun.*
 181. Mohammed, S.A.; Nasir, A.M.; Aziz, F.; Kumar, G.; Sallehuddin, W.; Jaafar, J.; Lau, W.J.; Yusof, N.; Salleh, W.N.W.; Ismail, A.F. CO₂/N₂ selectivity enhancement of PEBAX MH 1657/Aminated Partially Reduced Graphene Oxide Mixed Matrix Composite Membrane. *Sep. Purif. Technol.* **2019**.
 182. Anastasiou, S.; Bhorla, N.; Pokhrel, J.; Reddy, K.S.K.; Srinivasakannan, C.; Wang, K.; Karanikolos, G.N. Metal-organic framework / graphene oxide composite fillers in mixed-matrix membranes for CO₂ separation. *Mater. Chem. Phys.* **2018**, *212*, 513–522.
 183. Janakiram, S.; Ahmadi, M.; Dai, Z.; Ansaloni, L.; Deng, L. Performance of nanocomposite membranes containing 0D to 2D nanofillers for CO₂ separation: A review. *Membranes (Basel)*. **2018**, *8*.
 184. Yoo, B.M.; Shin, J.E.; Lee, H.D.; Park, H.B. Graphene and graphene oxide membranes for gas separation applications. *Curr. Opin. Chem. Eng.* **2017**, *16*, 39–47.
 185. Sun, M.; Li, J. Graphene oxide membranes: Functional structures, preparation and environmental applications. *Nano Today* **2018**, *20*, 121–137.
 186. Dong, C.; Wang, Z.; Yi, C.; Wang, S. Preparation of polyvinylamine/polysulfone composite hollow-fiber membranes and their CO₂/CH₄ separation performance. *J. Appl. Polym. Sci.* **2006**, *101*, 1885–1891.

187. Yi, C.; Wang, Z.; Li, M.; Wang, J.; Wang, S. Facilitated transport of CO₂ through polyvinylamine/polyethylene glycol blend membranes. *Desalination* **2006**, *193*, 90–96.
188. Schuttlefield, J.D.; Grassian, V.H. ATR-FTIR spectroscopy in the undergraduate chemistry laboratory part I: Fundamentals and examples. *J. Chem. Educ.* **2008**, *85*, 279–281.
189. Fout, T.; Zoelle, A.; Keairns, D.; Turner, M.; Woods, M.; Kuehn, N.; Shah, V.; Chou, V.; Pinkerton, L. Cost and Performance Baseline for Fossil Energy Plants Volume 1: Bituminous Coal and Natural Gas to Electricity. *Natl. Energy Technol. Lab.* **2015**, *1a*, 240.
190. Piccinini, E.; Giacinti Baschetti, M.; Sarti, G.C. Use of an automated spring balance for the simultaneous measurement of sorption and swelling in polymeric films. *J. Memb. Sci.* **2004**, *234*, 95–100.
191. Ossila Spin Coating: Complete Guide to Theory and Techniques Available online: <https://www.ossila.com/pages/spin-coating> (accessed on Jun 5, 2020).
192. (NIH), W.R. ImageJ Available online: <https://imagej.nih.gov/ij/index.html> (accessed on Oct 14, 2020).
193. Olivieri, L.; Aboukeila, H.; Giacinti Baschetti, M.; Pizzi, D.; Merlo, L.; Sarti, G.C. Humid permeation of CO₂ and hydrocarbons in Aquivion® perfluorosulfonic acid ionomer membranes, experimental and modeling. *J. Memb. Sci.* **2017**, *542*, 367–377.
194. Jin, M.; Hyeok, J.; Yeon, S.; Yeon, J.; Min, J.; Grasso, G.; Hyun, J.; Lee, D.; Jin, W.; Yeo, J. Defect control for large-scale thin- fi lm composite membrane and its bench- scale demonstration. *J. Memb. Sci.* **2018**, *566*, 374–382.
195. Zhao, D.; Ren, J.; Wang, Y.; Qiu, Y.; Li, H.; Hua, K.; Li, X.; Ji, J.; Deng, M. High CO₂ separation performance of Pebax®/CNTs/GTA mixed matrix membranes. *J. Memb. Sci.* **2017**, *521*, 104–113.
196. NIST - National Institute of Standards and Technology. Formic Acid Sodium salt IR Spectrum. Available online: <http://webbook.nist.gov/cgi/cbook.cgi?ID=B6010183&Mask=80> (accessed on Sep 18, 2020).
197. Infrared Spectroscopy Absorption Table Available online: https://chem.libretexts.org/Ancillary_Materials/Reference/Reference_Tables/Spectroscopic_Parameters/Infrared_Spectroscopy_Absorption_Table (accessed on Sep 18, 2020).
198. SigmaAldrich IR Spectrum Table & Chart.
199. Moghadam, F.; Lee, T.H.; Park, I.; Park, H.B. Thermally annealed polyimide-based mixed matrix membrane containing ZIF-67 decorated porous graphene oxide nanosheets with enhanced propylene/propane selectivity. *J. Memb. Sci.* **2020**, *603*, 118019.
200. Cho, Y.H.; Jeong, S.M.; Kim, S.; Kim, Y.; Lee, H.J.; Lee, T.H.; Park, H.B.; Park, H.; Nam, S.; Park, Y. Sacrificial graphene oxide interlayer for highly permeable ceramic thin film composite membranes. *J. Memb. Sci.* **2020**, 118442.
201. Lee, H.; Park, S.C.; Roh, J.S.; Moon, G.H.; Shin, J.E.; Kang, Y.S.; Park, H.B. Metal-organic frameworks grown on a porous planar template with an exceptionally high surface area: Promising nanofiller platforms for CO₂ separation. *J. Mater. Chem. A* **2017**, *5*, 22500–22505.
202. Moore, T.T.; Koros, W.J. Non-ideal effects in organic-inorganic materials for gas separation membranes. *J. Mol. Struct.* **2005**, *739*, 87–98.
203. Takahashi, S.; Paul, D.R. Gas permeation in poly(ether imide) nanocomposite membranes based on surface-treated silica. Part 1: Without chemical coupling to matrix. *Polymer (Guildf)*. **2006**, *47*, 7519–7534.
204. Vinh-Thang, H.; Kaliaguine, S. Predictive models for mixed-matrix membrane performance: A review. *Chem. Rev.* **2013**, *113*, 4980–5028.
205. Baig, Z.; Mamat, O.; Mustapha, M.; Mumtaz, A.; Munir, K.S.; Sarfraz, M. Investigation of tip sonication effects on structural quality of graphene nanoplatelets (GNPs) for superior solvent dispersion. *Ultrason. Sonochem.* **2018**, *45*, 133–149.
206. NIST - National Institute of Standards and Technology. NIST Benzoyl chloride - Infrared

Spectrum Available online: <https://webbook.nist.gov/cgi/cbook.cgi?ID=C98884&Type=IR-SPEC&Index=2#IR-SPEC> (accessed on May 9, 2020).

207. Chen, P.; Tang, M.; Zhu, W.; Yang, L.; Wen, S.; Yan, C.; Ji, Z.; Nan, H.; Shi, Y. Systematical mechanism of Polyamide-12 aging and its micro-structural evolution during laser sintering. *Polym. Test.* **2018**, *67*, 370–379.
208. Duddleston, L.J.L.; Puck, A.T.; Harris, A.; Doll, N.P.; Osswald, T.A. Differential scanning calorimetry (DSC) quantification of polyamide 12 (nylon 12) degradation during the selective laser sintering (SLS) process. *Annu. Tech. Conf. - ANTEC, Conf. Proc.* **2016**, *12*, 1–4.
209. Craft, G.M. Characterization of Nylon-12 in a Novel Additive Manufacturing Technology , and the Rheological and Spectroscopic Analysis of PEG-Starch Matrix Interactions by, 2018.
210. Dorigato, A.; Brugnara, M.; Pegoretti, A. Novel polyamide 12 based nanocomposites for industrial applications. *J. Polym. Res.* **2017**, *24*, 1–13.
211. Zhang, J.; Adams, A. Understanding thermal aging of non-stabilized and stabilized polyamide 12 using ¹H solid-state NMR. *Polym. Degrad. Stab.* **2016**, *134*, 169–178.
212. Gogolewski, S.; Czerniawska, K.; Gasiorek, M. Effect of annealing on thermal properties and crystalline structure of polyamides. Nylon 12 (polylauro lactam). **1980**, *1136*, 1130–1136.
213. Grassl, B.; Meurer, B.; Scheer, M.; Galin, J.C. Segmented Poly(tetramethylene oxide) Zwitterionomers and Their Homologous Ionenenes. 2. Phase Separation through DSC and Solid State ¹H-NMR Spectroscopy. *Macromolecules* **1997**, *30*, 236–245.